# Investigating the influence of the transcription factor Hindsight in a Notch-induced tumour model

by

Emily Baker

A thesis

presented to the University of Waterloo

in fulfillment of the

thesis requirement for the degree of

Master of Science

in

Biology

Waterloo, Ontario, Canada, 2023

© Emily Baker 2023

## Author’s Declaration

I hereby declare that I am the sole author of this thesis. This is a true copy of the thesis, including any required final revisions, as accepted by my examiners.

I understand that my thesis may be made electronically available to the public.

## Abstract

In *Drosophila* development, the adult salivary gland and hindgut are derived from populations of undifferentiated cells that are found in the larval stages and are known as the salivary gland imaginal ring (SGIR) and hindgut imaginal ring (HIR). The SGIR and HIR have recently been developed as models for tumourigenesis. In these tissues, the Notch signaling pathway normally regulates proliferation, whereas overactivation results in severe overproliferation. Upon further investigation of this tumour model, cells located at the boundary of the SGIR, and its neighbouring differentiated larval cells have been characterized as a polyploid transition zone (TZ) that is a hotspot for metastatic transformation (Yang et al., 2019; Wang et al., 2021). We report here that the zinc finger transcription factor Hindsight is expressed in the TZ cells of the SGIR as well as the most anterior cells of the HIR. In both of these contexts, ectopic expression of *hnt* throughout the imaginal rings is sufficient to suppress cell proliferation and promote cell growth through the endocycle. Moreover, such ectopic expression of *hnt* is also sufficient to completely suppress Notch-induced overproliferation in both the SGIR and HIR. Analysis of *hnt* somatic mosaics within the SGIR suggests that Hnt can function to regulate proliferation in a cell non-autonomous manner. Co-expression of the cell cycle regulator *string* and *hnt* resulted in a rescue of the *hnt* overexpression phenotype, consistent with a role of *hnt* in the downregulation of the expression of *string.* Interestingly, the overexpression of *hnt* in both the SGIR and HIR frequently resulted in apparent deposition of melanin, suggesting *hnt*

overexpression is capable of inducing trans-differentiation whereby undifferentiated cells adopt the fate of melanin-producing crystal cells.

## Acknowledgements

Thank you to my supervisor, Dr. Bruce Reed for encouraging my pursuit of an MSc. I am truly grateful for the opportunity to learn and grow as a researcher and scientific writer under your tutelage. Many thanks to my committee members, Dr. Moira Glerum and Dr. Dale Martin. Dr. Glerum, I'd like to express my gratitude for your support and guidance over coffee, your mentorship is much appreciated. Dr. Martin, thank you for your kind words and encouragement during our chats in the hall. I'd also like to thank Dr. Christine Dupont and Jane Russwurm for their kindness and encouraging me to be openminded about my future. Having clarity on my goals and aspirations has been one of the greatest things I have gained from my graduate studies and that is thanks to each of you.

To my past and present Reed lab mates, Brittney Lato, Richard Do, Mackenzie Valley, Alex Ng and neighbour down the hall Gyan Mishra, thank you for your friendship and laughs. Thank you to all my friends for making sure I still had fun while still working hard on my goals. I am so thankful for your care and support.

To my family. I'm not sure there is a word in the dictionary that would be able to express the amount of love and gratitude I have for all of you. Special thank you to my parents for providing me with a solid foundation and encouraging me to reach for the stars. Thank you for instilling in me the importance of hard work and dedication and that every challenge is an opportunity to learn something about myself or the world around me.

## Table of Contents

Author's Declaration ..... ii

Abstract ..... iii

Acknowledgements ..... v

List of Figures ..... x

List of Tables ..... xii

List of Abbreviations ..... xiii

Chapter 1 : Introduction ..... 1

1.1 The Endocycle ..... 1

1.2 Regulation of the Endocycle ..... 1

1.3 Endocycling Cells and Cell Death ..... 3

1.4 Hindsight: General Background ..... 5

1.5 String: General Background ..... 6

1.6 Notch: General Background ..... 6

1.7 The connection between Hindsight, String and Notch ..... 7

1.8 Imaginal Tissue ..... 8

1.9 Notch-induced Tumour Model ..... 10

1.10 Research Goals and Objectives ..... 11

Chapter 2 : Methods ..... 12

2.1 Fly Stocks ..... 12

2.2 The GAL4/UAS System ..... 12

*2.2.1 retained-GAL4* ..... 13

*2.2.2 Mmp1-GAL4* ..... 13

*2.3 NRE-EGFP* ..... 13

2.4 *UAS-NICD* and *UAS-N$^{\Delta 34a}$* constructs ..... 14

2.5 *UAS-hnt* lines ..... 14

2.6 Fluorescent Reporter System ..... 14

2.7 Anti-Hindsight Immunostaining ..... 15

2.8 Rearing Protocol for Larvae with Overactive Notch Signaling ..... 16

2.9 Mosaic Analysis ..... 17

2.10 Confocal Microscopy ..... 18

2.11 Cell Counts ..... 18

2.12 Quantitative Analysis ..... 18

Chapter 3 : *hnt* function is implicated in cell cycle regulation and when overexpressed is capable of suppressing Notch tumourigenesis in the salivary gland imaginal ring ..... 19

3.1 Confirmation of *retn* and *Mmp1* expression patterns for use as GAL4 drivers ..... 19

3.2 Overproliferation phenotype due to overactive Notch signaling is reproducible with *UAS-N$^{\Delta 34a}$* ..... 21

3.3 Hnt is expressed in the most posterior cells of the SGIR ..... 24

3.4 Hnt-expressing cells of the SGIR have reduced Notch signaling ..... 25

3.5 Hnt-expressing cells are not mitotically active in the SGIR ..... 27

3.6 Overexpression of Hnt alters cell number and morphology in SGIR ..... 30

3.7 Mosaic analysis indicates that the presence of *hnt$^{345x}$* mutant cells increases the SGIR cell population ..... 33

3.8 Notch-induced overproliferation is suppressed by *hnt* overexpression ..... 36

3.9 *string* overexpression is sufficient to rescue cell population of *hnt* overexpression phenotype ..... 38

Chapter 4 : *hnt* function is implicated in cell cycle regulation and when overexpressed is capable of suppressing Notch tumourigenesis in the hindgut imaginal ring ..... 41

4.1 Confirmation of *retn* and *Mmp1* expression patterns for use as GAL4 drivers ..... 41

4.2 Notch-induced overproliferation is achievable in the HIR using *UAS-NICD* and *UAS-$N^{\Delta 34a}$* ..... 43

4.3 Hnt is expressed in the HIR ..... 46

4.4 *hnt* expressing cells of the HIR have minimal Notch signaling ..... 47

4.5 Hnt expressing cells of the HIR are not mitotically active ..... 49

4.6 Overexpression of *hnt* in the HIR leads to severe tissue disruption and enlarged nuclei ..... 51

4.7 Notch-induced overproliferation is suppressed by *hnt* overexpression ..... 54

4.8 Partial Rescue of *hnt* overexpression is achieved with co-expression of *stg* ..... 56

Chapter 5 : Discussion ..... 58

5.1 Comparison of *UAS-$N^{\Delta 34a}$* and *UAS-NICD* in the imaginal rings ..... 58

5.2 Cells that express *hnt* are not mitotically active and enter the endocycle in the SGIR and HIR ..... 60

5.3 Melanotic phenotype observed with *hnt* overexpression suggests *hnt* is capable of forcing crystal cell fate ..... 64

5.4 Hnt regulates proliferation in the SGIR non-autonomously ..... 66

5.5 Threshold of ectopic *hnt* is sufficient to suppress Notch-induced overproliferation by mediating *stg* expression ..... 67

5.6 Notch and Hindsight interactions are highly context dependent ..... 70

5.7 Summary of salivary gland and hindgut imaginal ring results ..... 72
Chapter 6 : Future Directions ..... 73
6.1 Hnt directly or indirectly influences *stg* expression ..... 73
6.2 Exploration of melanin deposition by overexpression of *hnt* in imaginal rings ..... 74
6.3 Knockdown of *hnt* throughout the TZ and AHIR in both control and Notch-overexpression conditions ..... 75
6.4 Confirmation of Hnt as an inducer of the endocycle ..... 76
Letter of Copyright Permission ..... 78
References ..... 83
Appendix A: Methods Related ..... 96
A.1 Genetic Stocks ..... 96
A.2 Crossing Schemes ..... 98
A.3 Extended larval state (ELS) with Notch-induced overproliferation ..... 100
Appendix B: Raw Data and Calculations Associated with Results ..... 102
B.1 Cell counts and Student T-Tests ..... 102

## List of Figures

Figure 1.1 Oscillation of endocycle regulators. ..... 3
Figure 1.2 Regulation of string expression by Notch and Hindsight. ..... 8
Figure 1.3 Schematic Diagram of Drosophila Imaginal Rings. ..... 10
Figure 3.1 *retn* and *Mmp1* GAL4 drivers are differentially expressed in the SGIR. ..... 20
Figure 3.2 $N^{\Delta 34a}$ and *NICD* UAS constructs produce similar overproliferation phenotype with *retn-GAL4*. ..... 22
Figure 3.3 *UAS-*$N^{\Delta 34a}$ produces a stronger overproliferation phenotype than *UAS-NICD* in *Mmp1*-expressing cells. ..... 23
Figure 3.4 Hnt is expressed in the salivary gland imaginal rings. ..... 24
Figure 3.5 Hnt expressing cells in the SGIR have minimal Notch signaling. ..... 26
Figure 3.6 Minimal Notch Signaling is detected in the SGIR Transition Zone. ..... 26
Figure 3.7 *Mmp1*-expressing cells do not contribute to total cell population of SGIR. ..... 28
Figure 3.8 *hnt* overexpression alters cell number and morphology in SGIR. ..... 31
Figure 3.9 Cell death executed by effector caspases is not responsible for the *hnt* overexpression phenotype in the SGIR. ..... 32
Figure 3.10 *hnt* loss of function mosaic results in increased total cell population of SGIR. ..... 34
Figure 3.11 Overproliferation in Notch-induced tumours is suppressed by *hnt* overexpression. ..... 37
Figure 3.12 Partial rescue of *hnt* overexpression phenotype via overexpression of *stg*. ..... 39
Figure 4.1 *retn* and *Mmp1* GAL4 drivers are differentially expressed in the hindgut imaginal ring. ..... 42
Figure 4.2 Similar overproliferation phenotypes produced by *UAS-NICD* and *UAS-*$N^{\Delta 34a}$ constructs in HIR. ..... 44
Figure 4.3 *Mmp1-GAL4* driven overactive Notch signaling fails to produce overproliferation phenotype in HIR. ..... 45
Figure 4.4 Hnt is expressed in the HIR. ..... 46
Figure 4.5 Hindsight expressing cells in the HIR have minimal Notch signaling. ..... 48

Figure 4.6 Minimal Notch signaling is detected in anterior HIR cells. ..... 48
Figure 4.7. *Mmp1*-expressing cells of the HIR are not mitotically active. ..... 50
Figure 4.8 *hnt* overexpression alters morphology in HIR..... 52
Figure 4.9 Cell death executed by effector caspases is not responsible for the *hnt* overexpression phenotypes in HIR. ..... 53
Figure 4.10 Overproliferation in Notch-induced tumours is suppressed by *hnt* overexpression. ..... 55
Figure 4.11 Partial rescue of *hnt* overexpression phenotype via overexpression of *stg* in HIR. ..... 57
Figure A.2.1 Representative crossing scheme to generate *Drosophila* stocks …….107
Figure A.2.2 Crossing scheme to generate fluorescent reporter system ……..……108
Figure A.3.1 Notch-induced overproliferation in SGIR increases with extended larval state (ELS)……..109
Figure A.3.2 Notch-induced overproliferation in HIR increases with extended larval state (ELS) …….110

## List of Tables

Table 3.1 Quantitative analysis indicates *Mmp1*-expressing cells do not contribute to total cell population of SGIR. ..... 29
Table 3.2 Quantitative analysis indicates *hnt* loss of function mosaic results in increased total cell population of SGIR. ..... 35
Table 3.3 Quantitative analysis indicates rescue of *hnt* overexpression phenotype via overexpression of *stg* with respect to cell number. ..... 40
Table 5.1 Summary of the salivary gland (SGIR) and hindgut (HIR) imaginal ring results...72
Table A.1.1 List of Genetic Stocks ……..105
Table B.1.1 *cdc2-RNAi* SGIR experiment cell counts and statistical analysis …….111
Table B.1.2 Control and $hnt^{345x}$ mosaic cell count data and statistical analysis ……...…112
Table B.1.3 *5xUAS-hnt* and *string* SGIR rescue experiment cell counts and statistical analysis……...114

## List of Abbreviations

| | |
|---|---|
| AHIR | Anterior Hindgut Imaginal Ring |
| APC/C | Anaphase Promoting Complex/Cyclosome |
| BDSC | Bloomington *Drosophila* Stock Center |
| *Cdc2* | Cell Division Control 2 gene |
| Cdc2 | Cell Division Control 2 protein |
| CDK2 | Cyclin-dependent Kinase 2 |
| CDKs | Cyclin Dependent Kinases |
| Cyc | Cyclin |
| DIC | Differential Interference Contrast |
| *Dup* | Double-parked gene |
| ELS | Extended Larval State |
| FIMO | Find Individual Motif Occurrences |
| FLY-FUCCI | Fluorescent Ubiquitination-based Cell Cycle Indicator |
| Fzr | Fizzy-related protein |
| HIR | Hindgut Imaginal Ring |
| *His2Av-GFP* | Histone2Av-GFP transgene construct |

| | |
|---|---|
| *His2Av-RFP* | Histone2Av-RFP transgene construct |
| *hnt* | Hindsight gene |
| Hnt | Hindsight protein |
| ISC | Intestinal Stem Cell |
| M/E | Mitotic/Endocycle |
| *Mmp1* | Matrix metalloproteinase 1 gene |
| Mmp1 | Matrix metalloproteinase 1 protein |
| *N* | Notch gene |
| N | Notch protein |
| NGS | Normal Goat Serum |
| NICD | Notch Intracellular Domain |
| NRE | Notch Response Element |
| PBS | Phosphate-buffered saline |
| *retn* | Retained gene |
| Retn | Retained protein |
| RLSC | Reed Lab Stock Collection |
| RNAi | RNA Interference |
| RREB-1 | Ras-Responsive Element Binding protein-1 |

| | |
|---|---|
| SGIR | Salivary Gland Imaginal Ring |
| *stg* | String gene |
| Stg | String protein |
| *Su(H)* | Suppressor of Hairless gene |
| Su(H) | Suppressor of Hairless protein |
| TFBM | Transcription Factor Binding Motif |
| TZ | Transition Zone |
| UAS | Upstream Activating Sequence |
| UPS | Ubiquitin Proteasome System |

# Chapter 1: Introduction

## 1.1 The Endocycle

The endocycle is a variation of the cell cycle in which cells undergo alternating G and S phases. The elimination of M phase results in the production of polyploid nuclei (Smith & Orr-Weaver, 1991). This somatic polyploidy leads to an increase in cell size as well as greater transcriptional and metabolic output, all of which are necessary for the development of many larval and adult tissues in *Drosophila* (Edgar et al., 2014; Frawley & Orr-Weaver, 2015). Variations of programmed endocycles are found in the tissues of all multicellular organisms (Anatskaya & Vinogradov, 2022). Somatic polyploidy is associated with wound repair in *Drosophila* and is an example where polyploidy is utilized for an increase in cell size. Upon injury, post-mitotic differentiated cells respond by enlarging their size via the endocycle to restore tissue mass and integrity (Losick et al., 2013; Tamori & Deng, 2013; Losick, 2016). The endocycle is also responsible for large polyploid larval salivary gland cells and their well-known polytene chromosomes (Smith & Orr-Weaver, 1991). These cells possess a DNA content of up to 2048C as they are responsible for producing and secreting a high volume of protein (Rodman, 1967; Hammond & Laird, 1985; Campos-Ortega & Hartenstein, 1997).

## 1.2 Regulation of the Endocycle

Progression through the stages of the cell cycle relies on oscillating concentrations of cyclins. Cyclins (Cyc) are regulatory proteins that form active complexes with Cyclin-Dependent Kinases (CDKs) (Follette & O'Farrell, 1997). Cells entering the endocycle must

downregulate mitotic machinery, including CycA, CycB, CycB3, String/Cdc25 and CDK1 to prevent the transition to M phase while maintaining the oscillation of components that drive the endocycle (Sauer et al., 1995; Maqbool et al., 2010).

The primary cyclin that drives cells into S-phase is CycE and it forms a complex with Cyclin-Dependent Kinase 2 (CDK2) (Knoblich et al., 1994). *CycE* expression is regulated by the fluctuating levels of the transcription factor, E2f1. As E2F1 levels rise at the end of G phase, CycE levels increase and peak during S phase. E2F1 and CycE are degraded by the E3 ubiquitin ligases, CRL4-Cdt2 and CRL1-Ago, respectively, allowing for the completion of S phase (Zielke et al., 2011; Shibutani et al., 2007, 2008; Moberg et al., 2001, Shcherbata et al., 2004). Dacapo is an inhibitor of the CycE/CDK2 complex and peaks similarly to E2F1 during G phase to promote the licensing of DNA replication origins (Lane et al., 1996; Hong et al., 2003, 2007). *Dacapo* expression is upregulated by a second isoform of E2F1, E2F1b (Kim et al., 2021). Dacapo is subsequently degraded during S phase (Swanson et al., 2015). To prevent rereplication during S phase, Geminin is found at high levels during S phase to suppress helicase loading and is degraded at the end of S phase by the anaphase promoting complex/cyclosome (APC/C) (Narbonne-Reveau et al., 2008; Zielke et al., 2008). The APC/C is also responsible for degradation of CycA, CycB and CycB3 allowing for G/S phase oscillation (Sigrist & Lehner, 1997; Narbonne-Reveau et al., 2008; Edgar et al., 2014). Overall, the endocycle retains many of the key principles that apply to the regulation of the mitotic cycle (Lilly & Duronio, 2005).

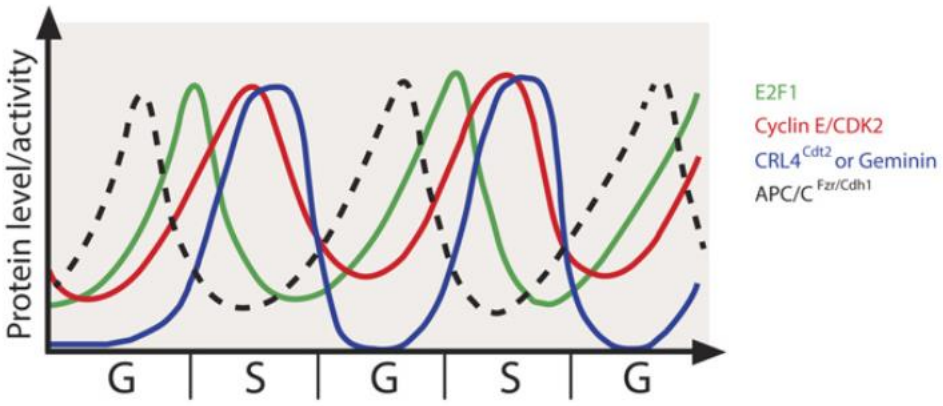



**Figure 1.1 Oscillation of endocycle regulators.** Levels of the E2F1 transcription factor rise at the end of G phase to turn on transcription of CycE and is degraded during S phase. Cyclin E/CDK2 activity rises at the start of S phase to initiate DNA replication and falls at the end of S phase after the completion of replication. The activity of the E3 ubiquitin ligase CRL4-Cdt2 peaks in S phase when it marks E2F1 for degradation. In addition, the activity of APC/C, Fizzy related (Fzr) peaks when CycE/CDK2 activity levels are low and targets Geminin for degradation during G phase (Hua & Orr-Weaver, 2017, with permission).

### 1.3 Endocycling Cells and Cell Death

Upon exposure to severe DNA damage, cells either undergo cellular senescence, which involves G1 phase arrest to halt growth, or they may initiate programmed cell death via apoptosis. In *Drosophila* as in many other eukaryotes, the regulation of the tumour suppressor protein, p53 promotes both of these processes depending on the context (Roos & Kaina, 2006; Saretzki, 2010; Surova & Zhivotosky, 2013).

It has been observed that the endocycle functions independently of cell differentiation as a protective mechanism against apoptosis by repressing genotoxic stress responses (Mehrotra et al., 2008; Hassel et al., 2014). In the adult *Drosophila* brain, polyploid cells are resistant to DNA damage-induced apoptosis (Nandakumar et al., 2020). Ectopic expression

of *Double-parked (Dup*) induces rereplication and triggers both p53-dependent and p53-independent apoptosis in mitotic cells of *Drosophila* larval and adult tissue. In contrast, endocycling cells fail to initiate apoptosis upon ectopic *Dup* expression and as a consequence, DNA damage accumulates in these cells (Mehrotra et al., 2008). Epigenetic silencing has been identified in endocycling salivary gland cells as one method by which these cells inhibit apoptosis. The regulatory regions of the proapoptotic genes *reaper* and *head involution defect* have higher levels of the chromatin silencing markers H3K9me and H3K27me3 in endocycling salivary gland cells than mitotically active cells. Interestingly, the locus where these genes reside is cytologically characterized as heterochromatic (Zhang et al., 2014). Targeted proteasomal degradation of p53 in endocycling cells functions as an additional mechanism to prevent apoptosis (Zhang et al., 2014). A model has been proposed based on experiments in the imaginal wing disc whereby the availability of CDK1 regulates the proapoptotic activity of p53. According to this model, mitotically active cells undergo apoptosis in response to DNA damage while endocycling cells that have down regulated CDK1 are unable to so (Ruiz-Losada et al., 2021). It is a striking and profound observation that endocycling cells do eventually succumb to developmentally programmed cell death during normal development. In particular, somatically polyploid salivary gland cells of third instar larvae which are recalcitrant to DNA damage pathways of programmed cell death, undergo developmentally programmed degradation via autophagy (Berry & Baehrecke, 2007).

### 1.4 Hindsight: General Background

The zinc finger transcription factor Hindsight (Hnt) consists of 14 putative $C_2H_2$ DNA binding motifs and is required for numerous developmental processes in *Drosophila melanogaster* (Yip et al., 1997; Wilk et al., 2000; Pickup et al., 2002). The expression of *hnt* has been identified in many embryonic tissues such as the midgut, peripheral nervous system, amnioserosa and tracheal system (Yip et al., 1997). *hnt* expression has also been reported in the crystal cells and eye imaginal discs of third instar larvae (Yip et al., 1997; Terriente-Felix et al., 2013). In the adult, Hnt is responsible for ovulation competency of follicles and has known roles in the establishment and maintenance of the adult intestinal stem cells (ISCs) (Baechler et al., 2015; Deady et al., 2017). Ras Responsive Element Binding protein 1 (RREB-1) is the human homolog of Hindsight and functions downstream of the small monomeric GTPase and proto-oncogene, RAS (Thiagalingam et al., 1996; Watzinger & Lion, 1999; Ming et al., 2013). RREB-1 has been linked to a multitude of human diseases including pancreatic cancer, leukemia, melanoma, and type II diabetes (Mahajan et al., 2014; Hui et al., 2019; Rahrmann et al., 2019; Yao et al., 2019). Interestingly, it has been recently discovered that the loss of a single copy of *RREB-1* in adult mice resembles a Noonan-like RASopathy syndrome (Kent et al., 2020). Individuals (humans) with Noonan syndrome and clinically related disorders may possess a wide variety of clinical features such as distinctive facial abnormalities, short stature, heart defects, and learning difficulties (Tartaglia et al., 2011).

### 1.5 String: General Background

String (Stg) is a Cdc25-type tyrosine phosphatase that functions as a dosage-dependent inducer of the G2 to M phase transition and is a Cdc2 kinase activator. In most mitotic cells, brief bursts of *stg* expression are responsible for triggering mitosis (Edgar & O'Farrell, 1989; Millar & Russell, 1992; Edgar et al., 1994). In the *Drosophila* embryo, the first 13 embryonic cell cycles are controlled by maternally expressed proteins (Rabinowitz, 1941; Edgar & O'Farrell, 1989). Maternal *stg* mRNA is degraded in early interphase 14 and by the end of interphase 14, zygotic *stg* mRNA accumulates, driving cells into mitosis 14, under the control of the zygotic genome. Zygotic *stg* expression subsequently determines the timing of the postblastoderm mitotic divisions (cell cycles 14-16) (Edgar & O'Farrell, 1989; Edgar & O'Farrell, 1990; Edgar et al., 1994).

### 1.6 Notch: General Background

Notch (N) is a transmembrane protein that functions as a receptor in an intracellular signalling pathway that shows a high degree of evolutionary conservation, being found in all kingdoms (Yamamoto et al., 2014; Vlachakis et al., 2020). When Notch physically interacts with one of its ligands (Serrate or Delta), a cleavage site is exposed, prompting proteolytic cleavage that results in the release of the Notch intracellular domain (NICD) from the membrane. The NICD can subsequently translocate to the nucleus where it will contribute to transcriptional regulation (Yamamoto et al., 2014). The main transcriptional effector of the Notch pathway in *Drosophila* is known as Suppressor of Hairless (Su(H)) (Schweisguth & Posakony, 1992). While N functions in a rather simple core pathway, it contributes to a

myriad of developmental processes, many of which seem diametrically opposed such as either promoting cellular differentiation or cell death. While in other circumstances, N signaling can promote cellular proliferation (Bray, 2006; 2016).

### 1.7 The connection between Hindsight, String and Notch

In several cases, *hnt* has been found to be expressed in a Notch-dependent manner (Sun & Deng, 2007; Krejci et al., 2009; Terriente-Felix et al., 2013). With regards to follicle cells, it has been suggested that *hnt* expression is upregulated by N signaling to induce the mitotic cycle/endocycle (M/E) transition by downregulating *cut* and *string* expression. Premature expression of Hnt is sufficient to promote early endocycle entry and Hnt loss of function mutants have delayed endocycle entry (Sun & Deng, 2007). As displayed in Figure 1.2, *stg* is also a putative direct target of N signaling and it has been proposed that *stg* is regulated simultaneously by N and Hnt in a feed-forward loop to generate a narrow window of Stg activity (Krejci et al., 2009). In support of this model, premature ectopic expression of Hnt in a model cell line for adult *Drosophila* myoblasts resulted in reduced mitotic activity, resembling the Notch knockdown phenotype. Additionally, this same study demonstrated that ectopic expression of Hnt is sufficient to inhibit a *stg* lacZ reporter *(*Krejci et al., 2009). Taken together, these experiments align with the interpretation that Hnt represses the expression of *stg* whose protein product is a positive regulator of the G2 to M phase transition (Edgar & O'Farrell, 1989), as outlined in the model shown in Figure 1.2.

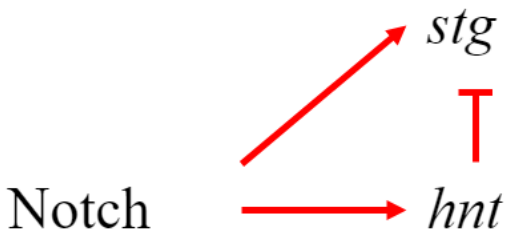



**Figure 1.2 Regulation of string expression by Notch and Hindsight.** Suggested feed-forward loop whereby Notch upregulates both *string* and *hnt* expression while the upregulation of *hnt* allows for its protein product to repress *stg*, creating a narrow window of Stg activity (Krejci et al., 2009).

### 1.8 Imaginal Tissue

*Drosophila* are holometabolous insects that undergo complete metamorphosis (Jindra, 2019; Truman & Riddiford, 2019). Collections of primarily diploid, undifferentiated cells undergo rapid proliferation as early as the second instar larval stage to displace apoptotic larval tissue with progenitor cells that will differentiate into adult (imago) tissue. Larval cells are distinguishable from the imaginal precursor cells because they do not proliferate after embryonic stage 5 and the larval nuclei become polytene (Curtiss & Heilig, 1995). There are 19 imaginal discs that are derived from invaginations of the embryonic epithelium and are not directly associated with the larval integument; therefore, they are considered excorporate (Curtiss & Heilig, 1995; Held, 2005). These imaginal precursor cell clusters are responsible for the external appendages such as the wings and eyes (Mandaravally, Madhavan & Schneiderman, 1977; Sato et al., 2008). In contrast, incorporate imaginal cells include those that are located within larval tissue which are arranged in nests or rings such as the precursors of the adult tracheal and digestive systems as well as the adult brain (Curtiss &

Heilig, 1995). As displayed in Figure 1.3, the imaginal rings, which are responsible for the adult digestive system are located in the salivary gland, foregut, and midgut/hindgut junction (Mandaravally, Madhavan & Schneiderman, 1977; Sato et al., 2008; Yang & Deng, 2018). At the posterior of the salivary gland imaginal ring (SGIR), a transition zone (TZ) has been described as a region where diploid imaginal ring cells and polyploid gland cells are juxtaposed (Yang et al., 2019). Such transition zones, being the junctions where two cell types meet, have been associated with tumour hotspots. These sites are likely to receive a variety of signaling cues from both tissue types, creating a unique microenvironment and a potential niche for stem cells to become dysregulated (Mcnairn & Guasch, 2011). Interestingly, in humans, 90% of cervical cancers are derived from TZ cells; in addition, squamous cell carcinoma of the eye is frequently derived at the limbus, a junction between the cornea and conjunctiva, another TZ (Burghardt & Ostör, 1983; McKelvie et al., 2002).

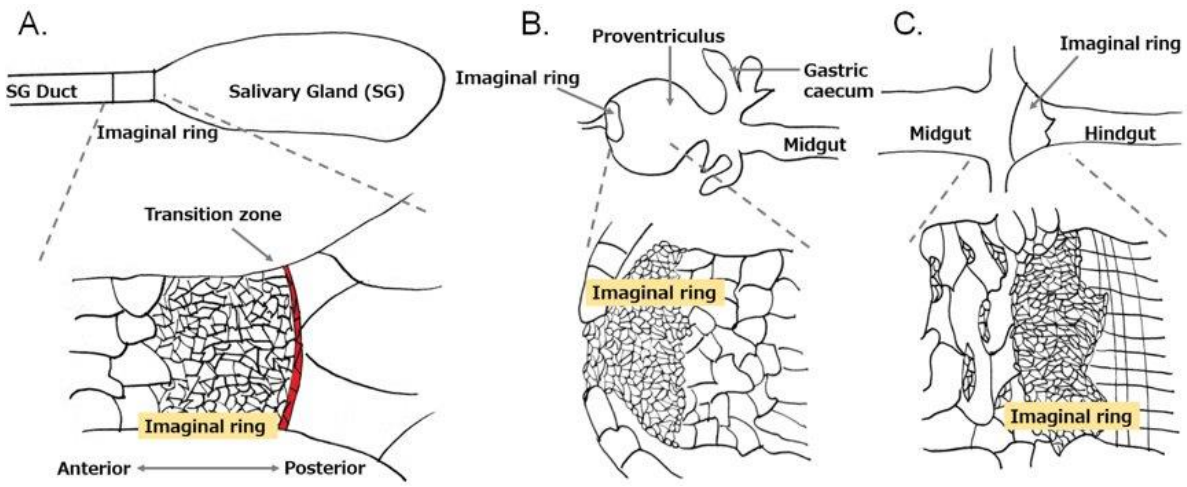



**Figure 1.3 Schematic Diagram of Drosophila Imaginal Rings.** (A) The salivary gland imaginal ring is located between the duct and gland itself and is a single layer of cells that are arranged in a cylindrical shape (B) The foregut imaginal ring is found in the proventriculus. (C) The hindgut imaginal ring is between the midgut and hindgut (Adapted from Yang & Deng 2018; Yang et al., 2019).

### 1.9 Notch-induced Tumour Model

Notch signalling is active in the salivary gland imaginal ring (SGIR), foregut imaginal ring and hindgut imaginal ring (HIR) of wild-type larvae and positively regulates the proliferation of these progenitor cells at the third instar larval stage (Yang & Deng, 2018). Of these three imaginal rings, the SGIR has been the most extensively investigated. It was found that persistent upregulation of Notch signalling by transgenic expression of a constitutively active form of N forces larvae into an extended larval state (ELS) and induces neoplastic transformation at the TZ of the SGIR. In contrast, the anterior region of the SGIR was considered a coldspot for this overproliferation. In previously published work, tumours that developed from the TZ were excised and transplanted into a host abdomen where they continued to grow and display metastatic behaviour, demonstrating what seems to be true

neoplastic transformation (Yang et al., 2019). In contrast, overproliferation in this previous study could only be induced in the HIR with certain GAL4 drivers and was not pursued as a topic of investigation. As for the foregut, overproliferation was never achieved via Notch upregulation, which perhaps demonstrates the high degree to which a particular cellular context responds to alterations in N signaling (Yang & Deng, 2018).

Further investigation of this tumour model located in the salivary gland led to the observation that during normal development, TZ cells are polyploid as they participate in endoreduplication. When N activation is upregulated, these polyploid cells re-enter mitosis via *stg* upregulation resulting in ploidy heterogeneity and aneuploidy, both of which contribute to tumour progression (Wang et al., 2021). This previously reported result has led to much speculation as to the contribution of polyploid mitosis in human oncogenesis (Coward & Harding, 2014; Pienta et al., 2021).

### 1.10 Research Goals and Objectives

The main objective of this research is to discern if Hnt plays a role in regulating cell proliferation and/or endocycle entry in the salivary gland and hindgut imaginal rings with typical Notch activity and when Notch is overexpressed in these two contexts. Additionally, it is also of interest to determine if there is any interaction of the cell cycle regulator *string* and Hnt.

# Chapter 2: Methods

## 2.1 Fly Stocks

All cultures were raised on standard *Drosophila* medium on a 12-hour light/dark cycle at 23˚C unless otherwise indicated. Standard *Drosophila* genetic crossing schemes were followed to create new stocks. Appendix A provides a list of all the genetic stocks (Table A.1.1) used and provides an outline of the crossing schemes utilized (Figure A.2.1 & A.2.2).

## 2.2 The GAL4/UAS System

GAL4 is a yeast transcription factor and powerful tool used by *Drosophila* geneticists in what is known as a bipartite system of inducible gene expression. GAL4 functions as a driver for any gene that is regulated by an enhancer element with a GAL4 binding site known as the Upstream Activating Sequence (UAS). The expression of the GAL4 driver can be temporally and spatially regulated by a tissue specific enhancer, thus placing the same constraints on any gene that is downstream of the UAS element. Without the presence of the GAL4 driver, the gene under control of a UAS-responder is transcriptionally silent. In addition to inducing ectopic expression of the gene of interest, RNA interference (RNAi)-mediated knockdown can be achieved by using a *UAS-RNAi* as the responder (Brand & Perrimon, 1993; Duffy, 2002).

### *2.2.1 retained-GAL4*

*retained (retn)* also known as *dead ringer,* encodes for a transcription factor that is part of the ARID-box family (Herrscher et al., 1995; Gregory et al., 1996). *retn-GAL4* expresses GAL4 under control of the DNA sequence in or near *retn* and was constructed as part of a collection of 7,000 transgenic lines to study the development of the adult central nervous system (Jenett et al., 2012). In addition to expression in the brain, *retn-GAL4* is expressed in the imaginal rings of larvae from the late second instar stage on (Yang & Deng, 2018).

### *2.2.2 Mmp1-GAL4*

*Matrix metalloproteinase 1 (Mmp1)* encodes for an enzyme that cleaves protein in the extracellular matrix (Matrisian, 1992). GAL4 is expressed under control of *Mmp1* regulatory sequences. The *Mmp1-GAL4* is part of a collection of ~1,000 transgenic lines that were randomly generated (Lee et al., 2018). *Mmp1-GAL4* was subsequently found to be expressed in the TZ of the SGIR (Wang et al., 2021).

## *2.3 NRE-EGFP*

*NRE-EGFP* is a transgenic construct that expresses EGFP under control of a Notch Response Element (NRE) and therefore, is a reporter for N signaling and is functional throughout many tissues during development. Knockdown of both N and Suppressor of Hairless (Su(H)) resulted in a loss of EGFP expression in tissues where N signaling is active (Saj et al., 2010). *NRE-EGFP* is expressed in each imaginal ring from first instar to late third instar (Yang & Deng, 2018).

### 2.4 *UAS-NICD* and *UAS-$N^{\Delta 34a}$* constructs

Two UAS lines that induce overactive Notch signaling were used in this research. Both constructs are constitutively active as they lack the Notch extracellular domain and therefore are ligand independent. The description for the *NICD* construct is described as *$Notch^{nucl}$* in (Fortini et al., 1993) and *$N^{\Delta 34a}$* is described as *$N^{\Delta E}$* in (Fuerstenberg & Giniger, 1998); for further detail see Discussion, section 5.1.

### 2.5 *UAS-hnt* lines

*1xUAS-peb, 5xUAS-peb* and *10xUAS-peb* constructs were developed by the Freeman lab to create transgenic lines that possess varying degrees of *hnt* expression based on the number of UAS sequences present (M. Freeman, personal communication, January 23, 2018). These stocks were originally identified as *UAS-peb* lines, however, throughout this document they will be referred to as *UAS-hnt* lines (*1xUAS-hnt, 5xUAS-hnt, 10xUAS-hnt*) for simplicity. These unpublished stocks were gifted by the Freeman lab of the Vollum Institute at Oregon Health & Science University.

### 2.6 Fluorescent Reporter System

To visualize and image the results of experiments, a fluorescent reporter system was created using *GAL4>$Cherry^{nls}$* and *Histone2Av-GFP* (*His2Av-GFP*) to identify GAL4-expressing cells and all nuclei, respectively. The crossing scheme for this system is outlined in Appendix Figure A.2.2.

## 2.7 Anti-Hindsight Immunostaining

Salivary glands and hindguts of third instar larvae were dissected in a phosphate-buffered saline (PBS) solution then fixed in 3.7% formalin in PBS for 20 minutes. Larvae were rinsed in PBS solution 3 times before being washed for 3x 10 minutes in PBT (PBS + 0.1% Triton X-100 + 2.5% BSA) solution. Following the washes, larvae were transferred to a blocking solution containing 5% Normal Goat Serum (NGS) and PBT for 40 minutes. Upon removal of the blocking solution, larvae were incubated overnight at 4˚C in primary antibody, NGS and PBT. The following day, larvae were washed with PBT for 3x 10 minutes and again blocked for a 40-minute period in NGS and PBT. Larvae were then placed in a tube wrapped in foil to prevent light exposure and were incubated overnight at 4˚C contained in a solution that contained fluorescently labelled secondary antibody, NGS as well as PBT. After overnight incubation, larvae were washed in PBT 3x for 10 minutes and then rinsed with PBS 3 times. Larvae were then transferred through a glycerol series (25%, 50%, 75%) and finally added to a 70% glycerol/2.5% (w/v) DABCO. Dissected tissue was mounted on a microscope slide and viewed using confocal microscopy (details below).

With respect to the *NRE-EGFP* anti-Hnt immunostaining, alterations were made to the protocol in order to enhance antibody signal and will be identified from now on as "Enhanced anti-Hnt immunostaining". Modified blocking solution consisted of: 50mM of glycine, 0.05% Tween 20, 0.1% Triton X-100, 0.1% BSA and 2% NGS. Antibody incubation solution was made of: 10mM of glycine, 0.1% Triton X-100, 0.05% Tween-20, 0.1% hydrogen peroxide ($H_2O_2$) and antibody. After both overnight incubations larvae were

washed in a PBS + 0.05% Tween 20 solution instead of PBT solution (Adapted from Rosas-Arellano et al., 2016).

The primary antibody, mouse monoclonal anti-Hindsight (Hnt) 27B8 1G9 was used at a dilution of 1:10 (Developmental Studies Hybridoma Bank) and the secondary antibody, TRITC-conjugated goat anti-mouse, was utilized at a dilution of 1:200 (Jackson Immunoresearch).

### 2.8 Rearing Protocol for Larvae with Overactive Notch Signaling

To prevent comparing larvae that were in various stages of a Notch-induced extended larval state (ELS), *Drosophila* crosses were set up for an overnight embryo collection and adults were removed the following day. Overnight embryo collections were performed for the following experiments: *retn>NICD, retn>*$N^{\Delta 34a}$*, retn>*$N^{\Delta 34a}$*+1xUAS-hnt, Mmp1>NICD* and *Mmp1>*$N^{\Delta 34a}$. Unless otherwise stated, all third instar larvae were imaged 7 days after cross initiation which is the first day that wandering third instar larvae appear in the culture (day 7). This ensured that third instar larvae could be confidently compared to other experiments without concern for larvae differing in their stage of ELS. Refer to Appendix A.3 for justification of this strict protocol.

## 2.9 Mosaic Analysis

To induce mitotic recombination in the salivary gland and obtain *His2Av-GFP/His2Av-RFP* twin spots, heat shock inducible FLP-FRT recombinase was used (Golic & Lindquist, 1989; Golic, 1991; Chou & Perrimon, 1992). The Reed Lab Stock Collection (RLSC) # 610 stock was used as a source of fluorescent markers to identify twin spots and is fully described as *y w P{w[+mC]=His2Av[T: Avic\GFP-S65T]}1 P{ry[+t7.2]=hsFLP}122 P{ry[+t7.2]=neoFRT}19A; P{w[+mC]=His2Av-mRFP1}III.1/TM6B, Tb.* Mutant clones were generated by crossing males of the previously described stock with virgin females of the Reed Lab Stock Collection (RLSC) # 1295 that are heterozygous for the loss of function $hnt^{345x}$ allele (Farley et al., 2018) which is located on the X chromosome (Gramates et al., 2022). Control clones were generated by crossing males of RLSC # 610 with virgin females of RLSC # 1300, which possess an X chromosome that is isogenic to RLSC # 1295 (Farley et al., 2018). Homozygous mutant cells were identified as those expressing *His2Av-RFP* only and associated twin spots were cells that lack RFP and possess two copies of *His2Av-GFP*. Both control and mutant vials were cleared one day after cross initiation (day 0) and heat shocked at 37˚C with 30-minute rest periods as follows: day 2, 2x45mins; day 6, 2x60mins; day 7 1x60mins. Otherwise, vials were maintained at 25˚C. Heat shocks early in development are more likely to yield larger clones than heat shocks later in development (Struhl & Basler, 1993).

### 2.10 Confocal Microscopy

Third instar larvae were dissected in halocarbon oil on microscope slides and imaged using a Nikon Eclipse 90i microscope equipped with a Nikon D eclipse C1 Scan head using a 20x objective. Z stacks of salivary gland and hindgut imaginal rings were processed by 2.00 µm slices with Nikon EZ-C1 software. All cultures that were not immunostained, spent a minimum of 24 hours at 29˚C, the optimal temperature for the GAL4/UAS system, prior to dissection (Duffy, 2002).

### 2.11 Cell Counts

Projections of Z stacks for quantitative analysis of SGIR images were made only using the top half of the Z stack in order to prevent inaccurate cell counts of what is a side view of a three-dimensional ring. ImageJ was then used to count cells via fluorescently labeled nuclei (Schneider et al., 2012). With respect to the mosaic analysis conducted in section 3.8, cell counts were performed blind to prevent bias.

### 2.12 Quantitative Analysis

To quantitate the results in sections 3.5, 3.7, and 3.8 cell counts were conducted as described in section 2.11. Microsoft Excel was then used to perform Student T-Tests (=T.TEST; two-tailed, two sample unequal variance test with inclusive median) and also to create box and whisker plots.

# Chapter 3: *hnt* function is implicated in cell cycle regulation and when overexpressed is capable of suppressing Notch tumourigenesis in the salivary gland imaginal ring

## 3.1 Confirmation of *retn* and *Mmp1* expression patterns for use as GAL4 drivers

Previously published work by the Deng lab utilized both *retn-GAL4* and *Mmp1-GAL4* to drive Notch-induced tumour development in the SGIR (Yang & Deng, 2018; Yang et al., 2019; Wang et al., 2021). To confirm the expression pattern and therefore the usefulness of these GAL4 drivers, confocal microscopy was used to observe *retn-GAL4>Cherry*$^{nls}$ and *Mmp1-GAL4>Cherry*$^{nls}$ expression in the SGIR's of dissected third instar larvae. *His2Av-GFP* was used to label all nuclei and allowed for the visualization of the entire imaginal ring. As shown in Figure 3.1A-A", *retn>Cherry*$^{nls}$ is expressed in the SGIR as a gradient from posterior to anterior. The most anterior cells of the SGIR do not express *retn>Cherry*$^{nls}$. In contrast, *Mmp1>Cherry*$^{nls}$ expression is restricted to the most posterior row of cells in the SGIR (Fig 3.1B-B"). These *Mmp1*-expressing cells are also those that express *retn* the strongest and have been identified as a transition zone (TZ) (Yang et al., 2019).

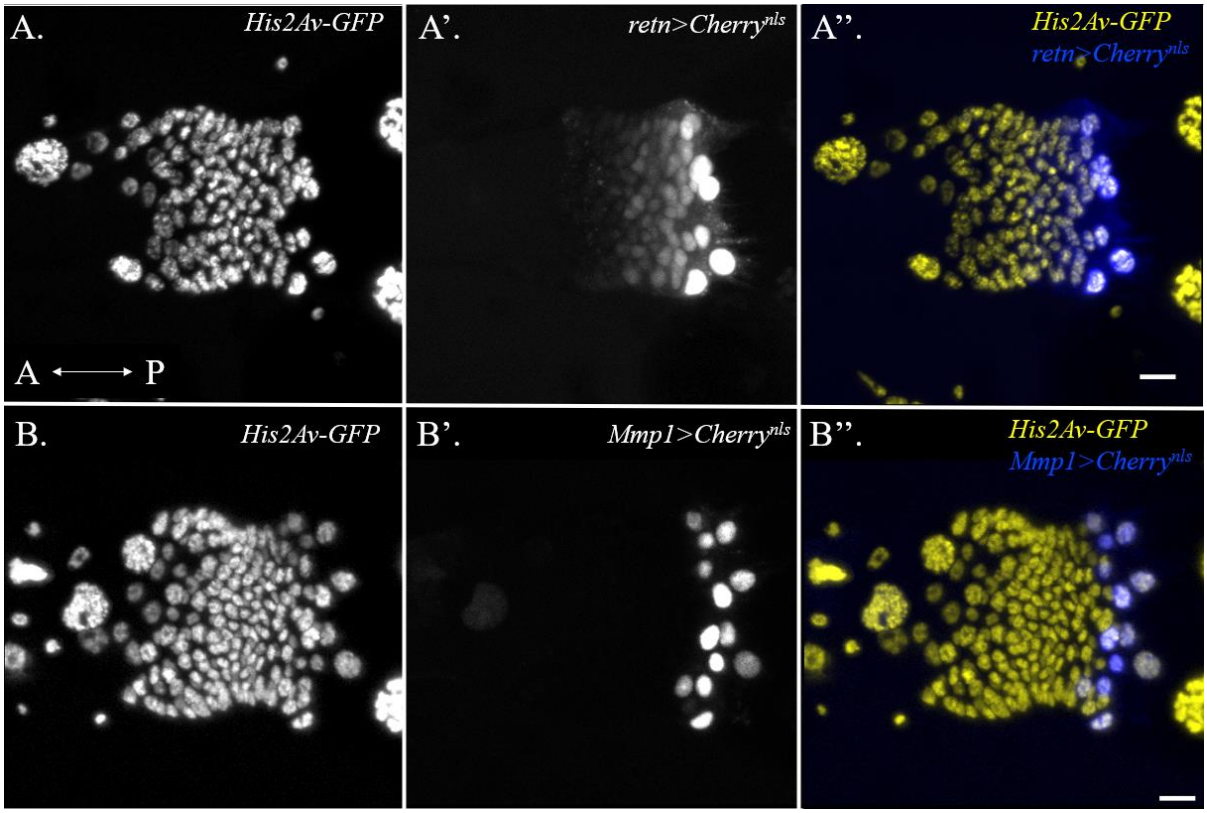



**Figure 3.1 *retn* and *Mmp1* GAL4 drivers are differentially expressed in the SGIR.** (A-A") *retn>Cherry*$^{nls}$ displays a gradient of expression in the SGIR, peaking in the posterior region. (B-B") *Mmp1>Cherry*$^{nls}$ expression is confined to the most posterior row of cells in the SGIR. *His2Av-GFP* was utilized as background to identify all nuclei. SGIRs are oriented in the same manner with anterior to the left. Scale bar: 10µm.

### 3.2 Overproliferation phenotype due to overactive Notch signaling is reproducible with *UAS-$N^{\Delta 34a}$*

Two UAS lines that cause overactive Notch signaling were used to induce overproliferation in the SGIR. *UAS-NICD* has been previously reported to induce tumour development in the SGIR of third instar larvae with *retn* and *Mmp1* GAL4 drivers. Additionally, overactive Notch signaling via *UAS-NICD* resulted in prolonged larval development and a giant larvae phenotype (Yang & Deng, 2018; Yang et al., 2019; Wang et al., 2021). These experiments were replicated and SGIRs of late third instar larvae that did not enter an extended larval state (ELS) (day 7) were dissected. Figure 3.2B-B" presents a representative image of the overproliferation phenotype of *retn>NICD.* An expansion of the posterior SGIR was evident as the total number of cells drastically increased. In contrast, *Mmp1>NICD* SGIRs failed to produce an overt phenotype without an ELS, replicating the previously reported results from (Wang et al., 2021) (Fig.3.3B-B"). Additionally, the degree of proliferation induced by *Mmp1>$N^{\Delta 34a}$* and *retn>UAS-$N^{\Delta 34a}$* was also investigated. While *retn>UAS-$N^{\Delta 34a}$* possessed an overproliferation phenotype similar to that of *retn>NICD,* (Fig. 3.2C-C" *cf.* Fig. 3.2B-B") *Mmp1>$N^{\Delta 34a}$* displayed a more protrusive phenotype in comparison to *Mmp1>NICD* (Fig. 3.3C-C" *cf.* Fig. 3.3B-B"). Day 7 *Mmp1> $N^{\Delta 34a}$* SGIRs contained more *Mmp1*-expressing cells that were larger in size when compared to both the control and *Mmp1>NICD* (Fig. 3.3).

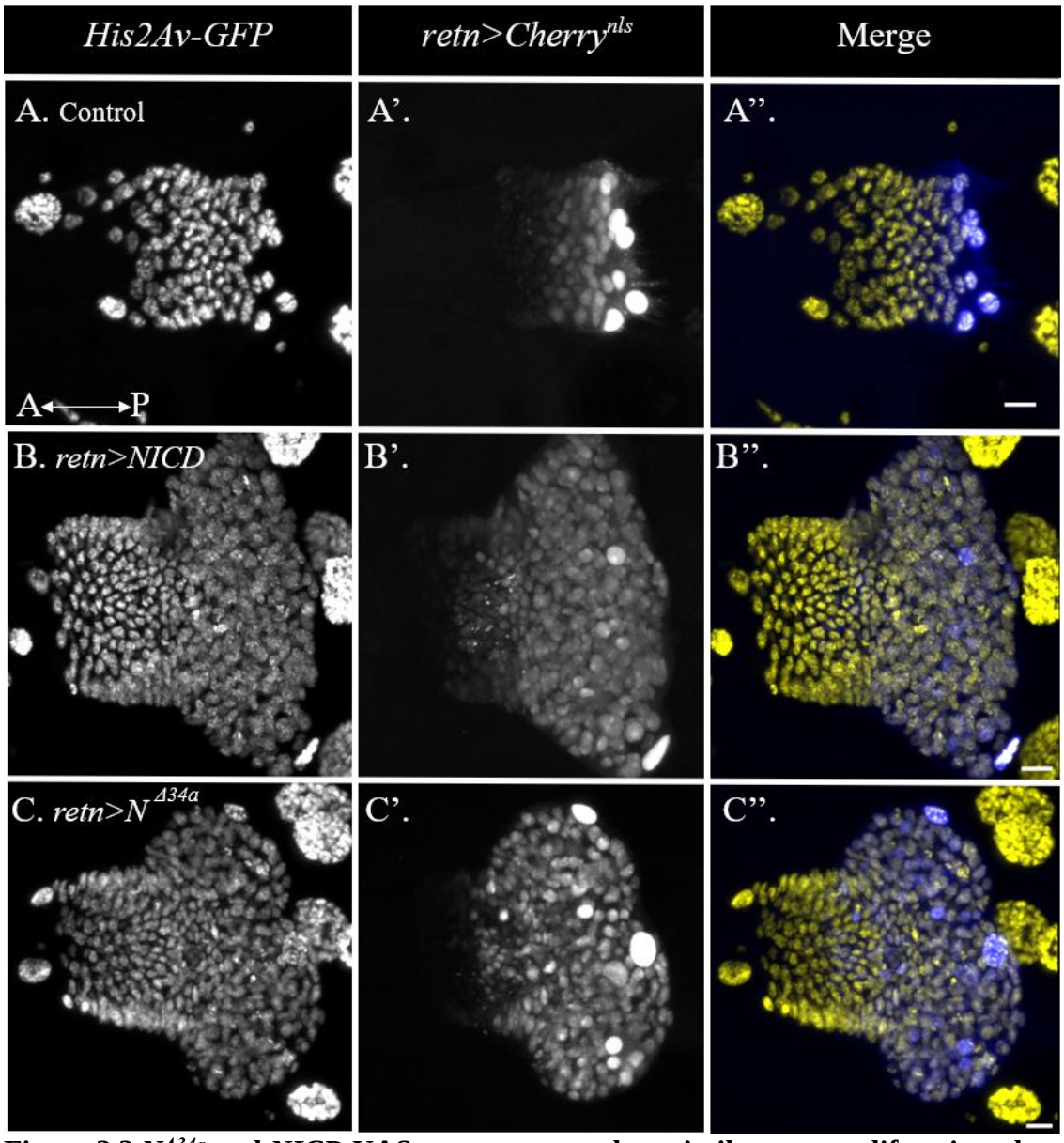



**Figure 3.2 $N^{\Delta 34a}$ and *NICD* UAS constructs produce similar overproliferation phenotype with *retn-GAL4*.** (A-A") Control SGIR to indicate typical cell population and morphology. (B-B", C-C") Representative images of SGIRs dissected from third instar larvae of an overnight collection (day 7). Both (B-B", C-C") show dramatic overproliferation and an expansion of the posterior region of the SGIR. *His2Av-GFP* was utilized as background to identify all nuclei. SGIRs are oriented in the same manner with anterior to the left. Scale bar: 10μm.

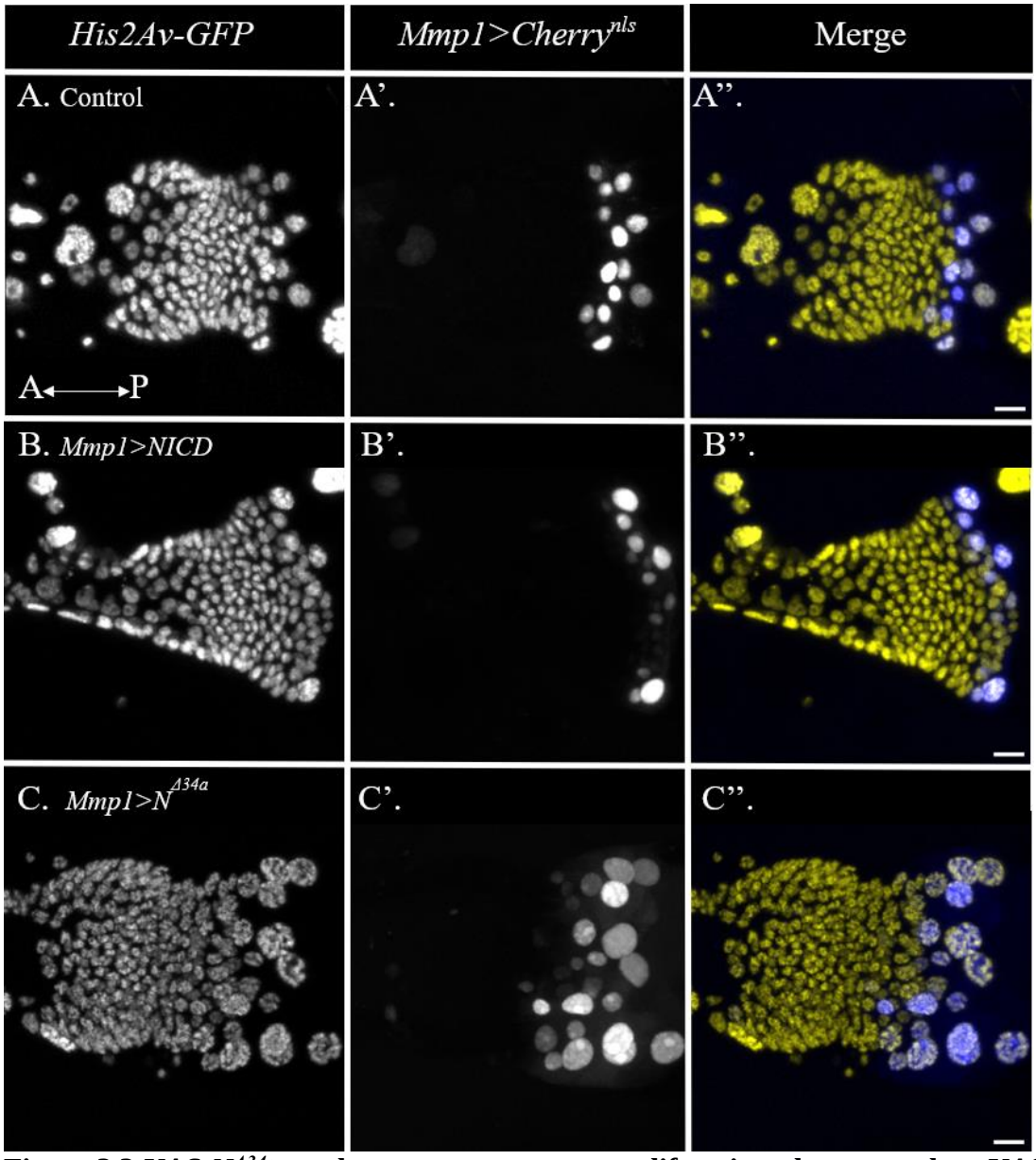



**Figure 3.3 *UAS-N$^{\Delta 34a}$* produces a stronger overproliferation phenotype than *UAS-NICD* in *Mmp1*-expressing cells.** (A-A") Control SGIR to indicate typical cell population and morphology. (B-B", C-C") Representative images of SGIRs dissected from third instar larvae of an overnight collection (day 7). (B-B") *Mmp1>NICD* fails to produce an overt phenotype with respect to the size of nuclei. (C-C") *Mmp1>N$^{\Delta 34a}$* results in many large *Mmp1*-expressing cells. *His2Av-GFP* was utilized as background to identify all nuclei. SGIRs are oriented in the same manner with anterior to the left. Scale bar: 10µm.

### 3.3 Hnt is expressed in the most posterior cells of the SGIR

In order to investigate the influence of Hindsight (Hnt) on the Notch-induced tumour model, it was first necessary to characterize the expression pattern of endogenous Hnt in the SGIR. Hnt expression has been previously reported in the SGIR of late third instar larvae using anti-Hnt immunohistochemical staining (Ming et al., 2013). Anti-Hnt immunostaining was performed on third instar larvae that expressed *UAS-GFP$^{nls}$* driven by *retn-GAL4* which allowed for the identification of the SGIR. As shown in Figure 3.4A-A", Hnt is only weakly expressed in the TZ of the SGIR as indicated by the co-expression of anti-Hnt immunostaining and *retn-GAL4>GFP$^{nls}$*. Hnt expression is dynamic in the salivary gland of third instar larvae and this accounts for the variable expression in the polytene gland cells of the anterior region of the salivary gland, shown posterior to the SGIR (Ming et al., 2013).

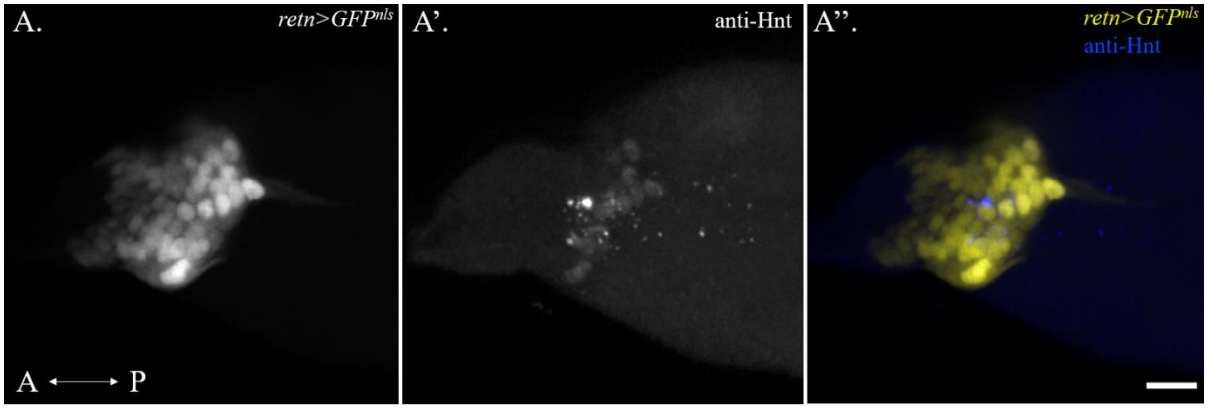



**Figure 3.4 Hnt is expressed in the salivary gland imaginal rings.** (A) *retn-GAL4* drives expression of *UAS-GFP$^{nls}$* in a gradient, greatest in the posterior of the SGIR. (A') Anti-Hnt immunostaining of the salivary gland indicates weak expression of Hnt in the most posterior region of the imaginal ring. Lack of Hnt expression in anterior polytene gland cells is due to dynamic expression of Hnt. (A'') Hnt positive cells that express *GFP$^{nls}$* are part of the imaginal ring. SGIR is oriented with anterior to the left. Scale bar: 10µm.

### 3.4 Hnt-expressing cells of the SGIR have reduced Notch signaling

It has been demonstrated that Notch signaling is active in the SGIR, with highest activity in the middle region (Yang & Deng, 2018). However, the level of Notch activity in relation to the expression of Hnt has not been ascertained in this context. To discern this relationship, enhanced anti-Hnt immunostaining was performed on third instar larvae that express GFP when Notch signaling is active via *NRE-EGFP.* Figure 3.5 displayed apparent Hnt expression in the TZ while Notch activity was minimal. Notch activity was highest in the middle section of the SGIR and diminishes towards the anterior and posterior (Fig. 3.5A), aligning with previous reports (Yang & Deng, 2018). The polytene cells of the salivary gland were positive for Hnt but did not have *NRE-EGFP* expression (Fig 3.5). To confirm that Notch activity is minimal in the TZ where Hnt is expressed, SGIRs of third instar larvae with *NRE-EGFP; retn>Cherry*$^{nls}$ were examined. Again, minimal Notch activity was observed in the TZ which was identifiable by the strongest *retn* expressing cells (Fig 3.6).

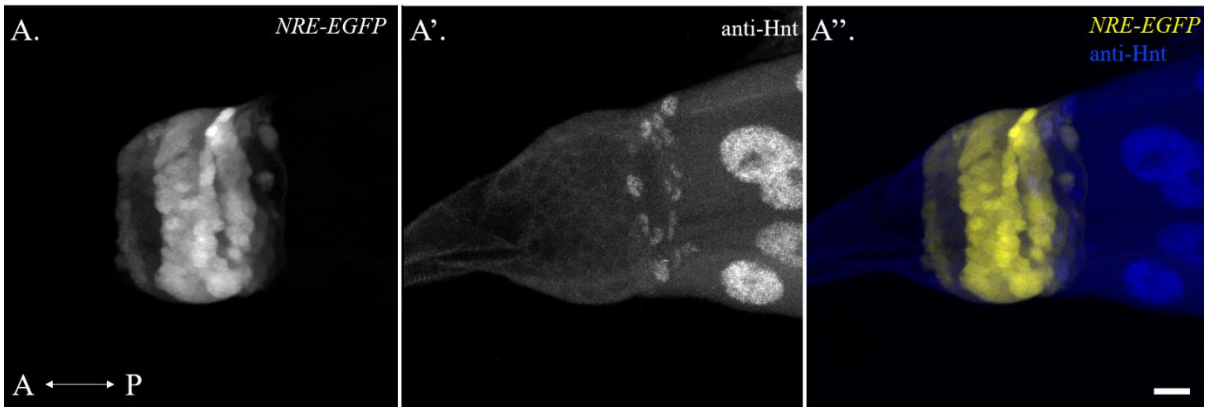



**Figure 3.5 Hnt expressing cells in the SGIR have minimal Notch signaling.** (A) *NRE-EGFP* has high activation in the middle of the SGIR and diminishes towards the anterior and posterior. (A') Enhanced anti-Hnt immunostaining of the salivary gland indicates weak expression of Hnt in the TZ and is expressed in polytene gland cells. (A'') Hindsight positive cells display little to no *NRE-EGFP* indicating low levels of Notch activity in these cells. SGIR is oriented with anterior to the left. Scale bar: 10µm.

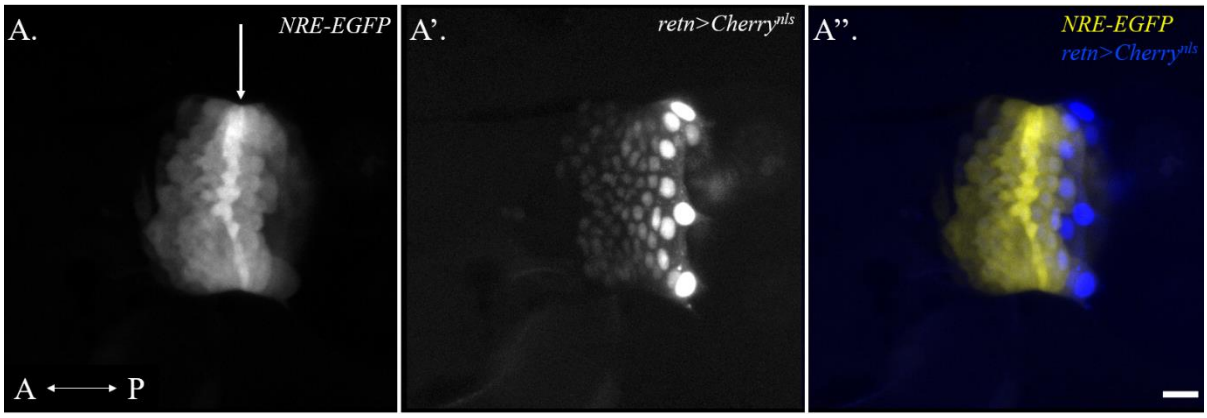



**Figure 3.6 Minimal Notch Signaling is detected in the SGIR Transition Zone.** (A) *NRE-EGFP* has high activation in the middle of the SGIR as indicated by the white arrow and diminishes towards the anterior and posterior. (A') *retn-GAL4* drives expression of *UAS-Cherry$^{nls}$* in a gradient, greatest in the posterior of the SGIR. (A'') Little to no Notch activity is observed in the TZ as evaluated by *NRE-EGFP*. SGIR is oriented with anterior to the left. Scale bar: 10µm.

### 3.5 Hnt-expressing cells are not mitotically active in the SGIR

It has been previously established (this study) that the TZ, which is identifiable as the cells of the SGIR that express *Mmp1*, is associated with weak Hnt expression (Fig. 3.4). The TZ cells have been classified as polyploid and undergo at least one endoreplication cycle during normal development and typically have an 8C or 16C value (Wang et al., 2021). To corroborate this statement and to ensure these TZ cells are not mitotically active, experiments with *UAS-cdc2-RNAi* were performed with *Mmp1-GAL4*, to target only Hnt positive cells, as well as *retn-GAL4*, to target the majority of imaginal ring cells. Cdc2, (cell division control 2) is a G2 to M phase inducer that requires dephosphorylation by String (Hayashi, 1996; Edgar & O'Farrell, 1989; Millar & Russell, 1992; Edgar et al., 1994). In third instar *cdc2* mutant larvae, certain diploid tissues are reduced in size and the cells appear larger because they enter the endocycle (Hayashi, 1996). *UAS-cdc2-RNAi* has also been reported to halt cell divisions (Somma et al., 2008), making it an excellent candidate for identifying the extent of mitotic activity between Hnt positive cells and the other cells of the imaginal rings. Cell counts were performed on the SGIRs of both *retn>cdc2-RNAi* and *Mmp1>cdc2-RNAi* (Fig. 3.7). In contrast to *retn>cdc2-RNAi* which had a statistically significant reduction in the overall number of SGIR cells, *Mmp1>cdc2-RNAi* was not sufficient to reduce the typical imaginal cell population (Table 3.1).

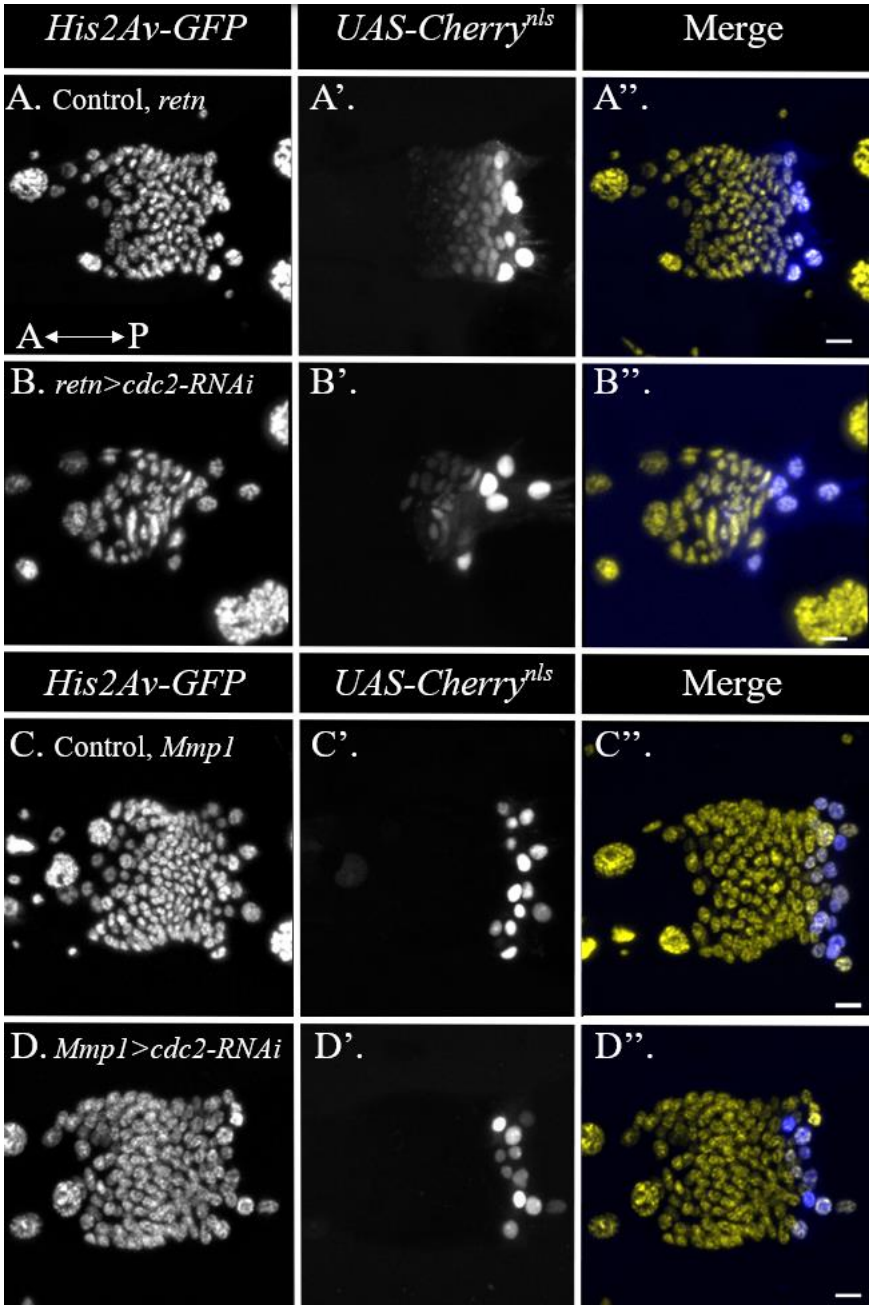



**Figure 3.7 *Mmp1*-expressing cells do not contribute to total cell population of SGIR.** (A-A") Representative control SGIR of *retn>UAS-Cherry*$^{nls}$ without *cdc2-RNAi.* (C-C") Representative control SGIR of *Mmp1>UAS-Cherry*$^{nls}$ without *cdc2-RNAi.* Knockdown of *Cdc2* is mediated by RNAi in *retn* (B-B") and *Mmp1*-expressing cells (D-D"). (B-B") Displays a severe reduction in the overall number of SGIR cells in comparison to the control (A-A"). (D-D") Lacks a discernable phenotype upon comparison to (C-C"). *His2Av-GFP* was utilized as background to identify all nuclei. SGIRs are oriented in the same manner with anterior to the left. Scale bar: 10μm.

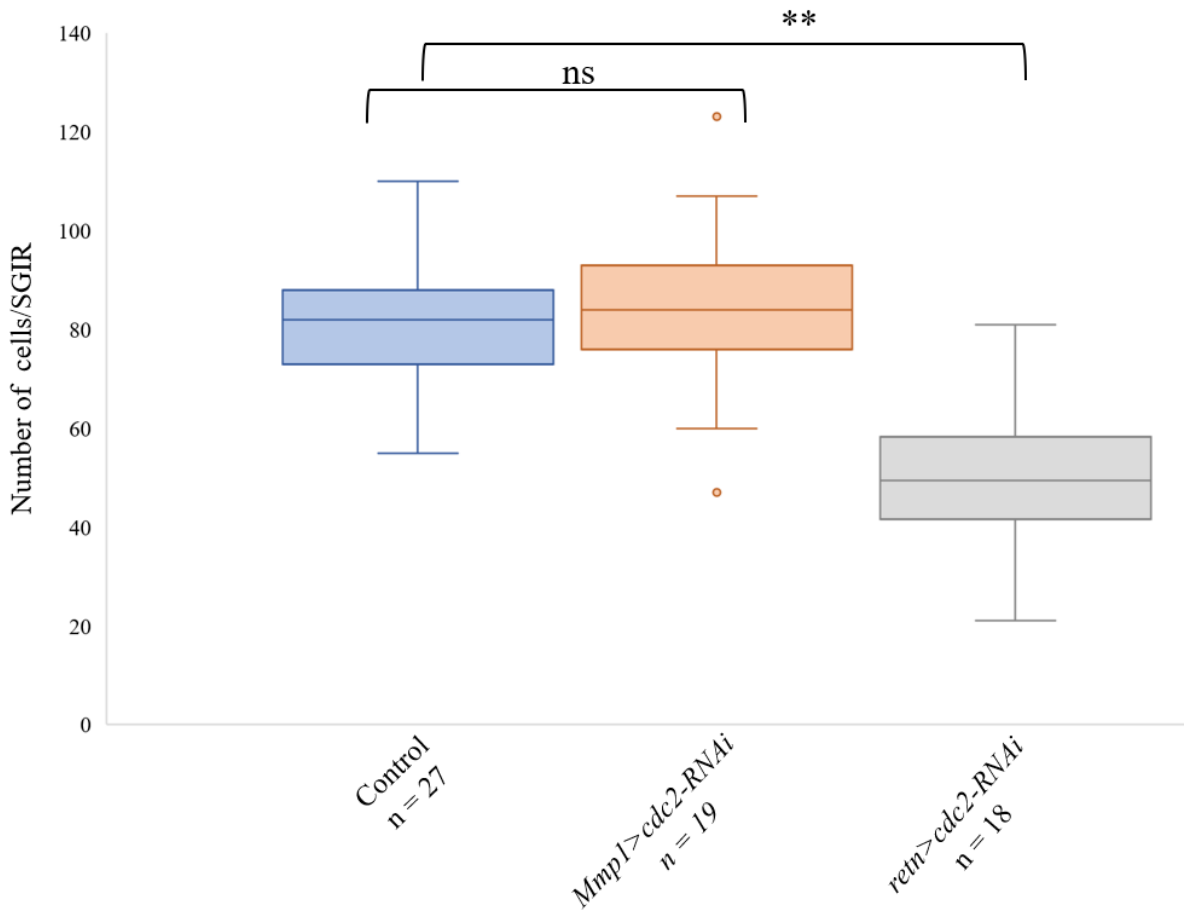



**Table 3.1 Quantitative analysis indicates *Mmp1*-expressing cells do not contribute to total cell population of SGIR.** Box and whisker plot diagram displays the difference in SGIR cell counts between control, *Mmp1>cdc2-RNAi* and *retn>cdc2-RNAi*. Only *retn-cdc2-RNAi* was found to have a statistically significant reduction in the number of cells/SGIR when compared to the control. **, $p<0.005$; ns, not significant; n = number of SGIRs. The median value is indicated by the horizontal line in each box. Whiskers indicate the minimum and maximum values of the data set that are not considered outliers. Outliers are indicated by the circles beyond the whiskers.

### 3.6 Overexpression of Hnt alters cell number and morphology in SGIR

Hnt has been implicated as a regulator of the mitotic/endocycle (M/E) switch in follicle cells of the adult ovary. Ectopic *hnt* expression in these follicle cells forced them into premature endocycle entry (Sun & Deng, 2007). To test the effect of *hnt* overexpression in the SGIR, *retn-GAL4* was used to drive *UAS-hnt* lines with varying degrees of expression. While *1xUAS-hnt* (Fig. 3.8B) failed to produce an overt phenotype, both *5xUAS-hnt* (Fig. 3.8C) and *10xUAS-hnt* (Fig. 3.8D) lines displayed a reduction in cell number, large nuclei, and disorganization of the tissue. An intriguing characteristic of the *hnt* overexpression phenotype was the production of darkly pigmented deposits, suggestive of melanin that were visible using Differential Interference Contrast (DIC) microscopy for *retn>5xUAS-hnt* (Fig. 3.8E) as well as *retn>10xUAS-hnt* (not shown).

To confirm that the reduction in cell number is due to fewer cell divisions and not cell death associated with activation of effector caspases, *Drosophila* stocks were created that co-express each of the *UAS-hnt* lines with *UAS-p35*. p35 is an inhibitor of effector caspases and therefore, prevents cell death executed by effector caspases when expressed in a given tissue (Hay et al., 1994; Zoog et al., 2002). As evident in Figure 3.9B-B", the expression of *p35* in the SGIR does not exhibit a phenotype that is distinct from the control (Fig. 3.9A-A"). Moreover, co-expression of *p35* with *5xUAS-hnt* and *10xUAS-hnt* failed to rescue the *retn>UAS-hnt* phenotypes (only *retn>5xUAS-hnt* shown, Fig. 3.9C-C", D-D").

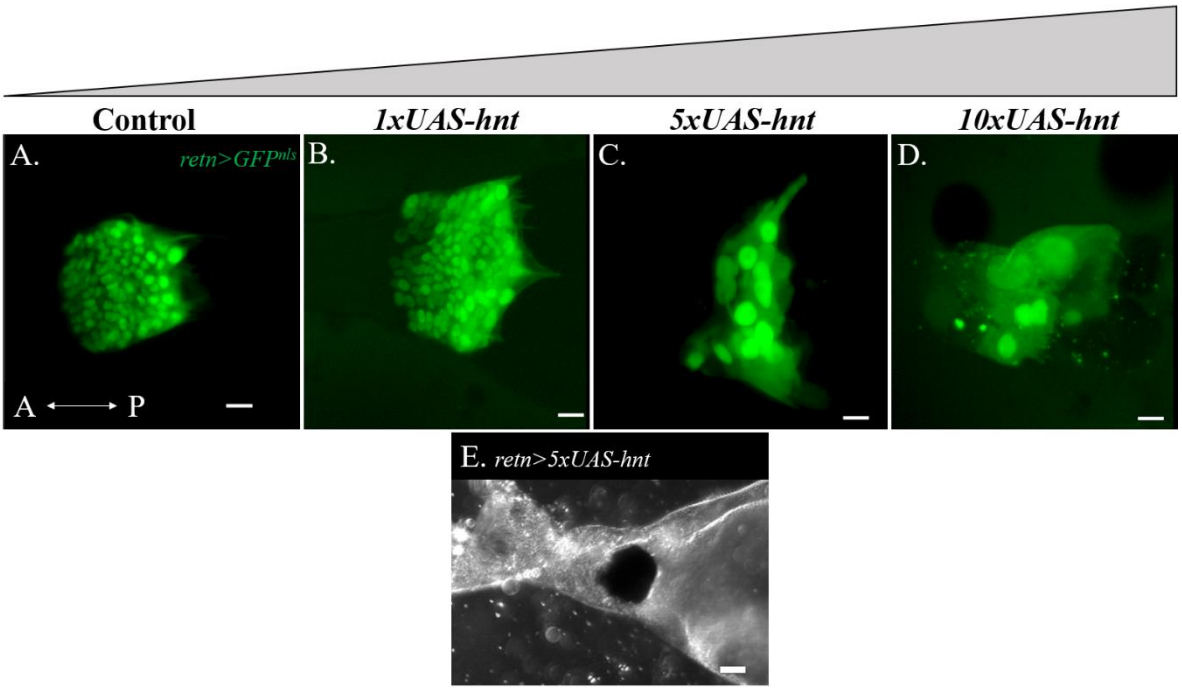



**Figure 3.8 *hnt* overexpression alters cell number and morphology in SGIR.** As the level of *hnt* expression increases, so does the severity of the phenotype. (A) Represents the control phenotype of the SGIR with *retn>GFP*$^{nls}$. Increasing *hnt* in *retn*-expressing cells via *UAS-hnt* constructs results in a reduction of the number of cells, large nuclei, and disorganization of the tissue as evident in (C & D) whereas *1xUAS-hnt* fails to produce an overt phenotype (B). *(*A-D) Scale bar: 10µm. (E) DIC image of *retn>5xUAS-hnt* possesses an accumulation of dark pigment. Scale bar: 20µm. Imaginal rings are oriented in the same manner with anterior to the left.

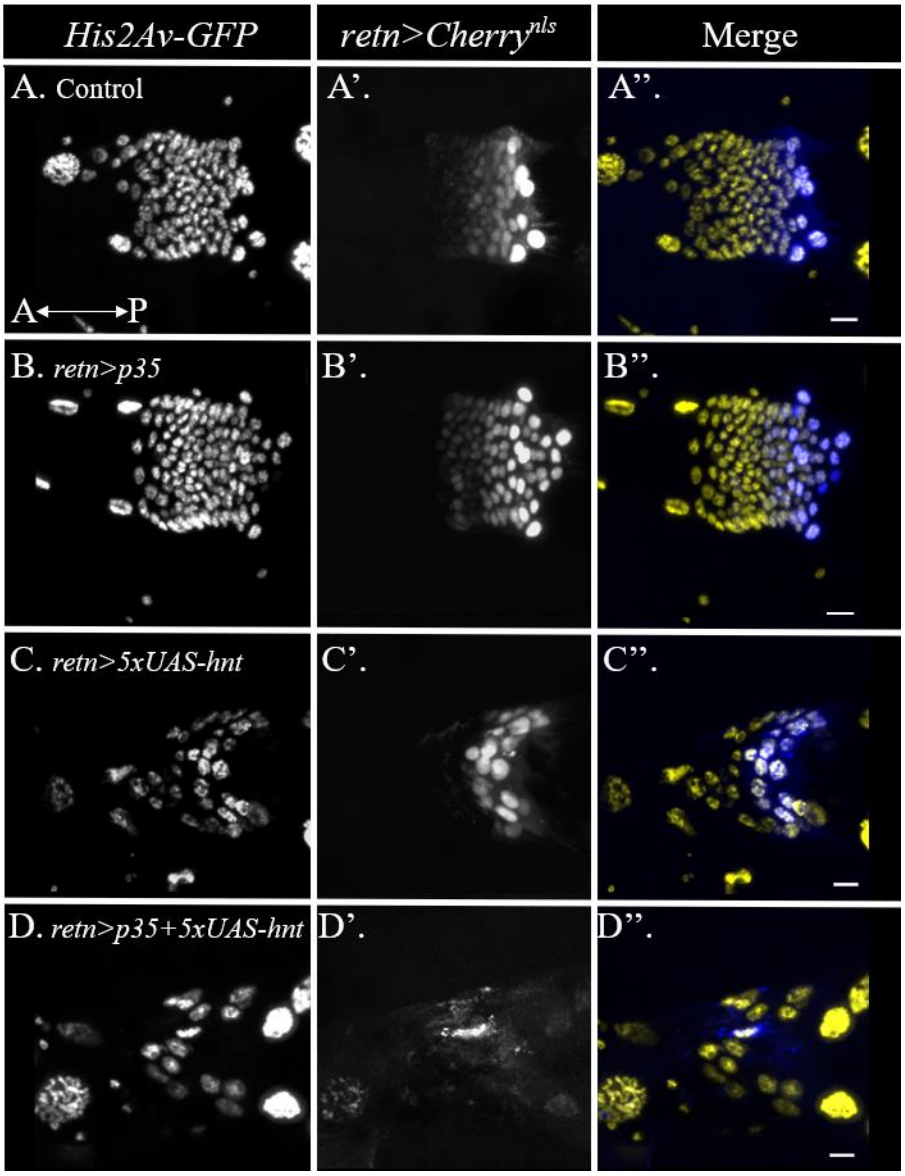



**Figure 3.9 Cell death executed by effector caspases is not responsible for the *hnt* overexpression phenotype in the SGIR.** (A-A") *retn>GFP*$^{nls}$ control SGIR for reference. (B-B") Expression of *p35* via *retn-GAL4* fails to produce an overt phenotype in the SGIR. (C-C") *retn>5xUAS-hnt* results in a decrease in the total number of SGIR cells. (D-D") *retn>p35+5xUAS-hnt* does not rescue the *5xUAS-hnt* phenotype (C-C"). *His2Av-GFP* was utilized as background to identify all nuclei. SGIRs are oriented in the same manner with anterior to the left. Scale bar: 10µm.

### 3.7 Mosaic analysis indicates that the presence of *hnt*$^{345x}$ mutant cells increases the SGIR cell population

While the results in section 3.6 demonstrated that the overexpression of *hnt* leads to a decrease in the number of cells, it is also necessary to observe the effect of *hnt* loss of function in the SGIR. Since the *hnt*$^{345x}$ loss of function allele is embryonic lethal (Farley et al., 2018) the technique of somatic recombination was used to recover larvae whose mitotically active tissues are genetic mosaics for *hnt* (i.e., *hnt* $^{-}$/+ with patches of +/+ and *hnt* $^{-}$/*hnt* $^{-}$, known as twin spots). Mosaic SGIRs for *hnt*$^{345x}$ were created by inducing mitotic recombination with a heat-shock inducible FLP recombinase (Farley et al., 2018). In Figure 3.10B, clones that are RFP$^{+}$/GFP$^{-}$ are homozygous for *hnt*$^{345x}$, while clones that are RFP$^{-}$/GFP$^{+}$ are homozygous for *hnt*$^{+}$. Cells that co-express *His2Av-RFP* and *His2Av-GFP* (RFP$^{+}$/GFP$^{+}$) did not undergo mitotic recombination. Blind cell counts for both control and *hnt*$^{345x}$ SGIRs were performed and indicate that *hnt*$^{345x}$ mosaic SGIRs have significantly more cells than control SGIRs (Table 3.2). However, the percentage of RFP$^{+}$/GFP$^{-}$ cells (which are *hnt* $^{-}$/*hnt* $^{-}$) between experiment and control SGIRs was not statistically significant (Appendix Table B.1.2).

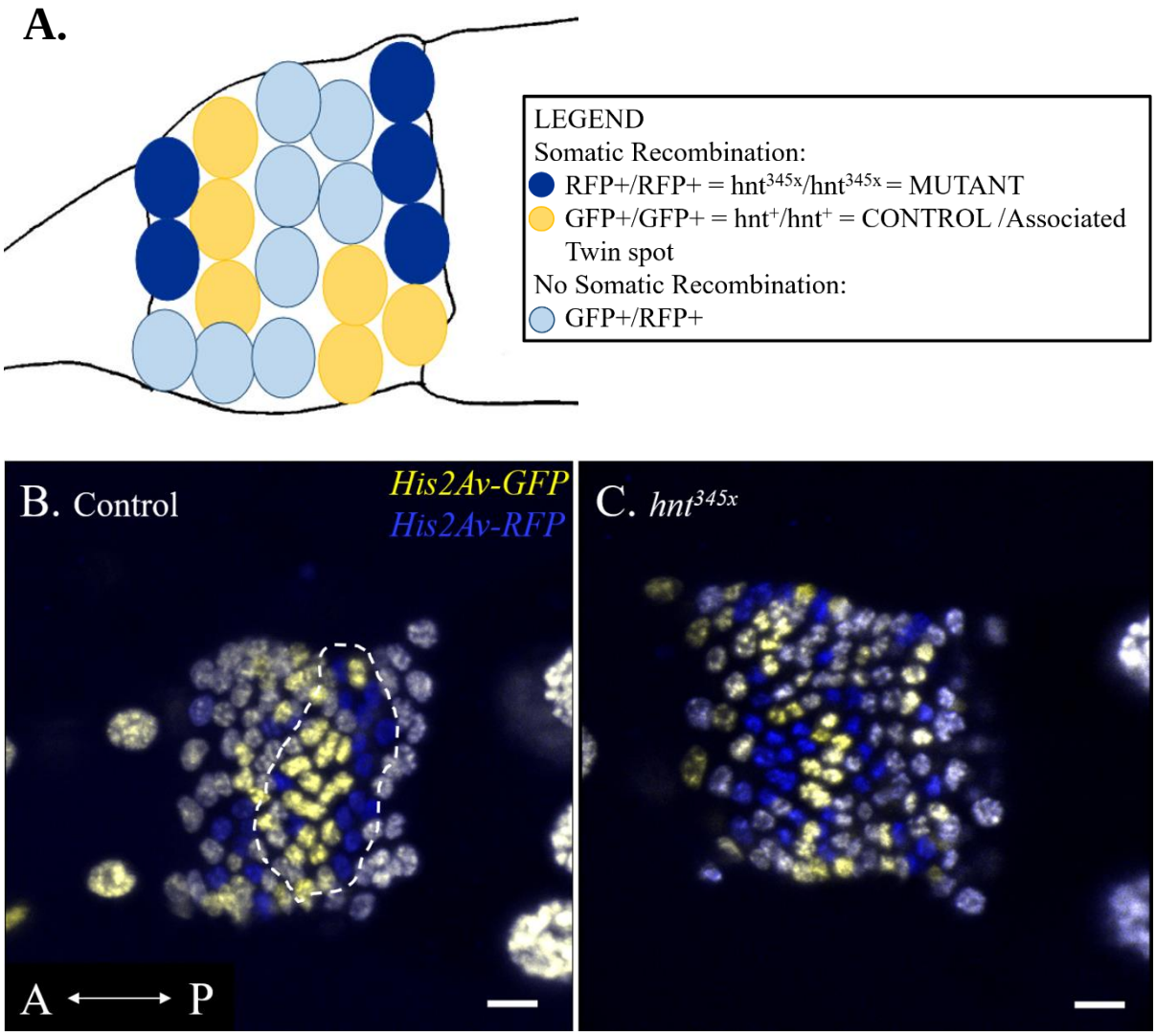



**Figure 3.10 *hnt* loss of function mosaic results in increased total cell population of SGIR.** (A) Schematic diagram to illustrate somatic recombination induced in the SGIR. Representative images of somatic recombination induced in both wild-type control (B) and *hnt*$^{345x}$ mutant (B) lines. A twin spot outlined with white dashes in (B) indicates successful somatic recombination in control SGIR. (C) SGIR is mosaic for *hnt* loss of function where *His2Av-RFP* only cells are homozygous for the *hnt*$^{345x}$ allele and *His2Av-GFP* only cells are homozygous for wild-type. Cells that co-express *His2Av-GFP* and *His2Av-RFP* did not undergo mitotic recombination. SGIRs are oriented in the same manner with anterior to the left and posterior to the right. Scale bar: 10µm.

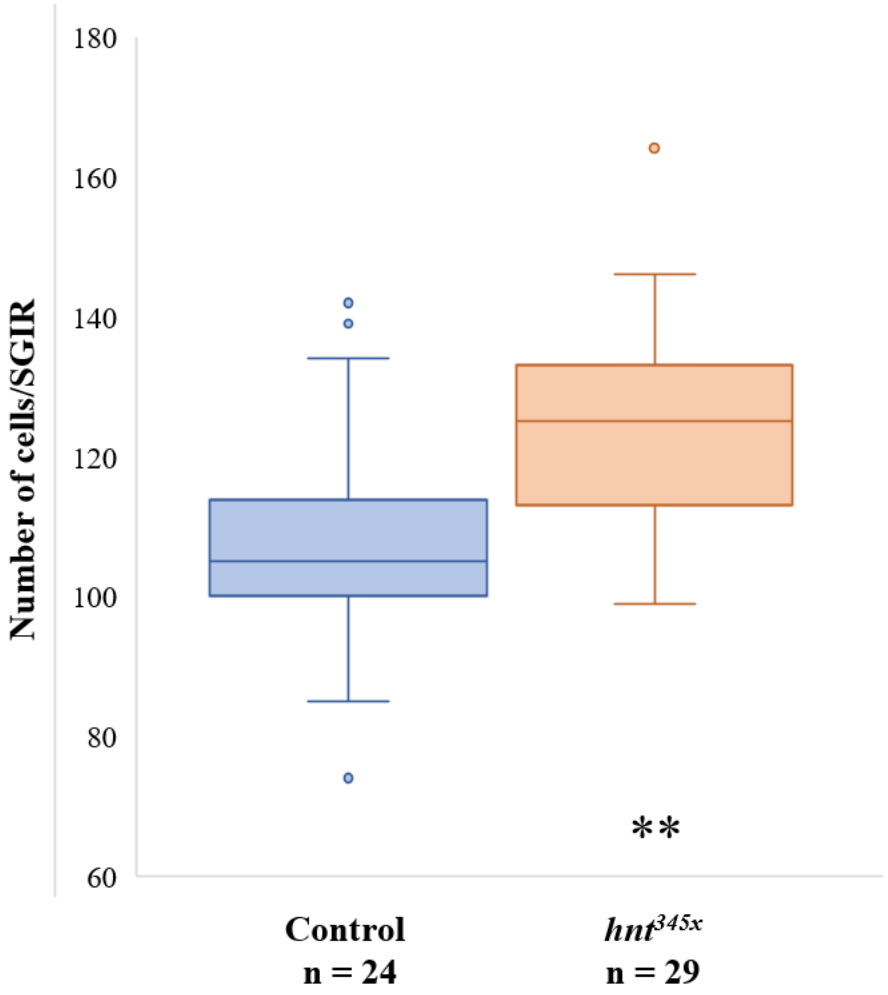



**Table 3.2 Quantitative analysis indicates *hnt* loss of function mosaic results in increased total cell population of SGIR.** Box and whisker plot diagram presents quantitative data associated with Fig. 3.10. SGIR cell counts were performed. Student T-Test confirmed statistically significant difference between the means of the two classes. **, $p<0.005$. n = number of SGIRs. The median value is indicated by the horizontal line in each box. Whiskers indicate the minimum and maximum values of the data set that are not considered outliers. Outliers are indicated by the circles beyond the whiskers.

### 3.8 Notch-induced overproliferation is suppressed by *hnt* overexpression

Given previous reports of Notch and Hnt interactions, it was of interest to address whether Hnt expression is sufficient to cease Notch-induced overproliferation in the SGIR (Sun & Deng, 2007; Krejci et al., 2009; Terriente-Felix et al., 2013). *Drosophila* stocks were created that used *retn-GAL4* to co-express each of the *UAS-hnt* lines (1x, 5x and 10x) with *UAS-*$N^{\Delta 34a}$. As evident in Figure 3.11, Notch-induced overproliferation is suppressed with the increase in *hnt* expression. The *retn>*$N^{\Delta 34a}$*+1xUAS-hnt* SGIR (Fig. 3.11C-C") maintains a significant amount of overproliferation and appears to have a greater number of enlarged nuclei than *retn>*$N^{\Delta 34a}$ (Fig. 3.11B-B"). In comparison, both *5xUAS-hnt* (Fig. 3.11D-D") and *10xUAS-hnt* (Fig. 3.11E-E") when co-expressed with $N^{\Delta 34a}$ severely reduced the number of cells in the SGIR. With respect to *retn>10xUAS-hnt+*$N^{\Delta 34a}$ (Fig. 3.11E-E") the few cells that are present have enlarged nuclei.

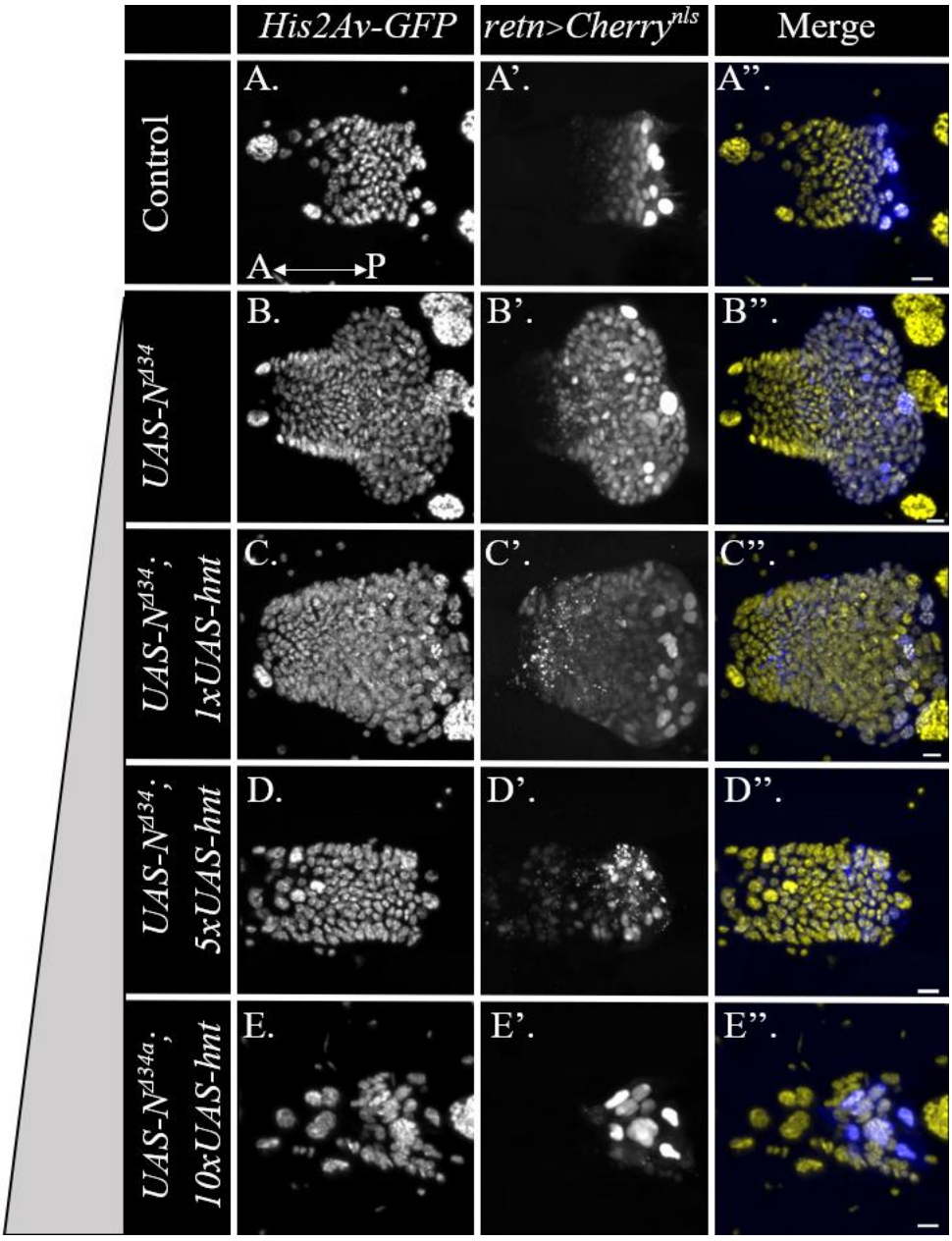



**Figure 3.11 Overproliferation in Notch-induced tumours is suppressed by *hnt* overexpression.** As the level of *hnt* expression increases in *retn>Cherry*$^{nls}$ expressing cells (B-E) the degree of overproliferation diminishes. (A-A") Control SGIR. (B-B") Representative image of *retn>UAS-N*$^{\Delta 3a}$. (C-C") Representative SGIR of *retn>N*$^{\Delta 34a}$*+1xUAS-hnt* possesses the overproliferation phenotype as observed in (B-B") with additional enlarged nuclei. (D-D") Representative SGIR of *retn>N*$^{\Delta 34a}$*+5xUAS-hnt* exhibits a reduction in the number of cells. (E-E") Representative SGIR of *retn>N*$^{\Delta 34a}$*+10xUAS-hnt,* has few cells, all of which possess enlarged nuclei. *His2Av-GFP* was utilized as background to identify all nuclei. SGIRs are oriented in the same manner with anterior to the left. Scale bar: 10µm.

### 3.9 *string* overexpression is sufficient to rescue cell population of *hnt* overexpression phenotype

Subsequent to the result that Hnt can suppress the Notch overexpression phenotype in the SGIR (this study), the next logical step was to work towards understanding the mechanism of this suppression. String (stg) is a strong candidate as Hnt has been proposed to downregulate *stg* in follicle cells and myoblasts (Sun & Deng, 2007; Krejci et al., 2009). Additionally, RNA-seq analysis of Notch-induced tumours of the SGIR TZ suggested *stg* to be upregulated in this context. Furthermore, RNAi-mediated knockdown of *stg* expression diminished the size of these tumours (Wang et al., 2021). As a G2 to M phase inducer (Edgar & O'Farrell, 1989), the overexpression of *stg* in the SGIR causes an increase in the total number of cells (Wang et al., 2021), an observation that was here reproduced (Fig. 3.12B-B"). The concurrent expression of *UAS-stg* and *5xUAS-hnt* by *retn-GAL4* (Fig. 3.12D-D") resulted in a striking recovery of the *5xUAS-hnt* phenotype (Fig. 3.12C-C") with respect to cell number. While the rescue experiment (Fig. 3.12D-D") restored the overall number of cells towards wild-type, the disorganization of the tissue and size of the nuclei do not reflect that of the control (Fig. 3.12A-A".). Table 3.3. illustrates that the *retn>stg+5xUAS-hnt* experiment significantly increased SGIR cell counts, in comparison to *retn>5xUAS-hnt.* Additionally, the rescue experiment did not have cell counts that significantly deviated from the control, further supporting the effectiveness of the rescue experiment with respect to cell divisions. SGIR cell counts for *retn>stg* were significantly higher than the control SGIR and *retn>5xUAS-hnt* cell counts were significantly lower than that of *retn>stg* (Table 3.3).

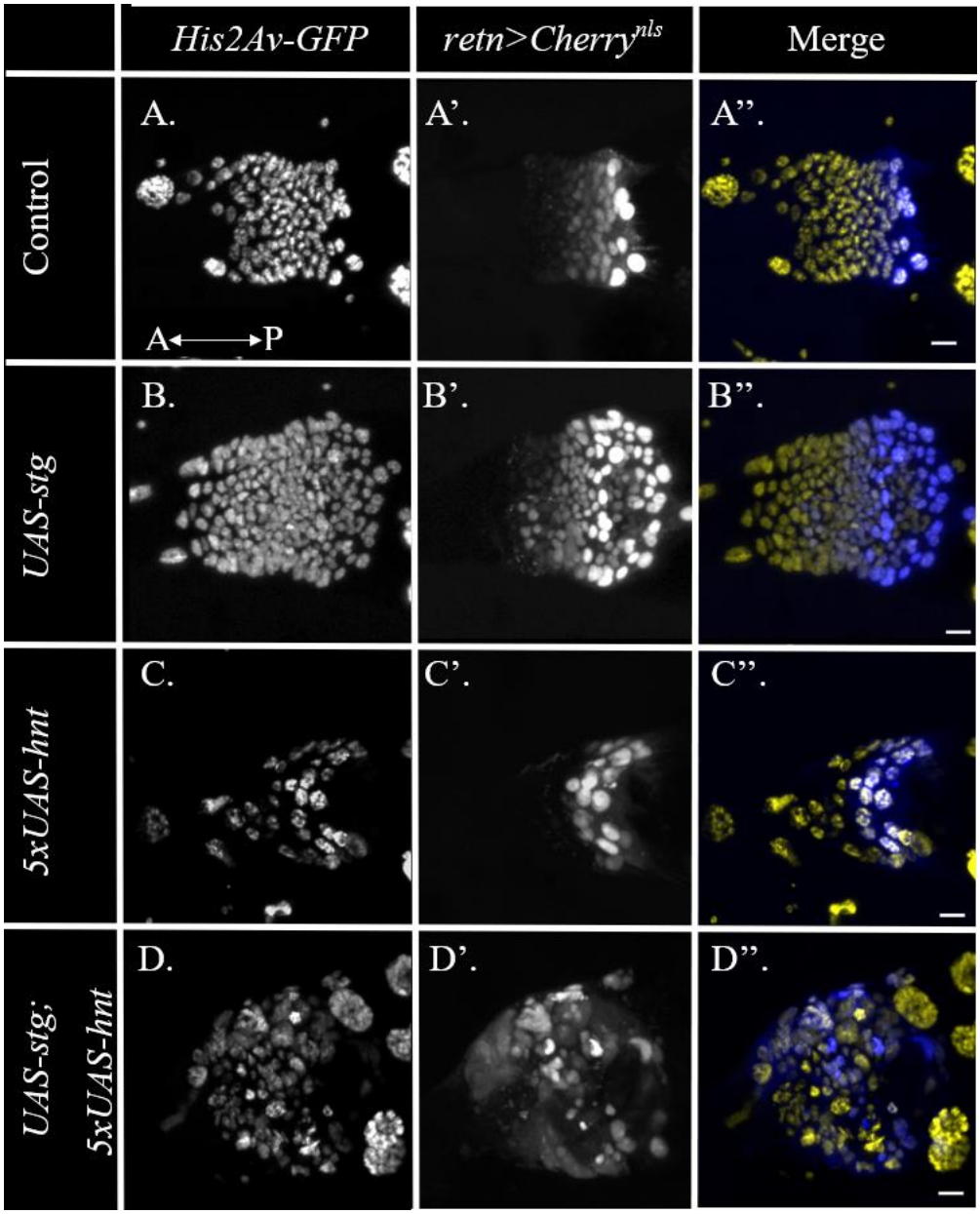



**Figure 3.12 Partial rescue of *hnt* overexpression phenotype via overexpression of *stg*.** (A-A") *retn-GAL4* control SGIR. (B-B") *retn>stg* exhibits a significant increase in the total number of cells in comparison to (A-A"). (C-C") *retn>5xUAS-hnt* displays a reduction in the typical cell population. (D-D") *retn>stg+5xUAS-hnt* disrupted cell morphology is evident, however, there is rescue of the SGIR total cell population in comparison to (C-C"). The SGIR lacks the proper organization found in the control (A-A"). *His2Av-GFP* was utilized as background to identify all nuclei. SGIRs are oriented in the same manner with anterior to the left. Scale bar: 10µm.

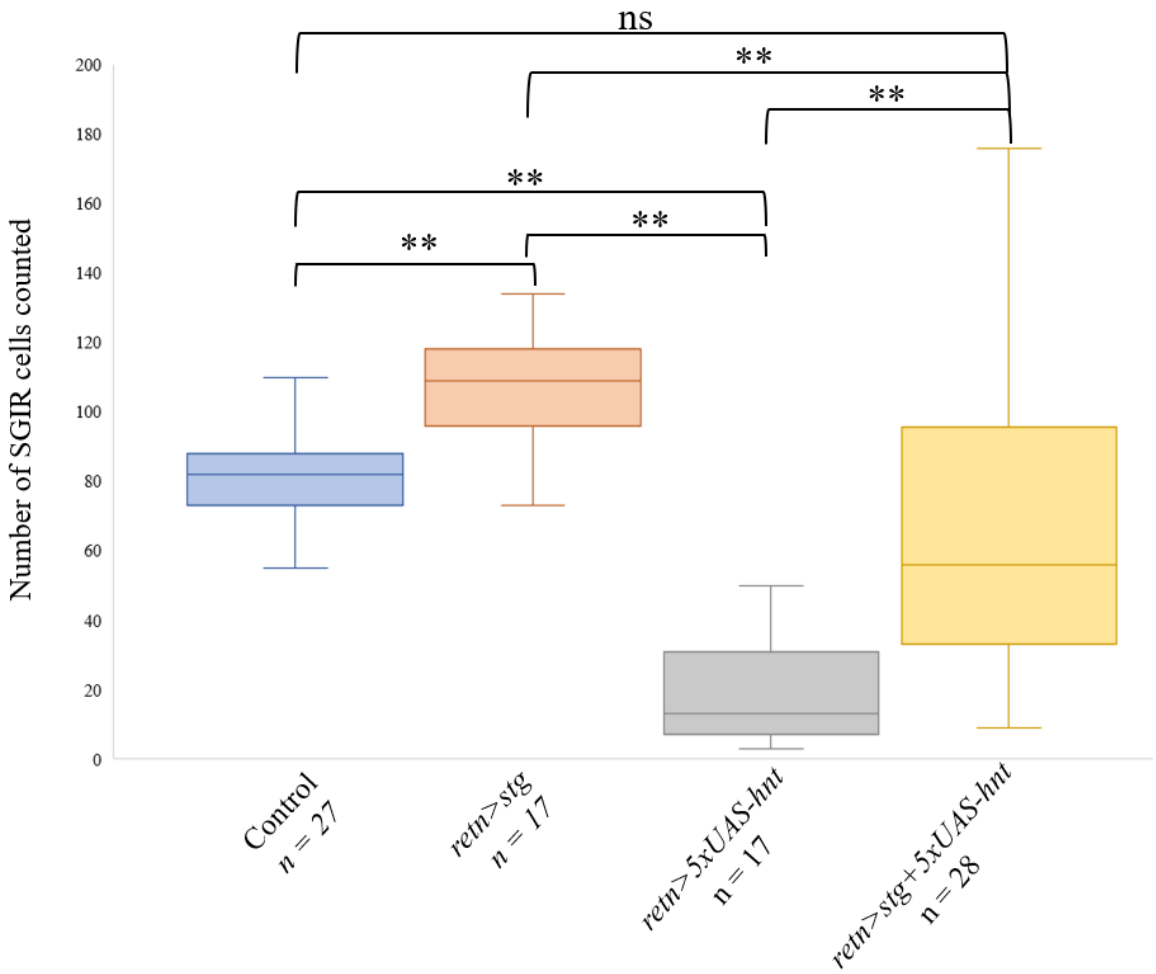



**Table 3.3 Quantitative analysis indicates rescue of *hnt* overexpression phenotype via overexpression of *stg* with respect to cell number.** Box and whisker plot diagram displays the difference in SGIR cell counts between the control, *retn>stg, retn>5xUAS-peb* and *retn>stg+5xUAS-peb.* Student T-Tests were conducted to identify statistical significance between genotypes. ** statistically significant ($p<0.005$); ns, not significant; n, number of SGIRs. The median value is indicated by the horizontal line in each box. Whiskers indicate the minimum and maximum values of the data set that are not considered outliers.

# Chapter 4: *hnt* function is implicated in cell cycle regulation and when overexpressed is capable of suppressing Notch tumourigenesis in the hindgut imaginal ring

*Note: Experiments in the Hindgut Imaginal Ring (HIR) were performed simultaneous to those in the SGIR so that the two contexts could be compared.*

## 4.1 Confirmation of *retn* and *Mmp1* expression patterns for use as GAL4 drivers

To confirm that *retn-GAL4* and *Mmp1-GAL4* were suitable genetic tools to conduct experiments in the HIR, the patterns of *retn-GAL4>Cherry*$^{nls}$ and *Mmp1-GAL4>Cherry*$^{nls}$ expression were observed in the HIR's of dissected late third instar larvae. *retn>Cherry*$^{nls}$ is expressed in the HIR as a gradient from anterior to posterior. The most posterior cells of the HIR do not express *retn>Cherry*$^{nls}$ (Fig 4.1A-A"). In contrast, *Mmp1>Cherry*$^{nls}$ expression is restricted to the most anterior row of cells in the HIR (Fig 4.1B-B"). These *Mmp1*-expressing cells are also those that most strongly express *retn.* Only the *retn-GAL4* expression pattern in the HIR has been previously reported and it is consistent with the observed results (Yang & Deng, 2018).

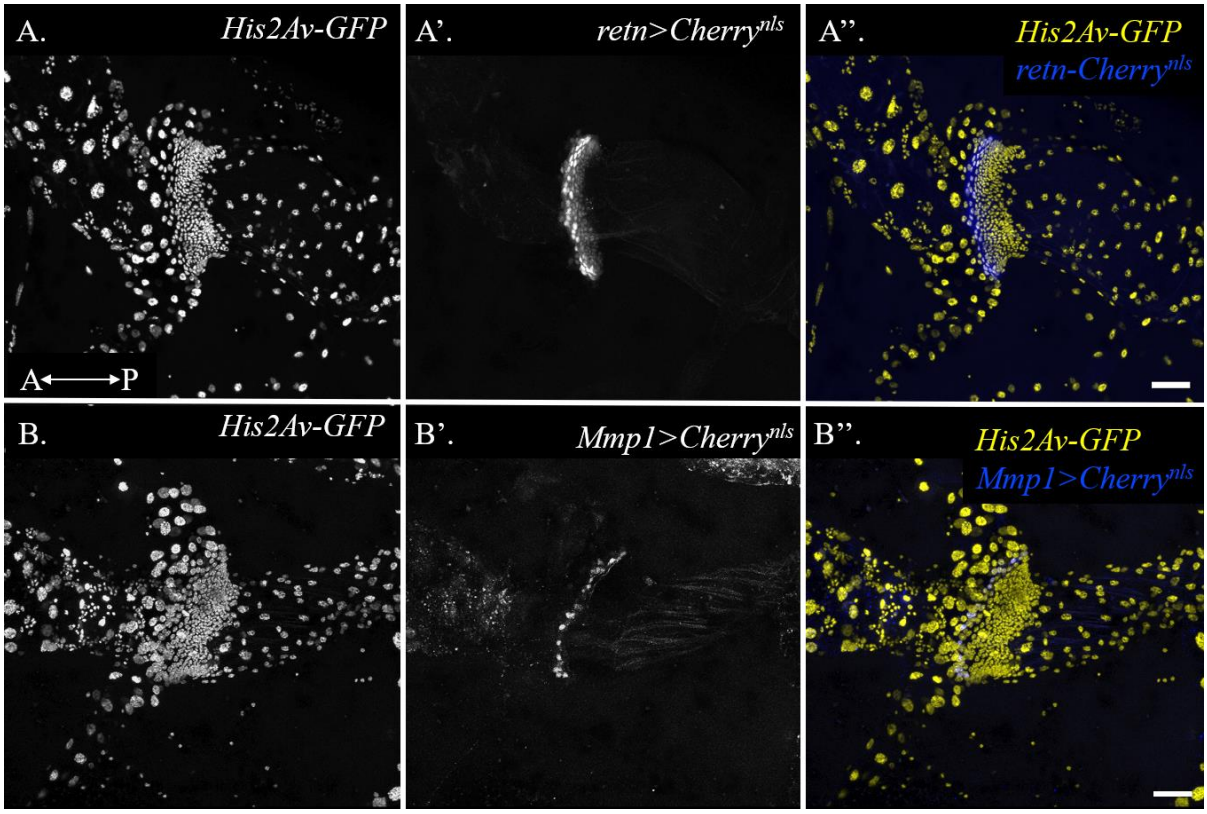



**Figure 4.1 *retn* and *Mmp1* GAL4 drivers are differentially expressed in the hindgut imaginal ring.** (A-A") *retn>Cherry*$^{nls}$ display a gradient of expression in the HIR, peaking in the anterior region. (B-B") *Mmp1>Cherry*$^{nls}$ expression is confined to the most anterior cells of the HIR. *His2Av-GFP* was utilized as background to identify all nuclei. HIRs are oriented in the same manner with anterior to the left. Scale bar: 40µm.

### 4.2 Notch-induced overproliferation is achievable in the HIR using *UAS-NICD* and *UAS-$N^{\Delta 34a}$*

Notch-induced overproliferation via *retn>NICD* and *NRE-GAL4>NICD* in the HIR has been previously explored. It was previously reported that the mitotic index was only significantly higher than that of control HIRs for *NRE-GAL4>NICD* and was not significant for *retn-GAL4.* Overall, it was suggested that the HIR is competent to undergo Notch-induced overproliferation, but it is dependent on the GAL4 driver (Yang & Deng, 2018). To test the competency of the HIR to Notch-induced overproliferation, both *Mmp1* and *retn-GAL4* drivers were paired with the two UAS lines that were used for the SGIR experiments, *UAS-NICD* and *UAS-$N^{\Delta 34a}$*. In Figure 4.2, and in contrast to the previously published results, severe overproliferation of the HIR was evident when *retn-GAL4* was used to drive either *UAS-NICD* or *UAS-$N^{\Delta 34a}$*. The tissue of both *retn>NICD* (Fig.4.2B-B") and *retn>$N^{\Delta 34a}$* (Fig.4.2C-C") was expanded in comparison to the control (Fig. 4.2A-A"). The anterior region of the hindgut imaginal ring (AHIR) of *retn>NICD* and *retn>$N^{\Delta 34a}$* displayed large nuclei and were striking in having strong *$Cherry^{nls}$* expression. All other nuclei in the HIR were much smaller in comparison. Neither *Mmp1>NICD* or *Mmp1>$N^{\Delta 34a}$* third instar HIRs that were dissected on day 7 produced a discernable overproliferation phenotype (Fig. 4.3B-B", C-C"). Overall, these results are consistent with the SGIR experiments, but are not in agreement with previously published results (Yang & Deng, 2018).

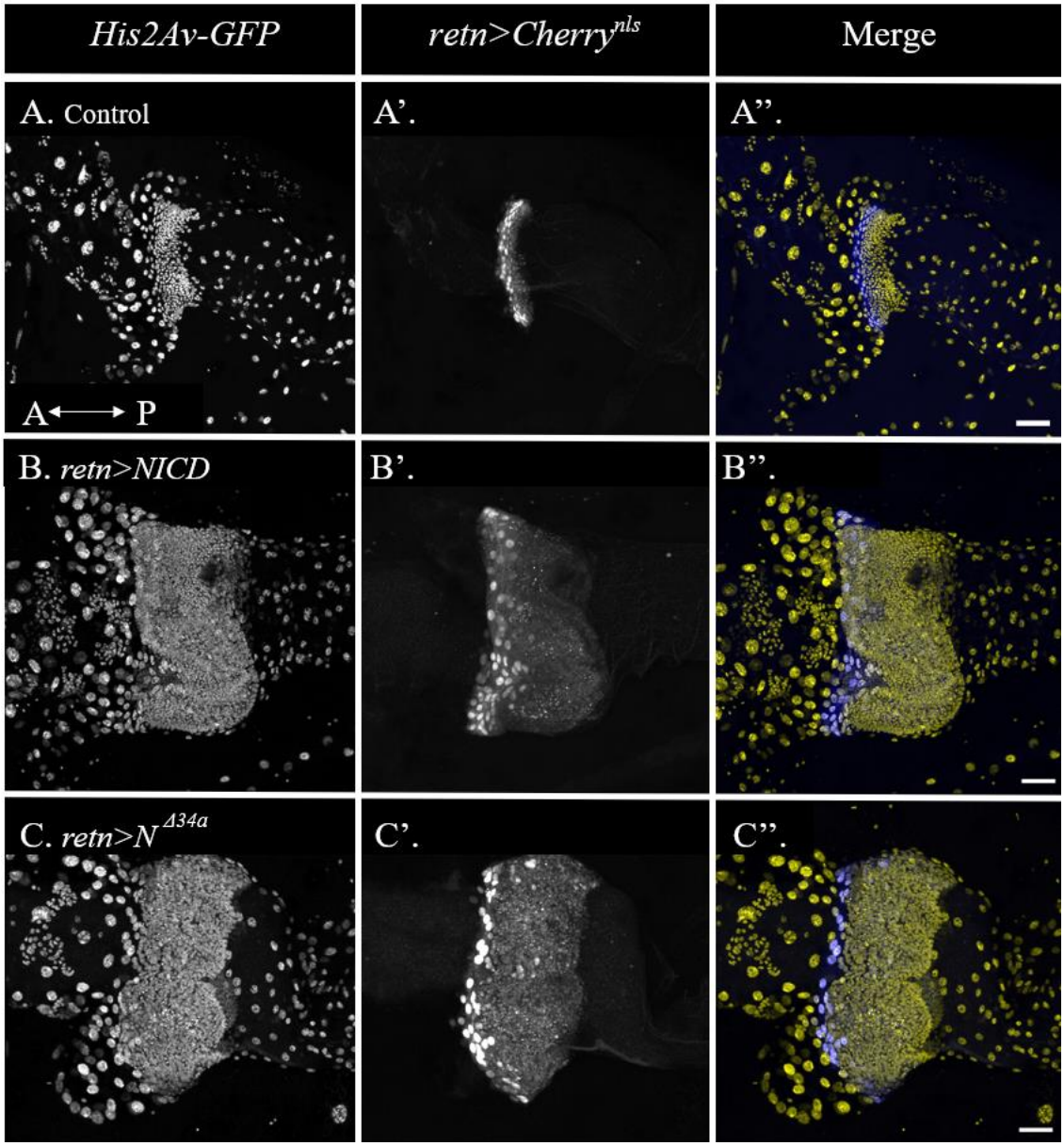



**Figure 4.2 Similar overproliferation phenotypes produced by *UAS-NICD* and *UAS-N$^{\Delta 34a}$* constructs in HIR.** (A-A") *retn-GAL4* control HIR. (B-B", C-C") Representative images of HIRs that were dissected from third instar larvae of an overnight collection (day 7). Both *retn>NICD* (B-B") and *retn>N$^{\Delta 34a}$* (C-C") display prominent overproliferation and tissue expansion in the HIR. Large nuclei are only evident in the AHIR. *His2Av-GFP* was utilized as background to identify all nuclei. HIRs are oriented in the same manner with anterior to the left. Scale bar: 40µm.

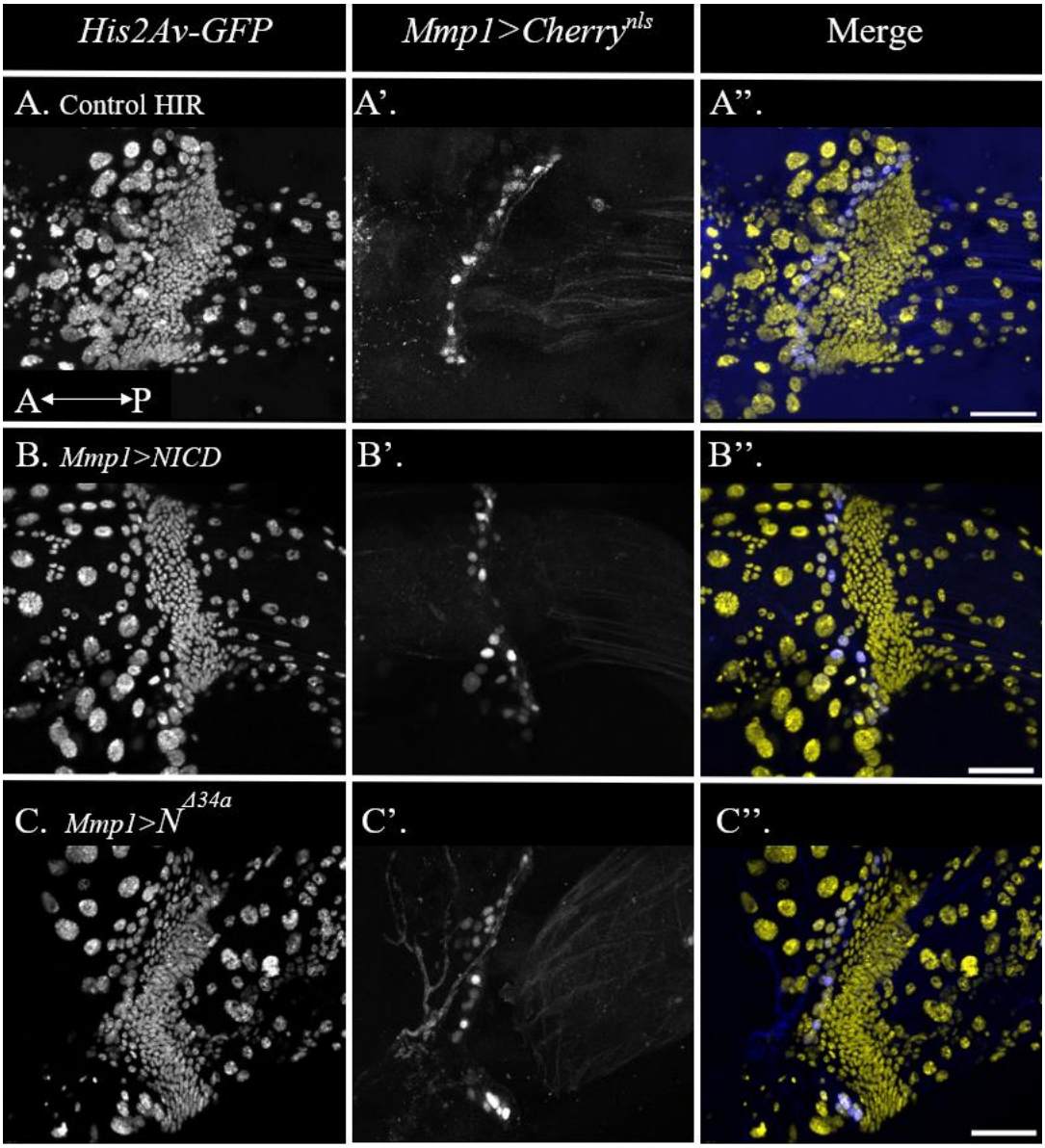



**Figure 4.3 *Mmp1-GAL4* driven overactive Notch signaling fails to produce overproliferation phenotype in HIR.** (A-A") *Mmp1-GAL4* control HIR. (B-B" , C-C") Representative images of HIRs that were dissected from third instar larvae of an overnight collection (day 7). Neither *Mmp1>NICD* (B-B") or *Mmp1>N$^{\Delta 34a}$* (C-C") have phenotypes that are distinct from the control (A-A"). *His2Av-GFP* was utilized as background to identify all nuclei. HIRs are oriented in the same manner with anterior to the left. Scale bar: 40µm.

### 4.3 Hnt is expressed in the HIR

To determine whether or not Hnt is also capable of suppressing the Notch overproliferation phenotype in the HIR, the endogenous expression pattern of Hnt in this context must be established. Unpublished work by the Reed lab, identified that Hnt is expressed in the anterior region of the HIR which will be referred to as the AHIR. Anti-Hnt immunostaining was performed on *retn>GFP$^{nls}$* third instar larvae. As shown in Figure 4.4, there is endogenous expression of Hnt in the HIR. Note that a tissue tear acquired during dissection or mounting of the HIR surreptitiously highlights that endogenous Hnt expression is strongest in the AHIR.

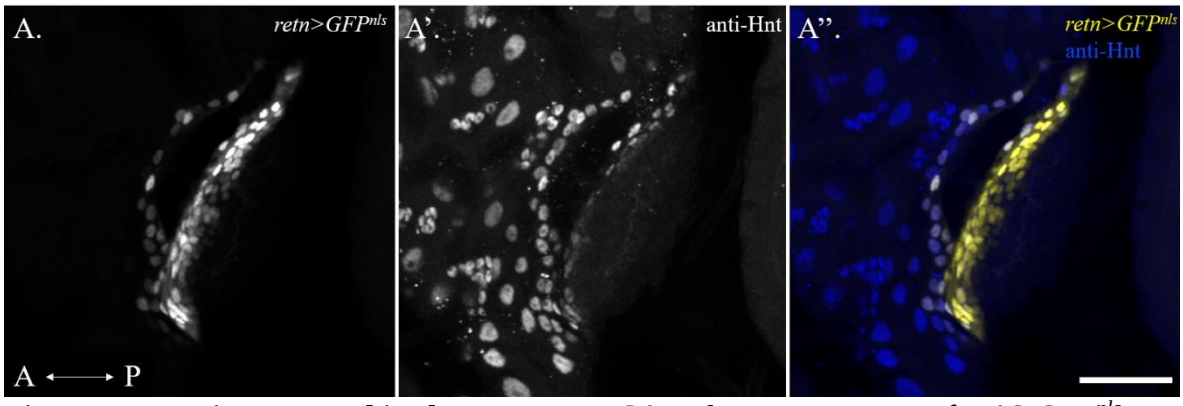



**Figure 4.4 Hnt is expressed in the HIR.** *retn-GAL4* drives expression of *UAS-GFP$^{nls}$* in a gradient, which is greatest in the anterior of the hindgut imaginal ring. During dissection or mounting, the HIR was torn causing a separation in the tissue that highlights the distinct endogenous pattern of Hnt that is restricted to the most anterior cells. (A') Anti-Hnt immunostaining of the hindgut shows expression of Hnt in the anterior-most region of the imaginal ring as well as the intestinal stem cells, enteroblasts and enterocytes. (A'') cells that express *GFP$^{nls}$* and anti-Hnt indicate imaginal ring cells that express Hnt. HIR is oriented with anterior to the left. Scale bar: 40µm.

### 4.4 *hnt* expressing cells of the HIR have minimal Notch signaling

It was previously reported that Notch signaling is most active in the posterior region of the HIR (Yang & Deng, 2018). To determine if cells in the HIR share the same relationship between Notch activity and Hnt expression as the SGIR (this study), enhanced anti-Hnt immunostaining was performed on *NRE-EGFP* third instar larvae (Fig. 4.5). Active Notch signaling detected by *NRE-EGFP* expression marked highest activity in the posterior of the HIR and diminished towards the anterior where Hnt is expressed. There is a small degree of overlap between the regions showing *NRE-EGFP* and Hnt. To reinforce these results, *NRE-EGFP; retn>Cherry*$^{nls}$ third instar larvae were also dissected (Fig. 4.6). The strongest *retn>Cherry*$^{nls}$ expressing cells, which are located in the AHIR, were identified as Hnt positive in Figure 4.5, have little to no Notch activity as evaluated by *NRE-EGFP* (Fig 4.6).

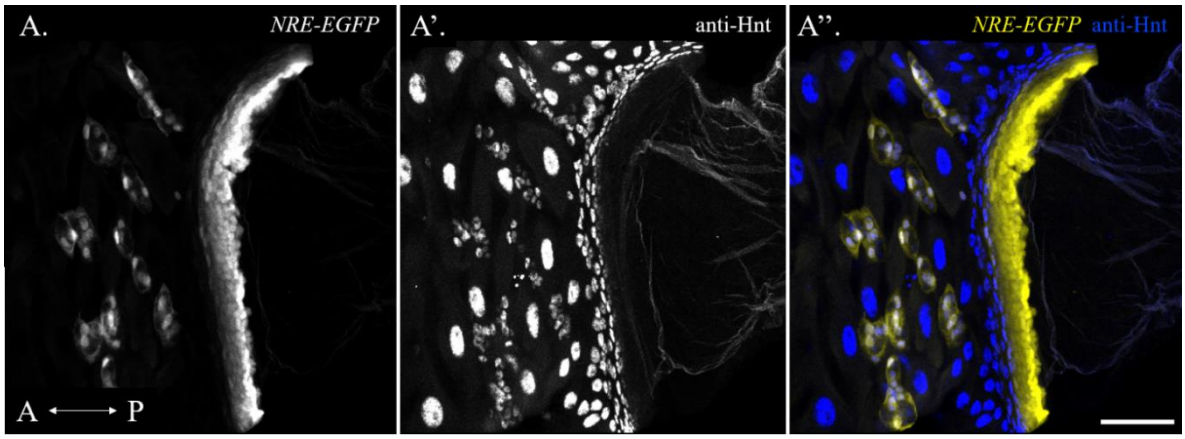



**Figure 4.5 Hindsight expressing cells in the HIR have minimal Notch signaling.** (A) *NRE-EGFP* displays high Notch activation in the posterior of the HIR and diminishes towards the anterior. *NRE-EGFP* is also expressed in the intestinal stem cells and enteroblasts. (A') Enhanced anti-Hnt immunostaining in the larval digestive tract indicates expression of Hnt in the most anterior region of the imaginal ring as well as the intestinal stem cells, enteroblasts and enterocytes. (A'') Not all Hnt expressing cells in the HIR co-express *NRE-EGFP*, indicating little to no Notch activity in these cells. HIR is oriented with anterior to the left. Scale bar 40µm.

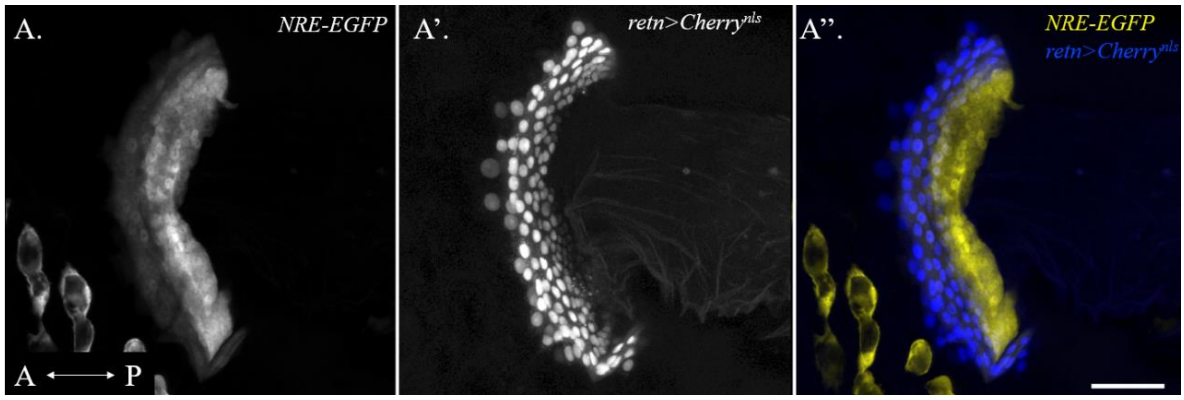



**Figure 4.6 Minimal Notch signaling is detected in anterior HIR cells.** (A) *NRE-EGFP* indicates active Notch signaling. Little to no Notch activity is observed in the AHIR. These anterior cells of the HIR are identified as the strongest *retn*-expressing cells (A''). HIR is oriented with anterior to the left. Scale bar: 40µm.

### 4.5 Hnt expressing cells of the HIR are not mitotically active

A transition zone (TZ) has yet to be identified in the HIR, nor has it been determined if any of the imaginal cells are polyploid. What has been discerned (this study), is that the AHIR is Hnt positive and also expresses *Mmp1*. To identify if the AHIR cells are mitotically active, the impact of the *UAS-cdc2-RNAi* experiments were also investigated in this tissue (Fig. 4.7). For technical reasons, performing cell counts in the HIR was not tractable, therefore only qualitative analysis was conducted. The *cdc2-RNAi* experiments with both *retn* (Fig. 4.7B-B") and *Mmp1* (Fig. 4.7D-D") resulted in the production of cells with large nuclei. These results are consistent with the SGIR experiments as *cdc2* RNAi-mediated knockdown promoted the endocycle as indicated by the increase in nuclear size (section 3.5).

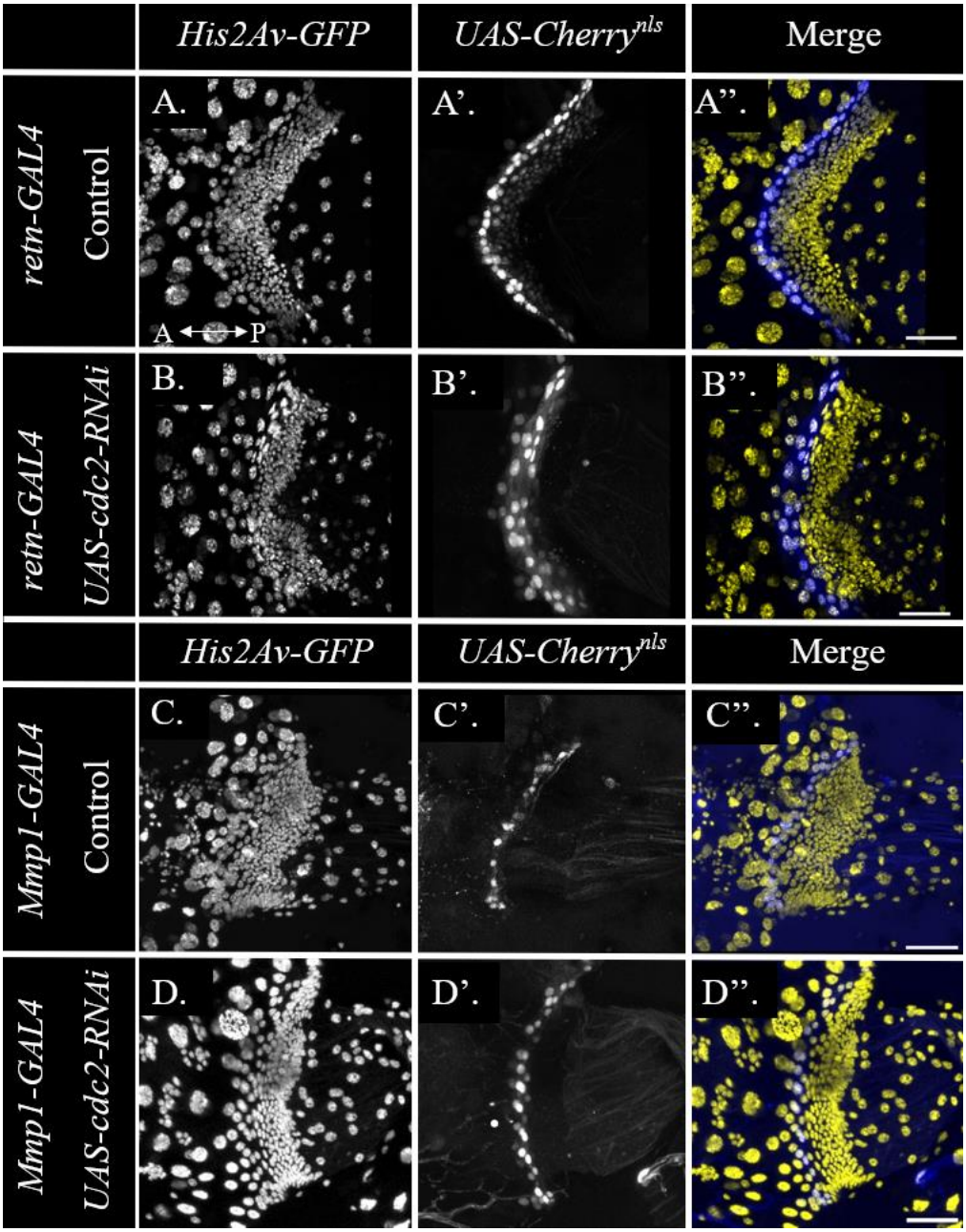



**Figure 4.7. *Mmp1*-expressing cells of the HIR are not mitotically active. (**A-A") Representative control HIR for the *retn* expression pattern without *cdc2-RNAi*. (B-B") *retn>cdc2-RNAi* displays a severe reduction in the overall number of HIR cells. *retn*-expressing cells appear enlarged. (C-C") Representative control HIR for the *Mmp1* expression pattern without *cdc2-RNAi*. (D-D") *Mmp1>cdc2-RNAi* appear to have slightly enlarged *Cherry*$^{nls}$ expressing nuclei. *His2Av-GFP* was utilized as background to identify all nuclei. HIRs are oriented in the same manner with anterior to the left. Scale bar: 40µm.

### 4.6 Overexpression of *hnt* in the HIR leads to severe tissue disruption and enlarged nuclei

The effect of *hnt* overexpression in the HIR was evaluated using the following *UAS-hnt* lines that were driven by *retn-GAL4*: *1xUAS-hnt*, *5xUAS-hnt* and *10xUAS-hnt* (Fig. 4.8). As evident in Figure 4.8, the level of *hnt* expression has a positive correlation with the severity of the HIR phenotype. While the size of the *1xUAS-hnt* HIR (Fig. 4.8B) appeared to have slightly increased relative to the control (Fig.4.8A), the morphology of both *5xUAS-hnt* (Fig.4.8C) and *10xUAS-hnt* (Fig. 4.8D) HIRs was severely disrupted and many greatly enlarged nuclei were observed. While the increase in size of the zone of *retn-GAL4* expression in the HIR was evident in the *5xUAS-hnt* (Fig. 4.8C) and *10xUAS-hnt* (Fig. 4.8D) larvae, a quantitative analysis was not tractable with the imaging system used. In particular, due to the high cell density of the HIR in relation to the SGIR, it was not possible to discern individual nuclei in the Z projections acquired in these experiments. It remains possible, however, that the overall increase in the area of the *retn-GAL4* expression is associated not with an increase in cell number, but an increase in growth via promotion of the endocycle. Additionally, and similar to the SGIR (Fig. 3.8E), using DIC, melanotic deposits were identified in the HIR with *retn>5xUAS-hnt* (Fig. 4.8E) and *retn>10xUAS-hnt* (not shown).

To confirm that the change in morphology of the HIR tissue is not due to cell death executed by effector caspases, *retn-GAL4* was used to co-express *UAS-p35* and *5xUAS-hnt*.

The co-expression of *UAS-p35* failed to rescue the *5xUAS-hnt* phenotype (Fig. 4.9D-D" *cf.* 4.9C-C") suggesting that this phenotype is not associated with the activation of effector caspases, leading to cell death.

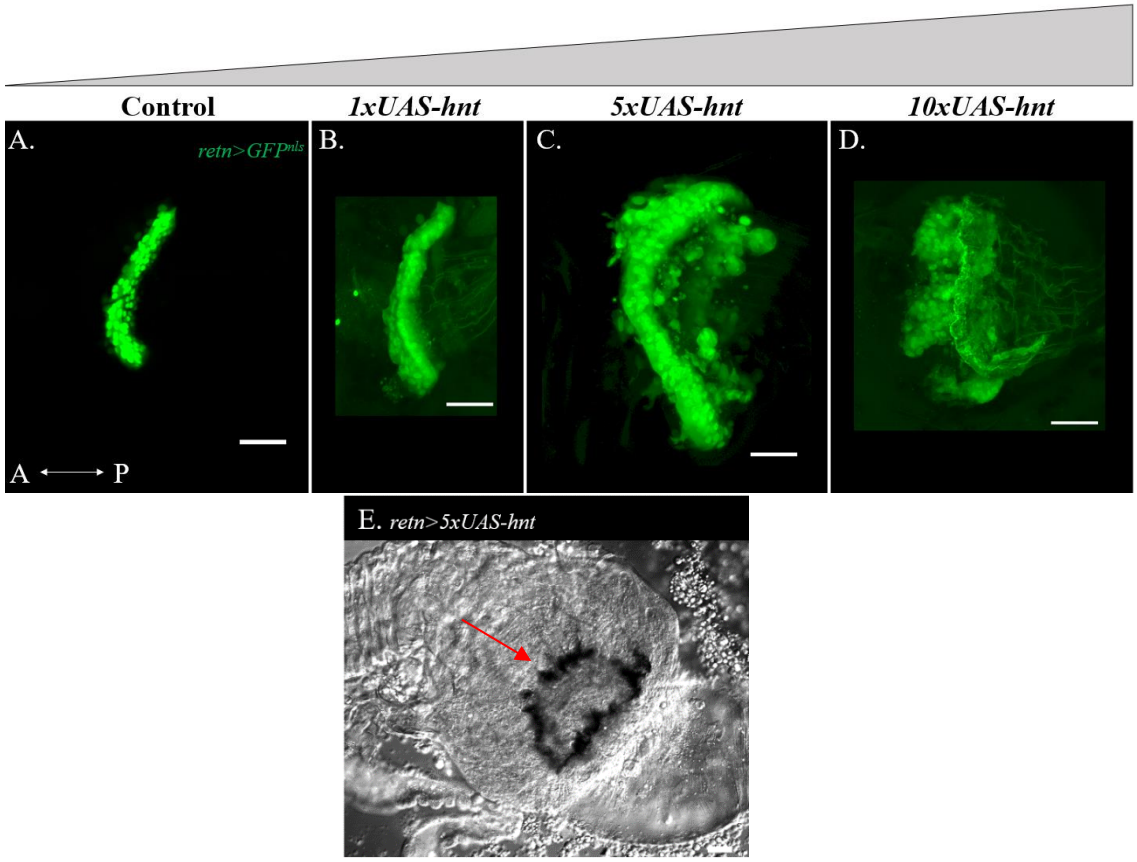



**Figure 4.8 *hnt* overexpression alters morphology in HIR.** (A) represents control HIR with *UAS-GFP*$^{nls}$ driven by *retn-GAL4.* (B) The HIR tissue of *1xUAS-hnt* appears slightly enlarged. Further increasing the level of *hnt* in *retn*-expressing cells increases the severity of the phenotype with large nuclei as well as disorganization and expansion of the tissue as evident in (C & D). (E) DIC image of *retn>5xUAS-hnt* exhibits darkly pigmented deposits as indicated by the arrow. Imaginal rings are oriented in the same manner with anterior to the left. Scale bar: 40µm.

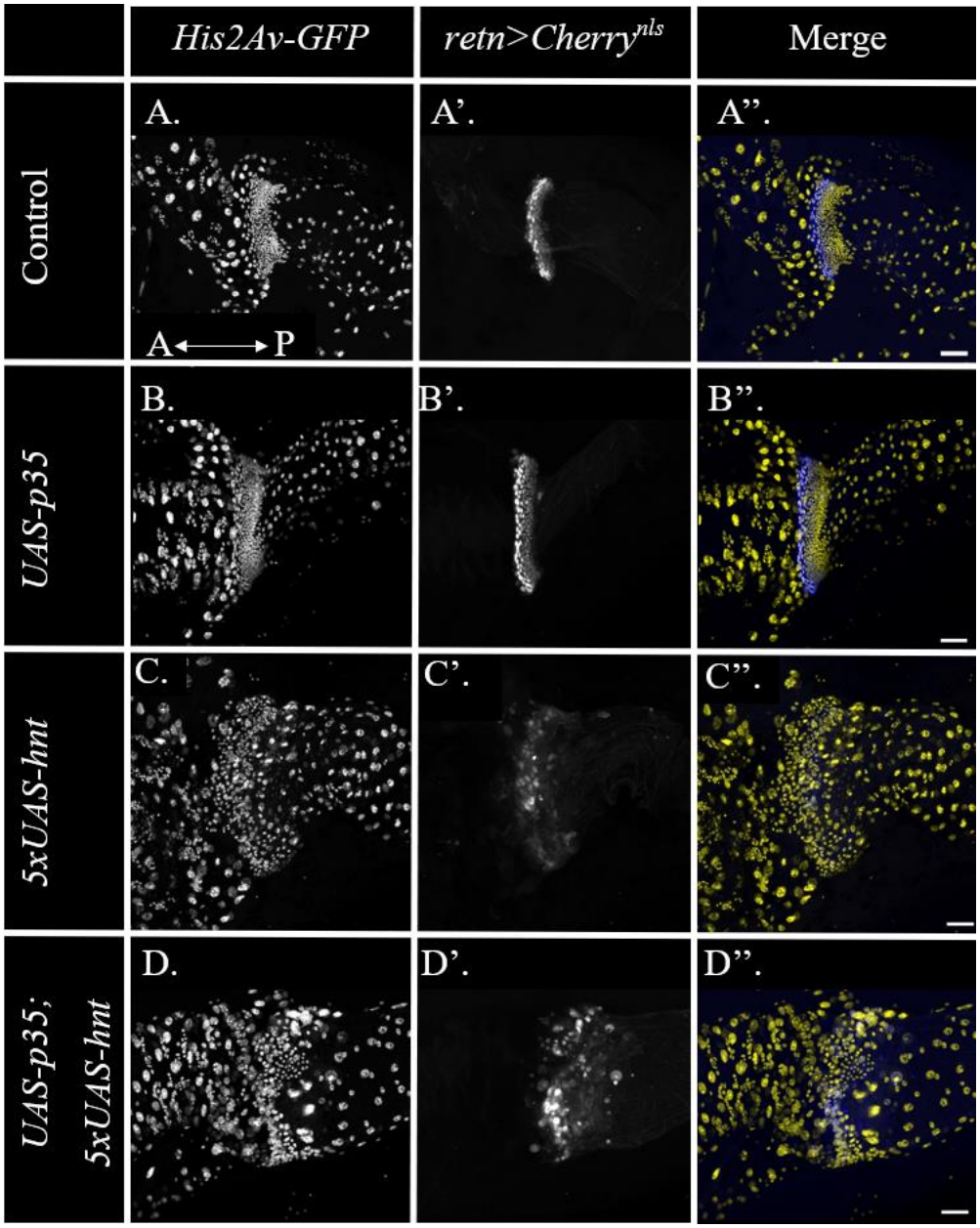



**Figure 4.9 Cell death executed by effector caspases is not responsible for the *hnt* overexpression phenotypes in HIR.** (A-A") Represents a *retn-GAL4* control HIR. (B-B") *retn>p35* lacks a distinct phenotype. (C-C") *retn>5xUAS-hnt* results in a decrease in the total number of imaginal cells. (D-D") *retn>p35+5xUAS-hnt* does not rescue the *5xUAS-hnt* phenotype. HIRs are oriented in the same manner with anterior to the left. Scale bar: 40µm.

### 4.7 Notch-induced overproliferation is suppressed by *hnt* overexpression

To further explore the degree of similarity between the SGIR and HIR, the impact of co-expressing each of the *UAS-hnt* lines (1x, 5x, 10x) with *UAS-$N^{\Delta 34a}$* in the HIR was investigated. As the level of *hnt* expression increased in *retn>$N^{\Delta 34a}$* cells, the degree of overproliferation in the HIR markedly diminished. *retn>$N^{\Delta 34a}$+1xUAS-hnt* (Fig. 4.10C-C") displays a similar degree of overproliferation to *retn>$N^{\Delta 34a}$* (Fig. 4.10B-B") and has enlarged nuclei in the AHIR (Fig. 4.10C-C" *cf.* Fig. 4.10A-A"). The same cannot be said for *retn>$N^{\Delta 34a}$+5xUAS-hnt* (Fig. 4.10D-D") or *retn>$N^{\Delta 34a}$+10xUAS-hnt* (Fig. 4.10E-E"). In the *retn>$N^{\Delta 34a}$+5xUAS-hnt* HIR (Fig. 4.10D-D"), there are very few large nuclei in the anterior of HIR and the overall size of the HIR tissue was diminished in comparison to *retn>$N^{\Delta 34a}$* (Fig 4.10B-B"). With respect to *retn>$N^{\Delta 34a}$+10xUAS-hnt* (Fig. 4.10E-E"), the sparsity of nuclei is evident, and the size of nuclei varies. The relative size of the *retn>$N^{\Delta 34a}$+10xUAS-hnt* HIR is reduced in comparison to *retn>$N^{\Delta 34a}$* (Fig.4.10B-B") and there is variation in the size of nuclei, many being large in size. Overall, suppression of Notch-induced overproliferation is dependent on the level of *hnt* expression.

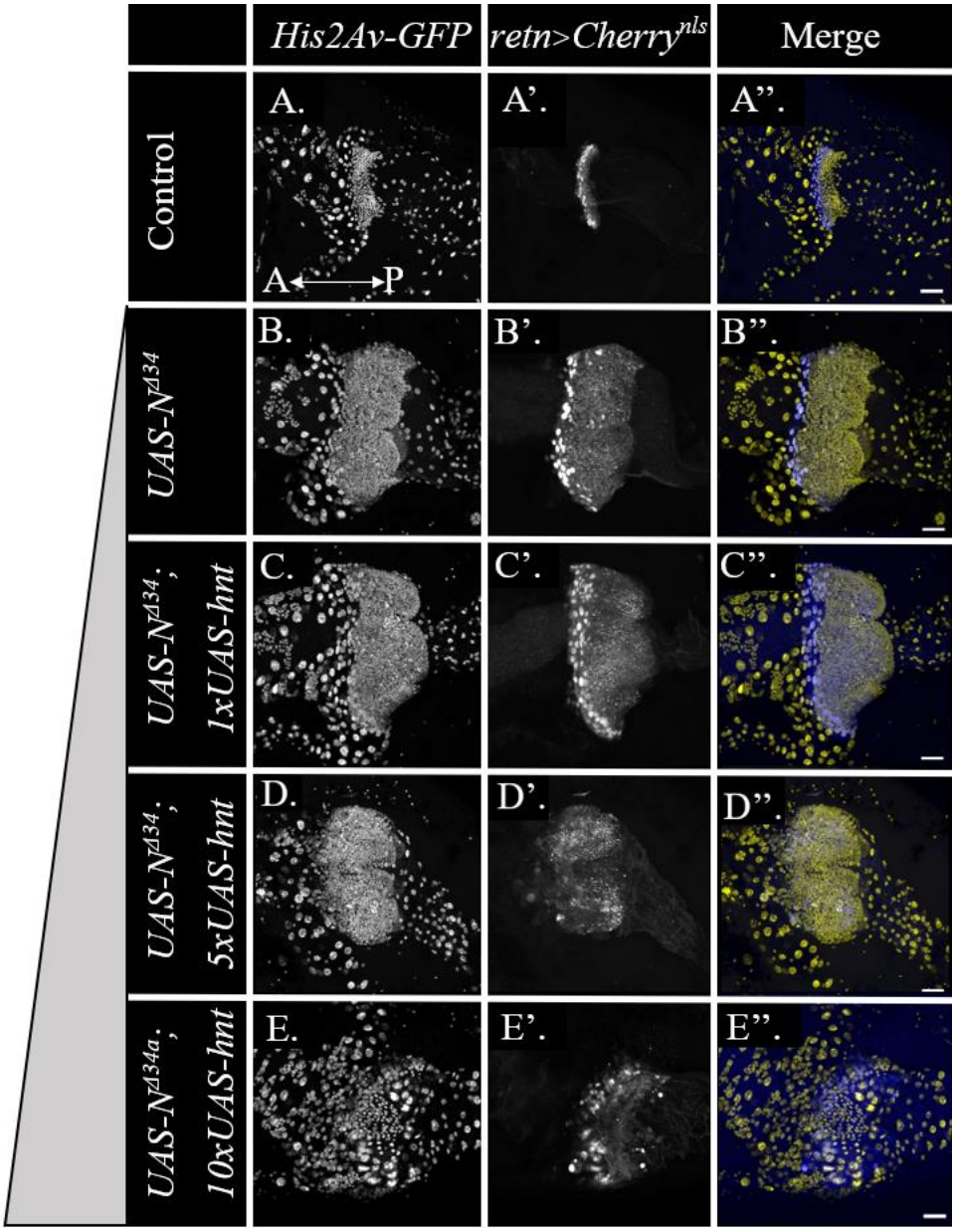



**Figure 4.10 Overproliferation in Notch-induced tumours is suppressed by *hnt* overexpression.** (A-A") Representative *retn-GAL4* control HIR. (B-B") Representative HIR of Notch-induced overproliferation via *retn>UAS-N$^{\Delta 34a}$* . Dense accumulation of cells and presence of large nuclei in the anterior HIR. (C-C") *retn>UAS-N$^{\Delta 34a}$+1xUAS-hnt* possesses a similar degree of proliferation to (B-B"). (D-D") *retn>UAS-N$^{\Delta 34a}$+5xUAS-hnt* does not have large nuclei in the AHIR and the tissue size has reduced. (E-E") *retn>UAS-N$^{\Delta 34a}$+10xUAS-hnt* HIR has scattered nuclei of various sizes. The HIR tissue is disorganized and diminished in size. *His2Av-GFP* was utilized as background to identify all nuclei. HIRs are oriented in the same manner with anterior to the left. Scale bar: 40µm.

### 4.8 Partial Rescue of *hnt* overexpression is achieved with co-expression of *stg*

Similar to the SGIR (section 3.9), it was also of interest to determine if the overexpression of *stg* could rescue the *hnt* overexpression phenotype in the HIR. Figure 4.11B-B" is a representative HIR of *retn>stg* which displayed a maintenance of tissue organization even though there was an increase in the number of *retn>Cherry*$^{nls}$ cells. In comparison to the *retn>5xUAS-hnt* (Fig.4.11C-C"), the *retn>stg+5xUAS-hnt* (Fig. 4.11D-D") resulted in a larger area of *retn* expression and an evident increase in cell number. This observation is consistent with a rescue of the *5xUAS-hnt* phenotype, similar to the SGIR. However, the disorganization and expansion of the HIR was retained with the co-expression of *stg* (Fig. 4.11D-D").

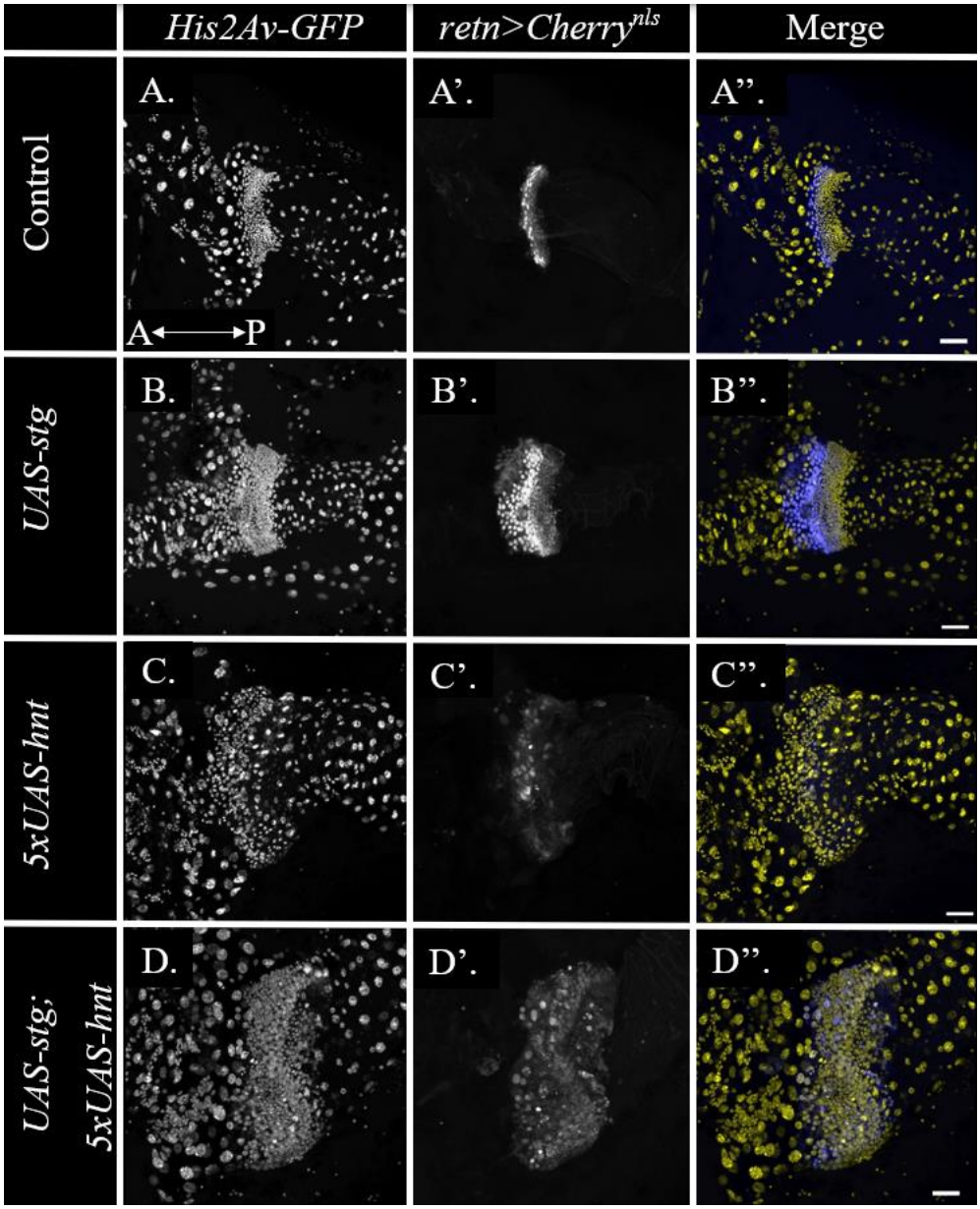



**Figure 4.11 Partial rescue of *hnt* overexpression phenotype via overexpression of *stg* in HIR.** (A-A") Represents a *retn-GAL4* control HIR. (B-B") *retn>stg* HIR possesses more cells than control (A-A"). (C-C") The *retn>5xUAS-hnt* HIR is disturbed, with fewer cells. The imaginal cells have nuclei of varied sizes. (D-D") The simultaneous overexpression of *5xUAS-hnt* and *UAS-stg* with *retn-GAL4* results in the rescue of the total number of cells in the HIR. Although the density of cells has improved with the co-expression of *stg*, the disorganization and expansion of the HIR remains. *His2Av-GFP* was utilized as background to identify all nuclei. HIRs are oriented in the same manner with anterior to the left. Scale bar: 40μm.

# Chapter 5: Discussion

## 5.1 Comparison of *UAS-N$^{\Delta 34a}$* and *UAS-NICD* in the imaginal rings

Upon introduction of overactive Notch signaling by either *UAS-NICD* (Fig.3.2B-B", Fig. 4.2B-B") or *UAS-N$^{\Delta 34a}$* (Fig. 3.2C-C", Fig. 4.2C-C"), overproliferation is exhibited with the use of *retn-GAL4* in both the salivary gland (SGIR) and hindgut (HIR) imaginal rings. Interestingly, this contradicts previous reports that stated the HIR was not permissive to Notch-induced overproliferation when *retn>NICD* was used (Yang & Deng, 2018). Further inspection of the methods used in (Yang & Deng, 2018), indicated that experiments were maintained and crossed at 21-22˚C. All experiments in this study were maintained and crossed at 23˚C and transferred to 29˚C a minimum of 24hrs prior to third instar larval dissection to ensure optimal GAL4 activity (Duffy, 2002). Differences in temperature are well-known to influence activity of GAL4/UAS expression and may explain why overproliferation was observed in *retn>NICD* HIRs at 29˚C.

A key distinction between the SGIR and HIR is the level of Hnt. With anti-Hnt immunostaining, Hnt was weakly detected in the transition zone (TZ) of the SGIR (Fig. 3.4). In contrast, anti-Hnt immunostaining was prominent in the anterior hindgut imaginal ring (AHIR) (Fig. 4.4). The difference in the level of Hnt emphasizes the need to consider the tissues as two separate contexts and may account for any dissimilarities that arise upon comparision.

One quality where the SGIR and HIR differ, is the presence of large nuclei. Experiments conducted with the *UAS-NICD* and *UAS-N$^{\Delta 34a}$* constructs driven by *retn-GAL4*, exhibited distinct arrangements of large nuclei in what appears to be the AHIR (Fig. 4.2B-B", C-C"). In contrast, few large nuclei are present in the SGIR (Fig. 3.2B-B", C-C"). Previous work performed by Wang et al. indicated that upon overactivation of Notch via *Mmp1>NICD*, additional rounds of the endocycle were detected prior to the polyploid SGIR transition zone (TZ) cells proliferating (Wang et al., 2021). Given that the AHIR has stronger Hnt expression than the TZ, these AHIR cells may be less responsive to overactive Notch signaling and undergo more endocycles than the TZ before re-entry into mitosis.

In comparison to the *retn-GAL4* experiments, *Mmp1>NICD* and *Mmp1>N$^{\Delta 34a}$* did not proliferate to the same extent in the SGIR (Fig. 3.3) and HIR (Fig. 4.3). These results may simply be due to the use of the *Mmp1-GAL4* driver (Fig. 3.1B-B", 4.1B-B") as it is expressed in fewer cells in comparison to *retn-GAL4* (Fig. 3.1A-A" , 4.1B-B"). Another possible consideration, however, is that the *Mmp1-GAL4* targeted cells may be less competent to proliferate because these cells also express Hnt and may have exited the mitotic cycle. Overproliferation with *Mmp1-GAL4* driver does occur in the context of an extended larval state (ELS) (Wang et al., 2021) however, the results in this study did not include such larvae.

The distinct difference in phenotype between the *Mmp1>NICD* (Fig. 3.3B-B") and *Mmp1>N$^{\Delta 34a}$* (Fig. 3.3C-C") in the SGIR, which included an increased size of nuclei and increased number of cells expressing *Mmp1-GAL4,* may be attributable to the design of the *UAS-N* constructs. In particular, the *UAS-N$^{\Delta 34a}$* construct lacks the C-terminal PEST domain which is responsible for degradation of the Notch protein. Without the PEST domain, the half-life and overall activity is modestly enhanced (Rogers et al., 1986; Fuerstenberg & Giniger, 1998). In contrast, the *UAS-NICD* construct retains the C-terminal domain (Fortini et al., 1993). An increased half-life and activity could explain why the *Mmp1>N$^{\Delta 34a}$* SGIR (Fig. 3.3C-C") displayed more cells with large nuclei in comparison to *Mmp1>NICD* (Fig. 3.3B-B").

### 5.2 Cells that express *hnt* are not mitotically active and enter the endocycle in the SGIR and HIR

Anti-Hnt immunostaining confirmed previous reports of Hnt in the SGIR TZ (Fig. 3.4) and the most anterior cells of the HIR (Fig. 4.4), (Ming et al., 2013; Reed, unpublished). Hnt is prominently expressed in the AHIR in comparison to the SGIR. It is also interesting to note that the Hnt expressing cells of the SGIR are the most posterior, while those in the HIR are the most anterior (Fig. 3.4, Fig. 4.4).

With respect to Notch activity, both Hnt positive cells in the SGIR (Fig. 3.5, Fig. 3.6) and HIR (Fig. 4.5, Fig. 4.6) lack significant *NRE-EGFP* expression. Therefore, Notch signaling is most active in cells that are not Hnt positive. The relationship between Hnt and Notch activity prompted the exploration as to whether or not Hnt expressing cells, which

have reduced Notch signaling, are mitotically active. *retn>cdc2-RNAi* and *Mmp1>cdc2-RNAi* knockdown experiments were conducted in both the SGIR (Fig 3.7) and HIR (Fig. 4.7). In the SGIR, only *retn>cdc2-RNAi* knockdown achieved a significant reduction in the cell population (Table 3.1). This indicates that during normal development, *retn-GAL4* expressing cells that do not express Hnt, are mitotically active (Fig. 3.7B-B"). *Mmp1>cdc2-RNAi* knockdown in the SGIR does not produce an overt phenotype (Fig. 3.7C-C"), which is consistent with the idea that *Mmp1*-expressing cells have less mitotic activity. Assessment of the effect of *cdc2-RNAi* knockdown in the HIR was performed qualitatively. There was a reduction in the number of HIR cells of *retn>cdc2-RNAi* knockdown larvae (Fig. 4.7B-B") and nuclei were larger in size in comparison to the control (Fig. 4.7A-A"). *Mmp1>cdc2-RNAi* in the HIR didn't alter cell numbers, but nuclei did appear to enlarge (Fig. 4.7D-D" *cf.* C-C"). Overall, these observations are consistent with the interpretation that Hnt positive cells are not mitotically active in the imaginal rings during normal development.

Upon comparison of the two contexts, these being the SGIR and HIR, the appearance of large presumably polyploid nuclei were evident only in the HIR *cdc2-RNAi* knockdown experiments and not those of the SGIR. Again, this may be the result of stronger Hnt expression. It is known that cells that lack *cdc2* expression halt the mitotic cycle and enter the endocycle (Hayashi, 1996; Somma et al., 2008). Given the stronger expression of *hnt* in the HIR, the endocycle may be further enhanced, resulting in large nuclei whereas the minimal *hnt* expression in the SGIR fails to do so.

The ectopic expression of *hnt* in *retn*-expressing cells is another indicator that Hnt positive cells are not mitotically active. While *retn>1xUAS-hnt* (Fig. 3.8B , Fig. 4.8B) did not display an overt phenotype, *retn>5xUAS-hnt* (Fig. 3.8C, Fig. 4.8C) and *retn>10xUAS-hnt* (Fig. 3.8D, Fig. 4.8D) in both the SGIR and HIR possessed large nuclei and a reduction in the total cell population in comparison to controls (Fig 3.8A Fig. 4.8A). It is well established that increased DNA content (polyploidy) is reflective of an increase in cell/nuclear size and can therefore be a means of identifying polyploid cells (Frawley & Orr-Weaver, 2015). *hnt* is only endogenously expressed in the polyploid TZ and AHIR. Therefore, these experiments indicate that a certain level of ectopic *hnt* is sufficient to induce the endocycle in *retn*-expressing cells, regardless of the typical Notch activity that promotes proliferation (Yang & Deng, 2018). Depending on the temperature at which the cross is maintained, the *retn>5xUAS-hnt* and *retn>10xUAS-hnt* genotypes are not fully penetrant lethals where lower temperatures (18-23˚C) show semi-lethality and higher temperatures (25-29˚C) possess greater lethality (data not shown). In the context of the Notch-induced tumour model (*retn>$N^{\Delta 34a}$*), the introduction of ectopic *hnt* (*5xUAS-hnt* and *10xUAS-hnt* only) is also sufficient to mitigate proliferation in both the SGIR (Fig. 3.11D-D", E-E") and HIR (Fig. 4.10D-D", E-E").

To further validate Hnt's role in promoting the endocycle, rescue experiments by co-expression of *UAS-p35* failed, indicating that the observed reduction in cell population is not due to cell death executed by effector caspases (Fig 3.9, Fig. 4.9). This, however, does not discount the possibility of caspase-independent cell death.

These results are consistent with previously published work which identified that endoreplication was responsible for the polyploidy of TZ cells in the SGIR (Wang et al., 2021). Furthermore, the results here presented support the interpretation that Hnt can function to suppress mitosis in a cell autonomous manner, regardless of the presence of Notch signaling. Hnt is also known to function cell autonomously in tracheal cells, the amnioserosa and R8 precursor cells of the eye disc (Wilk et al., 2004). In addition to the differences in mitotic activity here reported in the TZ and AHIR, there are two other examples in the literature that report a reduction of mitotic activity and/or entry into the endocycle in association with the expression of Hnt. The first of these examples concerns the follicle cells of the adult ovary, where Hnt is not found in mitotically active follicle cells. Additionally, ectopic expression of Hnt in follicle cells was sufficient to induce endocycles prematurely (Sun & Deng, 2007). The second example describes how low levels of Hnt are associated with mitotically active adult midgut progenitor cells and when Hnt expression is increased in these cells and adult intestinal stem cells, both cell types stop dividing (Baechler, 2014).

In addition to Hnt's influence on a cell's ability to enter mitosis, Hnt may also promote the progression of the endocycle. This is evident by the increase in nuclear size of cells in *retn>5xUAS-hnt* (Fig. 3.8C, Fig. 4.8C) and *retn>10xUAS-hnt* (Fig. 3.8.D, Fig. 4.8D) experiments. In support of this, Hnt is associated with regulating nuclear size in crystal cells and is expressed in endoreplicating Zone 1 tracheoblasts of the spiracular branch in embryos (Krzemien et al., 2010; Pitsouli & Perrimon, 2010; Terriente-Felix et al., 2013). In the adult

midgut, Hnt is required for differentiation of polyploid enterocytes (Baechler et al., 2015). With respect to sensory organ precursor cells, Hnt is a differentiation marker of these cells which have been reported to possess enlarged nuclei (Koelzer & Klein, 2003; Reeves & Posakony, 2005; Buffin & Gho, 2010; Troost et al., 2015). Overall, along with the support of literature, these experimental results demonstrate that cells that express *hnt* (endogenously or ectopically) are not mitotically active and polyploidy is associated with these cells in both imaginal rings.

### 5.3 Melanotic phenotype observed with *hnt* overexpression suggests *hnt* is capable of forcing crystal cell fate

One of the more unusual and unexpected observations of this study was the frequent presence of what appeared to be melanotic deposits associated with the overexpression of *hnt.* In general, the melanization pathway plays important roles in many physiological processes of *Drosophila* including colour patterning, wound repair and innate immunity (De Gregorio et al., 2002; Rämet et al., 2002; Wittkopp et al., 2002). Crystal cells, a type of polyploid hemocyte, are responsible for melanin deposition in response to injury or infection (Rizki, 1957; Rizki & Rizki, 1959; Tang et al., 2006; Bidla et al., 2007; Terriente-Felix et al., 2013). Pro-phenoloxidase (PPO) is released from crystal cells and subsequently cleaved into its active form, phenoloxidase (PO) by serine protease Hayan, as part of a serpin cascade (González-Santoyo & Córdoba-Aguilar, 2012; Nam et al., 2012). Melanin is produced when phenol oxidation is catalyzed by PO and the resulting quinones polymerize (González-Santoyo & Córdoba-Aguilar, 2012). The rupturing of crystal cells has been suggested as an ancestral origin to mammalian pyroptotic/pro-inflammatory cell death (Dziedziech &

Theopold, 2022). Polyploid crystal cell lysis is caspase-dependent and shares necrotic features with pyroptosis including swelling, rounding of the cell and cell rupture (Fink & Cookson, 2006; Bidla et al., 2007; Dziedziech & Theopold, 2022). Based on this evidence, crystal cell lysis was postulated to be independent of apoptosis which aligns with reports that polyploid cells do not perform this type of programmed cell death (Mehrotra et al., 2008; Zhang et al., 2014; Ruiz-Losada et al., 2021; Dziedziech & Theopold, 2022). Melanization can also occur without cell rupture as exhibited by *Black cells* mutants that possess black crystal cells (Rizki et al., 1980). This mutant phenotype is due to a point mutation in the *PPO1* gene (Neyen, et al., 2015).

Crystal cells are not the only cells that can cause melanin deposition. Previous work by Minakhina & Steward identified mutations in genes involved in processes such as the cell cycle that possessed melanotic phenotypes in both hematopoietic and non-hematopoietic tissues (Minakhina & Steward, 2006). Upon exposure to microorganisms, melanization can be induced in tracheal epithelial cells and is negatively regulated by serine protease Spn77Ba (Tang et al., 2008). Additionally, melanization of enterocytes is a hemocyte-independent event that is in response to chronic stress in the hindgut when larvae lack functional stress-protective mechanisms (Seisenbacher et al., 2011).

The overexpression phenotype of *retn>5xUAS-hnt* (Fig.3.8E, Fig. 4.8E) and *retn>10xUAS-hnt* (not shown) in both the SGIR and HIR possessed darkly pigmented deposits, suggestive of melanin and disrupted cell morphology. This phenotype is reminiscent of the previously described melanization pathway exhibited during normal

physiological processes and displayed in mutants. Hnt is known to be part of the differentiation program in crystal cells and dictates their nuclear size possibly by the promotion of the endocycle (Krzemien et al., 2010; Terriente-Felix et al., 2013). While rupturing of crystal cells is caspase-dependent (Dziedziech & Theopold, 2022), the *hnt* overexpression phenotype was not rescued in the SGIR or HIR by the prevention of effector caspase activation via co-expression of *UAS-p35* (Fig. 3.9 & Fig. 4.9). Caspase-independent cell death, however, cannot be ruled out. The lack of pigment deposition with *retn>1xUAS-hnt* (not shown) indicates that a threshold of ectopic *hnt* is required to produce these darkly pigmented deposits. Taken together, the *hnt* overexpression phenotype can be rationalized by more than one model. The favoured model is as described: upon overexpression of *hnt*, imaginal cells are forced into the endocycle and acquire a crystal cell fate which results in melanin deposition that is independent of the activation of effector caspases. Further experiments will be required to test this hypothesis.

### 5.4 Hnt regulates proliferation in the SGIR non-autonomously

Mosaic analysis revealed that on average, SGIRs that were mosaic for the *hnt* loss of function allele $hnt^{345x}$ had a greater total cell population than control SGIRs and this was statistically significant (Fig. 3.10 & Table 3.2). However, the percentage of $RFP^{+}/GFP^{-}$ cells between experiment and control SGIRs was not statistically significant (Appendix Table B.1.2). This suggests that Hnt regulates proliferation in a non-autonomous manner as homozygous $hnt^{345x}$ TZ cells could increase proliferation of all cells and is not exclusive to the TZ cells that are homozygous mutant.

This is not the first context that Hnt has been found to function in a non-autonomous manner. The R4 cells of the developing *Drosophila* eye are an example where Hnt has a non-autonomous effect on fate determination (Pickup et al., 2002). When *Drosophila* embryos lack Hnt in the amnioserosa, the typical expression of 3 genes, *apontic, Delta* and *decapentaplegic* is undetectable in adjacent leading-edge cells. Since wild-type embryos do not express Hnt in leading edge cells, these effects must be tissue non-autonomous (Wilk et al., 2004).

What is the possible non-autonomous function of Hnt in the SGIR? The SGIR transition zone (TZ) is located between two cell types, the diploid epithelial cells of the imaginal ring and the polyploid secretory cells of the salivary gland (Yang et al., 2019). While Notch activity is present in the imaginal ring, it is absent from the salivary gland and the Hnt expressing TZ cells (Fig. 3.5, Fig. 3.6). Therefore, in the context of the TZ of the SGIR, Hnt may function in a non-autonomous manner to regulate the degree of active Notch signaling in the proliferating SGIR cells.

### 5.5 Threshold of ectopic *hnt* is sufficient to suppress Notch-induced overproliferation by mediating *stg* expression

The results of this thesis suggest that ectopic expression of *hnt* (*retn>5xUAS-hnt* & *retn>10xUAS-hnt*) without overactive Notch signaling is sufficient to diminish mitotic activity and promote the endocycle in the SGIR and HIR (Fig. 3.8C-D", Fig. 4.8C-D"). Endogenous Hnt in the SGIR TZ and AHIR is not sufficient to prevent Notch-induced overproliferation (Fig. 3.11B-B" , Fig. 4.10B-B"). While *retn>$N^{34a}$+1xUAS-hnt* (Fig. 3.11C-

C”, Fig. 4.10C-C”) is not sufficient to prevent Notch-induced overproliferation, the presence of enlarged nuclei appears to increase in the SGIR and HIR. This suggests a threshold of Hnt is required to prevent proliferation, but low levels of Hnt are capable of inducing the endocycle. Consistent with this interpretation, TZ cells of the SGIR express minimal amounts of Hnt (Fig. 3.4) and have been identified as polyploid (Wang et al., 2021). With respect to the ectopic expression of *hnt* via *5xUAS-hnt* (Fig. 3.11D-D”, Fig. 4.10D-D”) and *10xUAS-hnt* (Fig. 3.11E-E”, Fig. 4.10E-E”), both are sufficient to repress the Notch overexpression phenotype. Additionally, large nuclei are observed with *retn>$N^{\Delta 34a}$+10xUAS-hnt* in both the SGIR and HIR further demonstrating a dosage-dependent effect associated with ectopic *hnt* expression. A threshold requirement has also been previously postulated with respect to *hnt* expression and enterocyte differentiation (Baechler et al., 2015) as well as the induction of ectopic *DPax2* expression in the embryo (Kim et al., 2019).

One of the main driving factors of the Notch-induced tumour model is the re-entry of mitosis by the polyploid TZ cells of the SGIR. Upon induction of NICD, polyploid cells exhibited an upregulation of *stg* and the knockdown of *stg* was sufficient to diminish the degree of proliferation and increase the nuclear size of cells in SGIRs of third instar larvae with *$Mmp1^{ts}$>stg-RNAi+NICD.* Moreover, *$Mmp1^{ts}$>stg* forced TZ polyploid cells to perform mitotic divisions (Wang et al., 2021). These previously published results clearly implicate the regulation of *stg* in the context of the SGIR. The proposed feed-forward loop as illustrated in Figure 1.2 suggests that Notch upregulates both *hnt* and *stg* while Hnt also represses *stg* to create a narrow window of *stg* activity (Krejci et al., 2009). Furthermore, in both the follicle

cells of the adult ovary and the Dmd8 cell line that models adult myoblasts, the ectopic expression of *hnt* had an inverse effect on the expression of a *stg::lacZ* reporter (Sun & Deng, 2007; Krejci et al., 2009). Informed by this model, and that *stg* is upregulated upon induction of NICD in the polyploid TZ cells (Wang et al., 2021), *stg* was a logical candidate to investigate as the means by which ectopic Hnt regulates proliferation in the SGIR and HIR with and without the Notch-overproliferation background. Stg promotes the G2 to M transition (Edgar & O'Farrell, 1989), and ectopic expression of *stg* (*retn>stg*) results in a significant increase in the total cell population in comparison to both control and *retn>5xUAS-hnt* SGIRs (Fig. 3.12, Table 3.3). With respect to the HIR, the number of imaginal ring cells also appeared to increase with *retn>stg* in comparison to the control (Fig. 4.11A-A", B-B"). Under control of *retn-GAL4* the co-expression of *UAS-stg* and *5xUAS-hnt* in both tissues attenuated the *hnt* overexpression phenotype as the total number of cells recouped (Fig. 3.12D-D", 4.11D-D"). The successful recovery of the cell population in the SGIR is evident by the fact that there is a statistically significant difference in cell counts between *retn>5xUAS-hnt* and the rescue experiment (*retn>stg+5xUAS-hnt)* (Table 3.3). Additionally, there is no statistically significant difference in cell counts between control SGIRs and *retn>stg+5xUAS-hnt* SGIRs (Table 3.3). While there was rescue of the cell population, morphological disruptions associated with the *retn>5xUAS-hnt* phenotype persisted (Fig. 3.12 & 4.11).

### 5.6 Notch and Hindsight interactions are highly context dependent

In a variety of contexts, Hnt has been implicated as an effector of Notch signaling. Using Chromatin Immunoprecipitation (ChIP), binding regions for Suppressor of Hairless, the main transcriptional activator of the Notch pathway (Schweisguth & Posakony, 1992), have been identified near *hnt* in two distinct cell lines (Krejci et al., 2009; Terriente-Felix et al., 2013). Hnt is upregulated by Notch signaling in follicle cells of the adult ovary to induce the mitotic/endocycle switch by downregulating *stg.* Follicle cell clones that overexpress *hnt* possess larger nuclei in comparison to their adjacent wildtype neighbours (Sun & Deng, 2007). With respect to differentiation of the Dmd8 cell line that models adult myoblasts, Notch and Hnt were proposed to participate in a feed-forward loop to regulate mitotic activity via *stg* (Krejci et al., 2009). Key experiments conducted in crystal cells demonstrated that *hnt* expression was positively correlated with the depletion or increase of Notch activity. In this context, Notch regulates nuclear size by upregulating *hnt* (Terriente-Felix et al., 2013). Furthermore, in the adult midgut, high levels of Notch signaling are involved in the differentiation of enteroblasts to polyploid enterocytes which also requires *hnt* (Ohlstein & Spradling, 2007; Baechler et al., 2015).

Overall, it is intriguing that the product of Notch and Hnt interactions is most often a reduction in mitotic activity that is associated with endocycle entry and can be indicated by an increase in nuclear size. In contrast, Notch is required to promote proliferation in the imaginal ring cells as well as in the imaginal discs and eyes (Baonza & Garcia-Bellido, 2000; Baonza & Freeman, 2005; Yang & Deng, 2018). Aside from the TZ and AHIR, Hnt is not

present in the imaginal ring tissue during normal development (Fig. 3.4, 4.4). Therefore, it is proposed that Hnt is absent in the majority of imaginal ring cells because they are required to proliferate in a Notch-dependent manner. When *hnt* is ectopically expressed in the SGIR and HIR it is consistent with the model that Hnt directly or indirectly impedes Notch-induced *stg* upregulation as previously postulated (Sun & Deng., 2007; Krejci et al., 2009). This argument is reinforced by the suppression of proliferation by ectopic *hnt* in both control and overactive Notch signaling conditions in the SGIR and HIR. Moreover, the *hnt* overexpression phenotype is rescued by the ectopic expression of *stg* in this circumstance. Overall, there is compelling evidence to suggest that *stg* could be a direct downstream target that is repressed by Hnt, but further investigations are required to establish the role of Hnt in this context.

## 5.7 Summary of salivary gland and hindgut imaginal ring results

| Experimental Result | SGIR | HIR |
|---|---|---|
| Overactive Notch signaling via *UAS-N$^{\Delta 34a}$* & *UAS-NICD* induces overproliferation | *Mmp1-GAL4** ✓ *(UAS-N$^{\Delta 34a}$ only)*<br>*retn-GAL4* ✓ | *Mmp1-GAL4* ✗<br>*retn-GAL4* ✓<br>*presence of large nuclei |
| Anti-Hnt immunostaining | Hnt is weakly expressed in TZ | Hnt is strongly expressed in anterior of HIR |
| Hnt expressing cells have weak Notch signaling | ✓ | ✓ |
| Hnt expressing cells are not mitotically active | ✓ | ✓<br>*presence of large nuclei |
| *hnt* overexpression leads to decrease in cell number, enlarged nuclei and tissue disruption; not due to cell death associated with effector caspase activation | ✓ | ✓ |
| *hnt* overexpression results in deposition of melanin | ✓ | ✓ |
| Mosaic analysis suggests cell non-autonomous role of *hnt* | ✓ | N/A |
| Notch-induced overproliferation is suppressed by *hnt* overexpression | ✓ | ✓ |
| *string* overexpression is sufficient to rescue cell population of *hnt* overexpression phenotype | ✓ | ✓ |

**Table 5.1 Summary of the salivary gland (SGIR) and hindgut (HIR) imaginal ring results.** Check mark indicates that tissue displayed experimental result described. An X mark indicates that the tissue did not display the experimental result described. N/A = not applicable.

# Chapter 6: Future Directions

## 6.1 Hnt directly or indirectly influences *stg* expression

It has been established (this study) that the reduction in cell population by the ectopic expression of *hnt* in the imaginal rings can be mitigated by the overexpression of *stg.* In the context of the Dmd8 cell line that models adult myoblasts, the ectopic expression of *hnt* hinders *stg::lacZ* (Krejci et al., 2009). Misexpression experiments with *hnt* in follicle cells also display an inverse correlation between *hnt* and *stg::lacZ* (Sun & Deng, 2007).

To discern if the transcription factor Hnt directly or indirectly effects *stg* expression, a combination of bioinformatic and molecular biology techniques will be required. *stg* RNA probes will have to be designed to perform *in situ* hybridization allowing for the identification of the *stg* expression pattern during normal development in the imaginal rings. *In situ* hybridization can then be repeated on *retn>5xUAS-hnt* third instar larvae to confirm whether or not *hnt* influences *stg* expression. If there is confirmation that ectopic *hnt* alters the expression of *stg*, the next step would be to identify if there are *stg* regulatory regions that are binding sites for Hnt. Chromatin Immunoprecipitation qPCR (ChIP-qPCR) can be used to identify if there are any direct transcriptional targets of Hnt in the *stg* regulatory region. An epitope Myc tagged version of Hnt described in (Farley et al., 2018), would be expressed in *retn>N$^{\Delta 34a}$* 3$^{rd}$ instar larvae. SGIR tissue would be dissected and standard ChIP protocol for *Drosophila* such as the one described in (Tran et al., 2012) would be followed to obtain purified DNA. qPCR would be performed on the purified DNA since only the *stg* locus is of interest. Final validation of Hnt directly regulating *stg* would require the use of *stg::lacZ*

reporter constructs. *stg::lacZ* reporter constructs were developed by (Lehman et al., 1999) to decipher >40kB of *stg* regulatory DNA. Initially, the sequences of each of these constructs can be scanned with the program Find Individual Motif Occurrences (FIMO) for Hnt transcription factor binding motifs (TFBM) using their associated position weight matrices (Grant et al., 2011; Zhu et al., 2011; Ming et al., 2013). Provided that some of these constructs contain putative TFBM's for Hnt, stocks with *stg::lacZ* constructs that are loss of function for *hnt* as well as those that overexpress *hnt* will be created. *stg::lacZ* constructs with alterations to the lacZ expression upon loss or overexpression of *hnt* would be selected. Deletions would be made at potential TFBM's in the selected *stg::lacZ* constructs and if the lacZ expression is altered this would be further verification that Hnt directly interacts with the *stg* regulatory region.

### 6.2 Exploration of melanin deposition by overexpression of *hnt* in imaginal rings

To our knowledge, this is the first report of ectopic *hnt* resulting in the deposition of dark pigment (Fig. 3.8E & 4.8E). *hnt* is involved in the differentiation program of crystal cells and dictates their nuclear size (Krzemien et al., 2010; Terriente-Felix et al., 2013). The proposed model described in (section 5.3) suggests that ectopic *hnt* forces imaginal ring cells to take on a crystal cell fate and leads to cell rupture causing melanin deposition, independent of effector caspase activation.

*In situ* hybridization with RNA probes for *lozenge*, an early marker of crystal cells or *PPO1*, a sensitive and specific marker of terminally differentiated crystal cells could be used to support or refute the model that *retn>5xUAS-hnt* and *retn>10xUAS-hnt* forces imaginal

ring cells to take on this new fate (Lebestky et al., 2003; Milchanowski et al., 2004). *PPO1* and *PPO2* are responsible for the production of prophenoloxidases in crystal cells (Rizki et al., 1980; Irving et al., 2005; Binggeli et al., 2014). Flies that are double mutants for $PPO1^{\Delta}$, $PPO2^{\Delta}$ are melanization-deficient (Binggeli et al., 2014). To confirm that ectopic expression of *hnt* in larvae is due to activation of PPO1 and/or PPO2, overexpression of *hnt* in these double mutant larvae should fail to produce melanin.

### 6.3 Knockdown of *hnt* throughout the TZ and AHIR in both control and Notch-overexpression conditions

While the $hnt^{345x}$ mosaic analysis indicated the non-autonomous effect of *hnt* on proliferation in the SGIR (Fig. 3.10), it is of interest to also explore if the knockdown of *hnt* via *Mmp1>hnt-RNAi* in the TZ and AHIR is also sufficient to increase the total cell population. Using a *UAS-hnt-RNAi* construct that has been identified to effectively knockdown *hnt* would ensure all cells in the TZ and AHIR are deficient for Hnt. This contrasts with the $hnt^{345x}$ mosaic analysis as it was not possible to obtain only $hnt^{345x}$ mutant cells in the TZ. The *Mmp1-GAL4* would be used to target only the TZ and AHIR. Along with co-expression of a fluorescent marker (i.e., $UAS\text{-}GFP^{nls}$) it would be possible to detect if Hnt has a cell autonomous effect by conducting cell counts. If the total cell counts for $GFP^{+}$ expressing cells have increased in comparison to the control, this suggests that cells that lack *hnt* expression undergo more cell divisions than cells that do express *hnt.* Furthermore, it would also be of interest to determine if the co-expression of *UAS-hnt-RNAi* and $UAS\text{-}N^{\Delta 34a}$ results in a stronger overproliferation phenotype.

### 6.4 Confirmation of Hnt as an inducer of the endocycle

Experiments conducted with co-expression of *UAS-p35* and *5xUAS-hnt* identified that cell death associated with the activation of effector caspases is not responsible for the reduction in cell population in the imaginal rings (Fig. 3.9, 4.9). The increase in nuclear size with the ectopic expression of *hnt* (Fig. 3.8D, E, Fig. 4.8D, E) aligns with the plethora of evidence that supports the theory that *hnt* regulates nuclear size (Sun & Deng, 2007; Krejci et al., 2009 Pitsouli & Perrimon, 2010; Terriente-Felix et al, 2013; Baechler, 2014). Techniques for identification of endocycle entry and polyploidy are available in *Drosophila.*

FLY-FUCCI (Fluorescent Ubiquitination-based Cell Cycle Indicator) is a reporter system based on the degradation of fluorescently tagged GFP-E2f1 and RFP-CycB degrons (Zielke et al., 2014). A degron is an element of a protein that is targeted by UPS (Ubiquitin Proteasome System)-mediated degradation (Clausen et al., 2019). The visualization of RFP and/or GFP indicate what stage of the cell cycle cells are in. Cells that are in the endocycle are identified by alternating GFP-E2F1 and RFP-CycB expression (Zielke et al., 2014). This genetic tool can be used to identify if cells that ectopically express *hnt* enter the endocycle.

Immunostaining for CycA and CycB, can also be performed on control and *retn>5xUAS-hnt* imaginal rings to detect if there is any change in the expression pattern of the mitotic markers (Lee & Orr-Weaver, 2003). With respect to ectopic expression of *hnt* in follicle cells, immunostaining for CycA and CycB revealed an extended presence of these mitotic markers as the entry into the endocycle was delayed in these cells (Sun & Deng, 2007). Comparing the intensity of DAPI staining between control and *retn>5xUAS-hnt*

imaginal rings is a method of verifying the change in nuclear size with ectopic *hnt* expression.

## Letter of Copyright Permission

OXFORD UNIVERSITY PRESS LICENSE

TERMS AND CONDITIONS

Jan 19, 2023

---

This Agreement between Miss. Emily Baker ("You") and Oxford University Press ("Oxford University Press") consists of your license details and the terms and conditions provided by Oxford University Press and Copyright Clearance Center.

| | |
|---|---|
| License Number | 5472781459739 |
| License date | Jan 19, 2023 |
| Licensed content publisher | Oxford University Press |
| Licensed content publication | Genetics |
| Licensed content title | DNA Replication Control During *Drosophila* Development: Insights into the Onset of S Phase, Replication Initiation, and Fork Progression |
| Licensed content author | Hua, Brian L; Orr-Weaver, Terry L |
| Licensed content date | Aug 31, 2017 |
| Type of Use | Thesis/Dissertation |

| | |
|---|---|
| Institution name | |
| Title of your work | Investigating the influence of the transcription factor Hindsight in a Notch-induced tumour model |
| Publisher of your work | University of Waterloo |
| Expected publication date | Jan 2023 |
| Permissions cost | 0.00 CAD |
| Value added tax | 0.00 CAD |
| Total | 0.00 CAD |
| Title | Investigating the influence of the transcription factor Hindsight in a Notch-induced tumour model |
| Institution name | University of Waterloo |
| Expected presentation date | Jan 2023 |
| Portions | Figure 2C, The endocycle is driven by oscillations in key cell cycle factors.p.34 |

| | |
|---|---|
| | Miss. Emily Baker<br>[redacted] |
| Requestor Location | [redacted]<br>Attn: Miss. Emily Baker |
| Publisher Tax ID | GB125506730 |
| Total | 0.00 CAD |

Terms and Conditions

**STANDARD TERMS AND CONDITIONS FOR REPRODUCTION OF MATERIAL FROM AN OXFORD UNIVERSITY PRESS JOURNAL**

1. Use of the material is restricted to the type of use specified in your order details.

2. This permission covers the use of the material in the English language in the following territory: world. If you have requested additional permission to translate this material, the terms and conditions of this reuse will be set out in clause 12.

3. This permission is limited to the particular use authorized in (1) above and does not allow you to sanction its use elsewhere in any other format other than specified above, nor does it apply to quotations, images, artistic works etc that have been reproduced from other sources which may be part of the material to be used.

4. No alteration, omission or addition is made to the material without our written consent. Permission must be re-cleared with Oxford University Press if/when you decide to reprint.

5. The following credit line appears wherever the material is used: author, title, journal, year, volume, issue number, pagination, by permission of Oxford University Press or the sponsoring society if the journal is a society journal. Where a journal is being published on behalf of a learned society, the details of that society must be included in the credit line.

6. For the reproduction of a full article from an Oxford University Press journal for whatever purpose, the corresponding author of the material concerned should be informed of the proposed use. Contact details for the corresponding authors of all Oxford University Press journal contact can be found alongside either the abstract or full text of the article concerned, accessible from www.oxfordjournals.org Should there be a problem clearing these rights, please contact journals.permissions@oup.com

7. If the credit line or acknowledgement in our publication indicates that any of the figures, images or photos was reproduced, drawn or modified from an earlier source it will be necessary for you to clear this permission with the original publisher as well. If this permission has not been obtained, please note that this material cannot be included in your publication/photocopies.

8. While you may exercise the rights licensed immediately upon issuance of the license at the end of the licensing process for the transaction, provided that you have disclosed complete and accurate details of your proposed use, no license is finally effective unless and until full payment is received from you (either by Oxford University Press or by Copyright Clearance Center (CCC)) as provided in CCC's Billing and Payment terms and conditions. If full payment is not received on a timely basis, then any license preliminarily granted shall be deemed automatically revoked and shall be void as if never granted. Further, in

the event that you breach any of these terms and conditions or any of CCC's Billing and Payment terms and conditions, the license is automatically revoked and shall be void as if never granted. Use of materials as described in a revoked license, as well as any use of the materials beyond the scope of an unrevoked license, may constitute copyright infringement and Oxford University Press reserves the right to take any and all action to protect its copyright in the materials.

9. This license is personal to you and may not be sublicensed, assigned or transferred by you to any other person without Oxford University Press's written permission.

10. Oxford University Press reserves all rights not specifically granted in the combination of (i) the license details provided by you and accepted in the course of this licensing transaction, (ii) these terms and conditions and (iii) CCC's Billing and Payment terms and conditions.

11. You hereby indemnify and agree to hold harmless Oxford University Press and CCC, and their respective officers, directors, employs and agents, from and against any and all claims arising out of your use of the licensed material other than as specifically authorized pursuant to this license.

12. Other Terms and Conditions: v1.4

**Questions? customercare@copyright.com or +1-855-239-3415 (toll free in the US) or +1-978-646-2777.**

## References


Anatskaya, O. V., & Vinogradov, A. E. (2022). Polyploidy as a Fundamental Phenomenon in Evolution, Development, Adaptation and Diseases. *International Journal of Molecular Sciences*, *23*(7), 3542. https://doi.org/10.3390/ijms23073542

Baechler, B. (2014). *Investigation of the role of Hindsight in the development of the Drosophila midgut* [Master's Thesis, University of Waterloo]. UWSpace.

Baechler, B. L., McKnight, C., Pruchnicki, P. C., Biro, N. A., & Reed, B. H. (2015). Hindsight/RREB-1 functions in both the specification and differentiation of stem cells in the adult midgut of Drosophila. *Biology Open*, *5*(1), 1–10. https://doi.org/10.1242/bio.015636

Baonza, A., & Freeman, M. (2005). Control of Cell Proliferation in the Drosophila Eye by Notch Signaling. *Developmental Cell*, *8*(4), 529–539. https://doi.org/10.1016/j.devcel.2005.01.019

Baonza, A., & Garcia-Bellido, A. (2000). Notch signaling directly controls cell proliferation in the Drosophila wing disc. *Proceedings of the National Academy of Sciences of the United States of America*, *97*(6), 2609–2614.

Berry, D. L., & Baehrecke, E. H. (2007). Growth arrest and autophagy are required for salivary gland cell degradation in Drosophila. *Cell*, *131*(6), 1137–1148. https://doi.org/10.1016/j.cell.2007.10.048

Bidla, G., Dushay, M. S., & Theopold, U. (2007). Crystal cell rupture after injury in Drosophila requires the JNK pathway, small GTPases and the TNF homolog Eiger. *Journal of Cell Science*, *120*(7), 1209–1215. https://doi.org/10.1242/jcs.03420

Binggeli, O., Neyen, C., Poidevin, M., & Lemaitre, B. (2014). Prophenoloxidase Activation Is Required for Survival to Microbial Infections in Drosophila. *PLoS Pathogens*, *10*(5), e1004067. https://doi.org/10.1371/journal.ppat.1004067

Brand & Perrimon (1993). Targeted gene expression as a means of altering cell fates and generating dominant phenotypes. *Development* 118:401–415.

Bray, S. J. (2006). Notch signalling: A simple pathway becomes complex. *Nature Reviews Molecular Cell Biology*, *7*(9), 678–689. https://doi.org/10.1038/nrm2009

Bray, S. J. (2016). Notch signalling in context. *Nature Reviews Molecular Cell Biology*, *17*(11), 722–735. https://doi.org/10.1038/nrm.2016.94

Buffin, E., & Gho, M. (2010). Laser Microdissection of Sensory Organ Precursor Cells of Drosophila Microchaetes. *PLoS ONE*, *5*(2), e9285. https://doi.org/10.1371/journal.pone.0009285

Burghardt, E., & Ostör, A. G. (1983). Site and origin of squamous cervical cancer: a histomorphologic study. *Obstetrics and gynecology*, *62*(1), 117–127.

Campos-Ortega, J. A., & Hartenstein, V. (1997). *The embryonic development of Drosophila melanogaster*. Berlin: Springer-Verlag Berlin and Heidelberg GmbH & Co. KG

Chou, T. B., & Perrimon, N. (1992). Use of a yeast site-specific recombinase to produce female germline chimeras in Drosophila. *Genetics*, *131*(3), 643–653. https://doi.org/10.1093/genetics/131.3.643

Clausen, L., Abildgaard, A. B., Gersing, S. K., Stein, A., Lindorff-Larsen, K., & Hartmann-Petersen, R. (2019). Chapter Two—Protein stability and degradation in health and disease. In R. Donev (Ed.), *Advances in Protein Chemistry and Structural Biology* (Vol. 114, pp. 61–83). Academic Press. https://doi.org/10.1016/bs.apcsb.2018.09.002

Coward, J., & Harding, A. (2014). Size Does Matter: Why Polyploid Tumor Cells are Critical Drug Targets in the War on Cancer. *Frontiers in Oncology*, *4*. https://doi.org/10.3389/fonc.2014.00123

Curtiss, J., & Heilig, J. S. (1995). Establishment of Drosophila imaginal precursor cells is controlled by the Arrowhead gene. *Development*, *121*(11), 3819–3828. https://doi.org/10.1242/dev.121.11.3819

De Gregorio, E., Han, S.-J., Lee, W.-J., Baek, M.-J., Osaki, T., Kawabata, S.-I., Lee, B.-L., Iwanaga, S., Lemaitre, B., & Brey, P. T. (2002). An Immune-Responsive Serpin Regulates the Melanization Cascade in Drosophila. *Developmental Cell*, *3*(4), 581–592. https://doi.org/10.1016/S1534-5807(02)00267-8

Deady, L. D., Li, W., & Sun, J. (2017). The zinc-finger transcription factor Hindsight regulates ovulation competency of Drosophila follicles. *ELife*, *6*, e29887. https://doi.org/10.7554/eLife.29887

Duffy, J. B. (2002). GAL4 system in drosophila: A fly geneticist's swiss army knife. *Genesis*, *34*(1–2), 1–15. https://doi.org/10.1002/gene.10150

Dziedziech, A., & Theopold, U. (2022). Proto-pyroptosis: An Ancestral Origin for Mammalian Inflammatory Cell Death Mechanism in Drosophila melanogaster. *Journal of Molecular Biology*, *434*(4), 167333. https://doi.org/10.1016/j.jmb.2021.167333

Edgar, B. A., & O'Farrell, P. H. (1989). Genetic Control of Cell Division Patterns in the Drosophila Embryo. *Cell*, *57*(1), 177–187.

Edgar, B., & O'Farrell, P. H. (1990). *The Three Postblastoderm Cell Cycles of Drosophila Embryogenesis Are Regulated in G2 by string*. https://doi.org/10.1016/0092-8674(90)90012-4

Edgar, B. A., Lehman, D. A., & O'Farrell, P. H. (1994). Transcriptional regulation of string (cdc25): A link between developmental programming and the cell cycle. *Development (Cambridge, England)*, *120*(11), 3131–3143.

Edgar, B. A., Zielke, N., & Gutierrez, C. (2014). Endocycles: A recurrent evolutionary innovation for post-mitotic cell growth. *Nature Reviews Molecular Cell Biology*, *15*(3), 197–210. https://doi.org/10.1038/nrm3756

Farley, J. E., Burdett, T. C., Barria, R., Neukomm, L. J., Kenna, K. P., Landers, J. E., & Freeman, M. R. (2018). Transcription factor Pebbled/RREB1 regulates injury-induced axon degeneration. *Proceedings of the National Academy of Sciences*, *115*(6), 1358–1363. https://doi.org/10.1073/pnas.1715837115

Fink, S. L., & Cookson, B. T. (2006). Caspase-1-dependent pore formation during pyroptosis leads to osmotic lysis of infected host macrophages. *Cellular Microbiology*, *8*(11), 1812–1825. https://doi.org/10.1111/j.1462-5822.2006.00751.x

Follette, P. J., & O'Farrell, P. H. (1997). Cdks and the Drosophila cell cycle. *Current Opinion in Genetics & Development*, *7*(1), 17–22.

Fortini, M. E., Rebay, I., Caron, L. A., & Artavanis-Tsakonas, S. (1993). An activated Notch receptor blocks cell-fate commitment in the developing Drosophila eye. *Nature*, *365*(6446), 555–557. https://doi.org/10.1038/365555a0

Frawley, L. E., & Orr-Weaver, T. L. (2015). Polyploidy. *Current Biology*, *25*(9), R353–R358. https://doi.org/10.1016/j.cub.2015.03.037

Fuerstenberg, S., & Giniger, E. (1998). Multiple Roles for Notch in Drosophila Myogenesis. *Developmental Biology*, *201*(1), 66–77. https://doi.org/10.1006/dbio.1998.8944

Golic, K. G., & Lindquist, S. (1989). The FLP recombinase of yeast catalyzes site-specific recombination in the drosophila genome. *Cell*, *59*(3), 499–509. https://doi.org/10.1016/0092-8674(89)90033-0

Golic, K.G. (1991). Site-specific recombination between homologous chromosomes in Drosophila. *Science* 252(5008): 958--961.

González-Santoyo, I., & Córdoba-Aguilar, A. (2012). Phenoloxidase: A key component of the insect immune system. *Entomologia Experimentalis et Applicata*, *142*(1), 1–16. https://doi.org/10.1111/j.1570-7458.2011.01187.x

Gramates, L. S., Agapite, J., Attrill, H., Calvi, B. R., Crosby, M. A., dos Santos, G., Goodman, J. L., Goutte-Gattat, D., Jenkins, V. K., Kaufman, T., Larkin, A., Matthews, B. B., Millburn, G., Strelets, V. B., & the FlyBase Consortium. (2022). FlyBase: A guided tour of highlighted features. *Genetics*, *220*(4), iyac035. https://doi.org/10.1093/genetics/iyac035

Grant, C. E., Bailey, T. L., & Noble, W. S. (2011). FIMO: Scanning for occurrences of a given motif. *Bioinformatics*, *27*(7), 1017–1018. https://doi.org/10.1093/bioinformatics/btr064

Gregory, S. L., Kortschak, R. D., Kalionis, B., & Saint, R. (1996). Characterization of the dead ringer gene identifies a novel, highly conserved family of sequence-specific DNA-binding proteins. *Molecular and Cellular Biology*, *16*(3), 792–799.

Hammond, M. P., & Laird, C. D. (1985). Control of DNA replication and spatial distribution of defined DNA sequences in salivary gland cells of Drosophila melanogaster. *Chromosoma*, *91*(3–4), 279–286. https://doi.org/10.1007/BF00328223

Hassel, C., Zhang, B., Dixon, M., & Calvi, B. R. (2014). Induction of endocycles represses apoptosis independently of differentiation and predisposes cells to genome instability. *Development*, *141*(1), 112–123. https://doi.org/10.1242/dev.098871

Hay, B. A., Wolff, T., & Rubin, G. M. (1994). Expression of baculovirus P35 prevents cell death in Drosophila. Development, 120(8), 2121–2129. https://doi.org/10.1242/dev.120.8.2121

Hayashi, S. (1996). *A Cdc2 dependent checkpoint maintains diploidy in Drosophila*. 8.

Held L.J. (2005) Imaginal discs. Cambridge University Press

Herrscher, R. F., Kaplan, M. H., Lelsz, D. L., Das, C., Scheuermann, R., & Tucker, P. W. (1995). The immunoglobulin heavy-chain matrix-associating regions are bound by Bright: A B cell-specific trans-activator that describes a new DNA-binding protein family. *Genes & Development*, *9*(24), 3067–3082. https://doi.org/10.1101/gad.9.24.3067

Hong, A., Lee-Kong, S., Iida, T., Sugimura, I., & Lilly, M. A. (2003). The p27cip/kip ortholog dacapo maintains theDrosophila oocyte in prophase of meiosis I. *Development*, *130*(7), 1235–1242. https://doi.org/10.1242/dev.00352

Hong, A., Narbonne-Reveau, K., Riesgo-Escovar, J., Fu, H., Aladjem, M. I., & Lilly, M. A. (2007). The cyclin-dependent kinase inhibitor Dacapo promotes replication licensing during Drosophila endocycles. *The EMBO Journal*, *26*(8), 2071–2082. https://doi.org/10.1038/sj.emboj.7601648

Hua, B. L., & Orr-Weaver, T. L. (2017). DNA Replication Control During *Drosophila* Development: Insights into the Onset of S Phase, Replication Initiation, and Fork Progression. *Genetics*, *207*(1), 29–47. https://doi.org/10.1534/genetics.115.186627

Hui, B., Ji, H., Xu, Y., Wang, J., Ma, Z., Zhang, C., Wang, K., & Zhou, Y. (2019). RREB1-induced upregulation of the lncRNA AGAP2-AS1 regulates the proliferation and migration of pancreatic cancer partly through suppressing ANKRD1 and ANGPTL4. *Cell Death & Disease*, *10*(3), 207. https://doi.org/10.1038/s41419-019-1384-9

Irving, P., Ubeda, J.-M., Doucet, D., Troxler, L., Lagueux, M., Zachary, D., Hoffmann, J. A., Hetru, C., & Meister, M. (2005). New insights into Drosophila larval haemocyte functions through genome-wide analysis. *Cellular Microbiology*, *7*(3), 335–350. https://doi.org/10.1111/j.1462-5822.2004.00462.x

Jenett, A., Rubin, G. M., Ngo, T.-T. B., Shepherd, D., Murphy, C., Dionne, H., Pfeiffer, B. D., Cavallaro, A., Hall, D., Jeter, J., Iyer, N., Fetter, D., Hausenfluck, J. H., Peng, H., Trautman, E. T., Svirskas, R. R., Myers, E. W., Iwinski, Z. R., Aso, Y., … Zugates, C. T. (2012). A GAL4-Driver Line Resource for Drosophila Neurobiology. *Cell Reports*, *2*(4), 991–1001. https://doi.org/10.1016/j.celrep.2012.09.011

Jindra, M. (2019). Where did the pupa come from? The timing of juvenile hormone signalling supports homology between stages of hemimetabolous and holometabolous insects. *Philosophical Transactions of the Royal Society B: Biological Sciences*, *374*(1783), 20190064. https://doi.org/10.1098/rstb.2019.0064

Kent, O. A., Saha, M., Coyaud, E., Burston, H. E., Law, N., Dadson, K., Chen, S., Laurent, E. M., St-Germain, J., Sun, R. X., Matsumoto, Y., Cowen, J., Montgomery-Song, A., Brown, K. R., Ishak, C., Rose, J. L., De Carvalho, D. D., He, H. H., Raught, B., … Rottapel, R. (2020). Haploinsufficiency of RREB1 causes a Noonan-like RASopathy via epigenetic reprogramming of RAS-MAPK pathway genes. *Nature Communications*, *11*(1), 4673. https://doi.org/10.1038/s41467-020-18483-9

Kim, M., Delos Santos, K., & Moon, N.-S. (2021). Proper CycE–Cdk2 activity in endocycling tissues requires regulation of the cyclin-dependent kinase inhibitor Dacapo by dE2F1b in Drosophila. *Genetics*, *217*(1), iyaa029. https://doi.org/10.1093/genetics/iyaa029

Kim, M., Du, O. Y., Whitney, R. J., Wilk, R., Hu, J., Krause, H. M., Kavaler, J., & Reed, B. H. (2019). A Functional Analysis of the Drosophila Gene hindsight: Evidence for Positive Regulation of EGFR Signaling. *G3: Genes|Genomes|Genetics*, *10*(1), 117–127. https://doi.org/10.1534/g3.119.400829

Knoblich, J. A., Sauer, K., Jones, L., Richardson, H., & Lehner, C. F. (1994). *Cyclin E Controls S Phase Progression and Its Down-Regulation during Drosophila Embryogenesis Is Required for the Arrest of Cell Proliferation*. 14.

Koelzer, S., & Klein, T. (2003). A Notch-independent function of Suppressor of Hairless during the development of the bristle sensory organ precursor cell of Drosophila. *Development*, *130*(9), 1973–1988. https://doi.org/10.1242/dev.00426

Krejci, A., Bernard, F., Housden, B. E., Collins, S., & Bray, S. J. (2009). Direct Response to Notch Activation: Signaling Crosstalk and Incoherent Logic. *Science Signaling*, *2*(55), ra1–ra1. https://doi.org/10.1126/scisignal.2000140

Krzemien, J., Oyallon, J., Crozatier, M., & Vincent, A. (2010). Hematopoietic progenitors and hemocyte lineages in the Drosophila lymph gland. *Developmental Biology*, *346*(2), 310–319. https://doi.org/10.1016/j.ydbio.2010.08.003

Lane, M. E., Sauer, K., Wallace, K., Jan, Y. N., Lehner, C. F., & Vaessin, H. (1996). Dacapo, a Cyclin-Dependent Kinase Inhibitor, Stops Cell Proliferation during Drosophila Development. *Cell*, *87*(7), 1225–1235. https://doi.org/10.1016/S0092-8674(00)81818-8

Lebestky, T., Jung, S.-H., & Banerjee, U. (2003). A Serrate-expressing signaling center controls Drosophila hematopoiesis. *Genes & Development*, *17*(3), 348–353. https://doi.org/10.1101/gad.1052803

Lee, L. A., & Orr-Weaver, T. L. (2003). Regulation of Cell Cycles in Drosophila Development: Intrinsic and Extrinsic Cues. *Annual Review of Genetics*, *37*(1), 545–578. https://doi.org/10.1146/annurev.genet.37.110801.143149

Lee, P.-T., Zirin, J., Kanca, O., Lin, W.-W., Schulze, K. L., Li-Kroeger, D., Tao, R., Devereaux, C., Hu, Y., Chung, V., Fang, Y., He, Y., Pan, H., Ge, M., Zuo, Z., Housden, B. E., Mohr, S. E., Yamamoto, S., Levis, R. W., … Bellen, H. J. (2018). A gene-specific T2A-GAL4 library for Drosophila. *ELife*, *7*, e35574. https://doi.org/10.7554/eLife.35574

Lehman, D., Patterson, B., Johnston, L., Balzer, T., Britton, J., Saint, R., & Edgar, B. (1999). Cis-regulatory elements of the mitotic regulator, string/Cdc25. *Development*, *126*, 1793–1803.

Lilly, M. A., & Duronio, R. J. (2005). New insights into cell cycle control from the Drosophila endocycle. *Oncogene*, *24*(17), 2765–2775. https://doi.org/10.1038/sj.onc.1208610

Losick, V. P. (2016). Wound-Induced Polyploidy Is Required for Tissue Repair. *Advances in Wound Care*, *5*(6), 271–278. https://doi.org/10.1089/wound.2014.0545

Losick, V. P., Fox, D. T., & Spradling, A. C. (2013). Polyploidization and Cell Fusion Contribute to Wound Healing in the Adult Drosophila Epithelium. *Current Biology*, *23*(22), 2224–2232. https://doi.org/10.1016/j.cub.2013.09.029

Mahajan, A., Go, M. J., Zhang, W., Below, J. E., Gaulton, K. J., Ferreira, T., Horikoshi, M., Johnson, A. D., Ng, M. C. Y., Prokopenko, I., Saleheen, D., Wang, X., Zeggini, E., Abecasis, G. R., Adair, L. S., Almgren, P., Atalay, M., Aung, T., Baldassarre, D., … Morris, A. P. (2014). Genome-wide trans-ancestry meta-analysis provides insight into the genetic architecture of type 2 diabetes susceptibility. *Nature Genetics*, *46*(3), 234–244. https://doi.org/10.1038/ng.2897

Mandaravally Madhavan, M., & Schneiderman, H. A. (1977). Histological analysis of the dynamics of growth of imaginal discs and histoblast nests during the larval development ofDrosophila melanogaster. *Wilhelm Roux's Archives of Developmental Biology*, *183*(4), 269–305. https://doi.org/10.1007/BF00848459

Maqbool, S. B., Mehrotra, S., Kolpakas, A., Durden, C., Zhang, B., Zhong, H., & Calvi, B. R. (2010). Dampened activity of E2F1–DP and Myb–MuvB transcription factors in *Drosophila* endocycling cells. *Journal of Cell Science*, *123*(23), 4095–4106. https://doi.org/10.1242/jcs.064519

Matrisian, L. M. (1992). The matrix-degrading metalloproteinases. *BioEssays*, *14*(7), 455–463. https://doi.org/10.1002/bies.950140705

McKelvie, P. A., Daniell, M., McNab, A., Loughnan, M., & Santamaria, J. D. (2002). Squamous cell carcinoma of the conjunctiva: A series of 26 cases. *The British Journal of Ophthalmology*, *86*(2), 168–173.

Mcnairn, A. J., & Guasch, G. (2011). Epithelial Transition Zones: Merging microenvironments, niches, and cellular transformation. *European Journal of Dermatology*, *21*(S1), 21–28. https://doi.org/10.1684/ejd.2011.1267

Mehrotra, S., Maqbool, S. B., Kolpakas, A., Murnen, K., & Calvi, B. R. (2008). Endocycling cells do not apoptose in response to DNA rereplication genotoxic stress. *Genes & Development*, *22*(22), 3158–3171. https://doi.org/10.1101/gad.1710208

Milchanowski, A. B., Henkenius, A. L., Narayanan, M., Hartenstein, V., & Banerjee, U. (2004). Identification and Characterization of Genes Involved in Embryonic Crystal Cell Formation During Drosophila Hematopoiesis. *Genetics*, *168*(1), 325–339. https://doi.org/10.1534/genetics.104.028639

Millar, J. B., & Russell, P. (1992). The cdc25 M-phase inducer: An unconventional protein phosphatase. *Cell*, *68*(3), 407–410. https://doi.org/10.1016/0092-8674(92)90177-e

Minakhina, S., & Steward, R. (2006). Melanotic Mutants in Drosophila: Pathways and Phenotypes. *Genetics*, *174*(1), 253–263. https://doi.org/10.1534/genetics.106.061978

Ming, L., Wilk, R., Reed, B. H., & Lipshitz, H. D. (2013). Drosophila Hindsight and mammalian RREB-1 are evolutionarily conserved DNA-binding transcriptional attenuators. *Differentiation*, *86*(4–5), 159–170. https://doi.org/10.1016/j.diff.2013.12.001

Moberg, K. H., Bell, D. W., Wahrer, D. C. R., Haber, D. A., & Hariharan, I. K. (2001). Archipelago regulates Cyclin E levels in Drosophila and is mutated in human cancer cell lines. *Nature*, *413*(6853), 311–316. https://doi.org/10.1038/35095068

Nam, H.-J., Jang, I.-H., You, H., Lee, K.-A., & Lee, W.-J. (2012). Genetic evidence of a redox-dependent systemic wound response via Hayan Protease-Phenoloxidase system in Drosophila. *The EMBO Journal*, *31*(5), 1253–1265. https://doi.org/10.1038/emboj.2011.476

Nandakumar, S., Grushko, O., & Buttitta, L. A. (2020). Polyploidy in the adult Drosophila brain. *ELife*, *9*, e54385. https://doi.org/10.7554/eLife.54385

Narbonne-Reveau, K., Senger, S., Pal, M., Herr, A., Richardson, H. E., Asano, M., Deak, P., & Lilly, M. A. (2008). APC/CFzr/Cdh1 promotes cell cycle progression during the *Drosophila* endocycle. *Development*, *135*(8), 1451–1461. https://doi.org/10.1242/dev.016295

Neyen, C., Binggeli, O., Roversi, P., Bertin, L., Sleiman, M. B., & Lemaitre, B. (2015). The Black cells phenotype is caused by a point mutation in the Drosophila pro-phenoloxidase 1 gene that triggers melanization and hematopoietic defects1Equal

contribution.1. *Developmental & Comparative Immunology*, *50*(2), 166–174. https://doi.org/10.1016/j.dci.2014.12.011

Ohlstein, B., & Spradling, A. (2007). Multipotent Drosophila Intestinal Stem Cells Specify Daughter Cell Fates by Differential Notch Signaling. *Science*, *315*(5814), 988–992. https://doi.org/10.1126/science.1136606

Pickup, A. T., Lamka, M. L., Sun, Q., Yip, M. L. R., & Lipshitz, H. D. (2002). Control of photoreceptor cell morphology, planar polarity and epithelial integrity during Drosophila eye development. *Development*, *129*(9), 2247–2258. https://doi.org/10.1242/dev.129.9.2247

Pienta, K. J., Hammarlund, E. U., Brown, J. S., Amend, S. R., & Axelrod, R. M. (2021). Cancer recurrence and lethality are enabled by enhanced survival and reversible cell cycle arrest of polyaneuploid cells. *Proceedings of the National Academy of Sciences*, *118*(7), e2020838118. https://doi.org/10.1073/pnas.2020838118

Pitsouli, C., & Perrimon, N. (2010). Embryonic multipotent progenitors remodel the Drosophila airways during metamorphosis. *Development*, *137*(21), 3615–3624. https://doi.org/10.1242/dev.056408

Rabinowitz, M. (1941). Studies on the cytology and early embryology of the egg of Drosophila melanogaster. *Journal of Morphology*, *69*(1), 1–49. https://doi.org/10.1002/jmor.1050690102

Rahrmann, E. P., Wolf, N. K., Otto, G. M., Heltemes-Harris, L., Ramsey, L. B., Shu, J., LaRue, R. S., Linden, M. A., Rathe, S. K., Starr, T. K., Farrar, M. A., Moriarity, B. S., & Largaespada, D. A. (2019). *Sleeping Beauty* Screen Identifies *RREB1* and Other Genetic Drivers in Human B-cell Lymphoma. *Molecular Cancer Research*, *17*(2), 567–582. https://doi.org/10.1158/1541-7786.MCR-18-0582

Rämet, M., Lanot, R., Zachary, D., & Manfruelli, P. (2002). JNK Signaling Pathway Is Required for Efficient Wound Healing in Drosophila. *Developmental Biology*, *241*(1), 145–156. https://doi.org/10.1006/dbio.2001.0502

Reeves, N., & Posakony, J. W. (2005). Genetic Programs Activated by Proneural Proteins in the Developing Drosophila PNS. *Developmental Cell*, *8*(3), 413–425. https://doi.org/10.1016/j.devcel.2005.01.020

Rizki, M. T. M. (1957). Alterations in the haemocyte population of Drosophila melanogaster. *Journal of Morphology*, *100*(3), 437–458. https://doi.org/10.1002/jmor.1051000303

Rizki, M. T. M., & Rizki, R. M. (1959). Functional Significance of the Crystal Cells in the Larva of Drosophila melanogaster. *The Journal of Biophysical and Biochemical Cytology*, *5*(2), 235–240.

Rizki, T. M., Rizki, R. M., & Grell, E. H. (1980). A mutant affecting the crystal cells inDrosophila melanogaster. *Wilhelm Roux's Archives of Developmental Biology*, *188*(2), 91–99. https://doi.org/10.1007/BF00848799

Rodman, T. C. (1967). DNA Replication in Salivary Gland Nuclei of DROSOPHILA MELANOGASTER at Successive Larval and Prepupal Stages. *Genetics*, *55*(3), 375–386.

Rogers, S., Wells, R., & Rechsteiner, M. (1986). Amino Acid Sequences Common to Rapidly Degraded Proteins: The PEST Hypothesis. *Science*, *234*(4774), 364–368.

Roos, W. P., & Kaina, B. (2006). DNA damage-induced cell death by apoptosis. *Trends in Molecular Medicine*, *12*(9), 440–450. https://doi.org/10.1016/j.molmed.2006.07.007

Rosas-Arellano, A., Villalobos-González, J. B., Palma-Tirado, L., Beltrán, F. A., Cárabez-Trejo, A., Missirlis, F., & Castro, M. A. (2016). A simple solution for antibody signal enhancement in immunofluorescence and triple immunogold assays. *Histochemistry and Cell Biology*, *146*(4), 421–430. https://doi.org/10.1007/s00418-016-1447-2

Ruiz-Losada, M., González, R., Peropadre, A., Gil-Gálvez, A., Tena, J. J., Baonza, A., & Estella, C. (2021). Coordination between cell proliferation and apoptosis after DNA damage in Drosophila. *Cell Death and Differentiation*. Scopus. https://doi.org/10.1038/s41418-021-00898-6

Saj, A., Arziman, Z., Stempfle, D., van Belle, W., Sauder, U., Horn, T., Dürrenberger, M., Paro, R., Boutros, M., & Merdes, G. (2010). A Combined Ex Vivo and In Vivo RNAi Screen for Notch Regulators in Drosophila Reveals an Extensive Notch Interaction Network. *Developmental Cell*, *18*(5), 862–876. https://doi.org/10.1016/j.devcel.2010.03.013

Saretzki G. (2010). Cellular senescence in the development and treatment of cancer. *Current pharmaceutical design*, *16*(1), 79–100.

Sato, M., Kitada, Y., & Tabata, T. (2008). Larval cells become imaginal cells under the control of homothorax prior to metamorphosis in the Drosophila tracheal system. *Developmental Biology*, *318*(2), 247–257. https://doi.org/10.1016/j.ydbio.2008.03.025

Sauer, K., J. A. Knoblich, H. Richardson, and C. F. Lehner, (1995). Distinct modes of cyclin E/cdc2c kinase regulation and S-phase control in mitotic and endoreduplication cycles of Drosophila embryogenesis. *Genes Dev.* 9: 1327–1339

Schneider, C. A., Rasband, W. S., & Eliceiri, K. W. (2012). NIH Image to ImageJ: 25 years of image analysis. *Nature Methods*, *9*(7), Article 7. https://doi.org/10.1038/nmeth.2089

Schweisguth, F., & Posakony, J. W. (1992). Suppressor of Hairless, the Drosophila homolog of the mouse recombination signal-binding protein gene, controls sensory organ cell fates. *Cell*, *69*(7), 1199–1212. https://doi.org/10.1016/0092-8674(92)90641-O

Seisenbacher, G., Hafen, E., & Stocker, H. (2011). MK2-Dependent p38b Signalling Protects Drosophila Hindgut Enterocytes against JNK-Induced Apoptosis under Chronic Stress. *PLoS Genetics*, *7*(8), e1002168. https://doi.org/10.1371/journal.pgen.1002168

Shcherbata, H. R., Althauser, C., Findley, S. D., & Ruohola-Baker, H. (2004). The mitotic-to-endocycle switch in Drosophila follicle cells is executed by Notch-dependent regulation of G1/S, G2/M and M/G1 cell-cycle transitions. *Development (Cambridge, England)*, *131*(13), 3169–3181. https://doi.org/10.1242/dev.01172

Shibutani, S., Swanhart, L. M., & Duronio, R. J. (2007). Rbf1-independent termination of E2f1-target gene expression during early Drosophila embryogenesis. *Development*, *134*(3), 467–478. https://doi.org/10.1242/dev.02738

Shibutani, S. T., de la Cruz, A. F. A., Tran, V., Turbyfill, W. J., Reis, T., Edgar, B. A., & Duronio, R. J. (2008). Intrinsic negative cell cycle regulation provided by PIP box- and Cul4Cdt2-mediated destruction of E2f1 during S phase. *Developmental Cell*, *15*(6), 890–900. https://doi.org/10.1016/j.devcel.2008.10.003

Sigrist, S. J., & Lehner, C. F. (1997). Drosophila fizzy-related Down-Regulates Mitotic Cyclins and Is Required for Cell Proliferation Arrest and Entry into Endocycles. *Cell*, *90*(4), 671–681. https://doi.org/10.1016/S0092-8674(00)80528-0

Smith, A. V., & Orr-Weaver, T. L. (1991). The regulation of the cell cycle during Drosophila embryogenesis: The transition to polyteny. *Development*, *112*, 997–1008.

Somma, M. P., Ceprani, F., Bucciarelli, E., Naim, V., De Arcangelis, V., Piergentili, R., Palena, A., Ciapponi, L., Giansanti, M. G., Pellacani, C., Petrucci, R., Cenci, G., Vernì, F., Fasulo, B., Goldberg, M. L., Di Cunto, F., & Gatti, M. (2008). Identification of Drosophila Mitotic Genes by Combining Co-Expression Analysis and RNA Interference. *PLoS Genetics*, *4*(7), e1000126. https://doi.org/10.1371/journal.pgen.1000126

Struhl, G., & Basler, K. (1993). Organizing activity of wingless protein in Drosophila. *Cell*, *72*(4), Article 4. https://doi.org/10.1016/0092-8674(93)90072-X

Sun, J., & Deng, W.-M. (2007). Hindsight Mediates the Role of Notch in Suppressing Hedgehog Signaling and Cell Proliferation. *Developmental Cell*, *12*(3), 431–442. https://doi.org/10.1016/j.devcel.2007.02.003

Surova, O., & Zhivotovsky, B. (2013). Various modes of cell death induced by DNA damage. *Oncogene*, *32*(33), 3789–3797. https://doi.org/10.1038/onc.2012.556

Swanson, C. I., Meserve, J. H., McCarter, P. C., Thieme, A., Mathew, T., Elston, T. C., & Duronio, R. J. (2015). Expression of an S phase-stabilized version of the CDK inhibitor Dacapo can alter endoreplication. *Development (Cambridge, England)*, *142*(24), 4288–4298. https://doi.org/10.1242/dev.115006

Tamori, Y., & Deng, W.-M. (2013). Tissue Repair through Cell Competition and Compensatory Cellular Hypertrophy in Postmitotic Epithelia. *Developmental Cell*, *25*(4), 350–363. https://doi.org/10.1016/j.devcel.2013.04.013

Tang, H., Kambris, Z., Lemaitre, B., & Hashimoto, C. (2006). Two Proteases Defining a Melanization Cascade in the Immune System of Drosophila*. *Journal of Biological Chemistry*, *281*(38), 28097–28104. https://doi.org/10.1074/jbc.M601642200

Tang, H., Kambris, Z., Lemaitre, B., & Hashimoto, C. (2008). A Serpin that Regulates Immune Melanization in the Respiratory System of Drosophila. *Developmental Cell*, *15*(4), 617–626. https://doi.org/10.1016/j.devcel.2008.08.017

Tartaglia, M., Gelb, B. D., & Zenker, M. (2011). Noonan syndrome and clinically related disorders. *Best Practice & Research. Clinical Endocrinology & Metabolism*, *25*(1), 161–179. https://doi.org/10.1016/j.beem.2010.09.002

Terriente-Felix, A., Li, J., Collins, S., Mulligan, A., Reekie, I., Bernard, F., Krejci, A., & Bray, S. (2013). Notch cooperates with Lozenge/Runx to lock haemocytes into a differentiation program. *Development (Cambridge, England)*, *140*(4), 926–937. https://doi.org/10.1242/dev.086785

Thiagalingam, A., De Bustros, A., Borges, M., Jasti, R., Compton, D., Diamond, L., Mabry, M., Ball, D. W., Baylin, S. B., & Nelkin, B. D. (1996). RREB-1, a novel zinc finger protein, is involved in the differentiation response to Ras in human medullary thyroid carcinomas. *Molecular and Cellular Biology*, *16*(10), 5335–5345.

Tran, V., Gan, Q., & Chen, X. (2012). Chromatin Immunoprecipitation (ChIP) using Drosophila tissue. *Journal of Visualized Experiments : JoVE*, *61*, 3745. https://doi.org/10.3791/3745

Troost, T., Schneider, M., & Klein, T. (2015). A Re-examination of the Selection of the Sensory Organ Precursor of the Bristle Sensilla of Drosophila melanogaster. *PLOS Genetics*, *11*(1), e1004911. https://doi.org/10.1371/journal.pgen.1004911

Truman, J. W., & Riddiford, L. M. (2019). The evolution of insect metamorphosis: A developmental and endocrine view. *Philosophical Transactions of the Royal Society B: Biological Sciences*, *374*(1783), 20190070. https://doi.org/10.1098/rstb.2019.0070

Vlachakis, D., Papageorgiou, L., Papadaki, A., Georga, M., Kossida, S., & Eliopoulos, E. (2020). An updated evolutionary study of the Notch family reveals a new ancient origin and novel invariable motifs as potential pharmacological targets. *PeerJ*, *8*, e10334. https://doi.org/10.7717/peerj.10334

Wang, X.-F., Yang, S.-A., Gong, S., Chang, C.-H., Portilla, J. M., Chatterjee, D., Irianto, J., Bao, H., Huang, Y.-C., & Deng, W.-M. (2021). Polyploid mitosis and depolyploidization promote chromosomal instability and tumor progression in a Notch-induced tumor model. *Developmental Cell*, S1534580721004779. https://doi.org/10.1016/j.devcel.2021.05.017

Watzinger, F., & Lion, T. (1999). RAS Family. *Atlas of Genetics and Cytogenetics in Oncology and Haematology*, *3*(2), 116–123.

Wilk, R., Pickup, A. T., Hamilton, J. K., Reed, B. H., & Lipshitz, H. D. (2004). Dose-sensitive autosomal modifiers identify candidate genes for tissue autonomous and tissue nonautonomous regulation by the Drosophila nuclear zinc-finger protein, hindsight. *Genetics*, *168*(1), 281–300. https://doi.org/10.1534/genetics.104.031344

Wilk, R., Reed, B. H., Tepass, U., & Lipshitz, H. D. (2000). The hindsight Gene Is Required for Epithelial Maintenance and Differentiation of the Tracheal System in Drosophila. *Developmental Biology*, *219*(2), 183–196. https://doi.org/10.1006/dbio.2000.9619

Wittkopp, P. J., True, J. R., & Carroll, S. B. (2002). Development of melanin patterns in Drosophila. *Development*, 10.

Yamamoto, S., Schulze, K. L., & Bellen, H. J. (2014). Introduction to Notch Signaling. In H. J. Bellen & S. Yamamoto (Eds.), *Notch Signaling: Methods and Protocols* (pp. 1–14). Springer. https://doi.org/10.1007/978-1-4939-1139-4_1

Yang, S.-A., & Deng, W.-M. (2018). Serrate/Notch Signaling Regulates the Size of the Progenitor Cell Pool in Drosophila Imaginal Rings. *Genetics*, *209*(3), 829–843. https://doi.org/10.1534/genetics.118.300963

Yang, S.-A., Portilla, J.-M., Mihailovic, S., Huang, Y.-C., & Deng, W.-M. (2019). Oncogenic Notch Triggers Neoplastic Tumorigenesis in a Transition-Zone-like Tissue Microenvironment. *Developmental Cell*, *49*(3), 461-472.e5. https://doi.org/10.1016/j.devcel.2019.03.015

Yao, J., Zhong, L., Zhong, P., Liu, D., Yuan, Z., Liu, J., Yao, S., Zhao, Y., Chen, M., Li, L., Liu, L., & Liu, B. (2019). RAS-Responsive Element-Binding Protein 1 Blocks the Granulocytic Differentiation of Myeloid Leukemia Cells. *Oncology Research*, *27*(7), 809–818. https://doi.org/10.3727/096504018X15451301487729

Yip, M. L., Lamka, M. L., & Lipshitz, H. D. (1997). Control of germ-band retraction in Drosophila by the zinc-finger protein HINDSIGHT. *Development*, *124*(11), 2129-2141.

Zhang, B., Mehrotra, S., Ng, W. L., & Calvi, B. R. (2014). Low Levels of p53 Protein and Chromatin Silencing of p53 Target Genes Repress Apoptosis in Drosophila Endocycling Cells. *PLoS Genetics*, *10*(9), e1004581. https://doi.org/10.1371/journal.pgen.1004581

Zhu, L. J., Christensen, R. G., Kazemian, M., Hull, C. J., Enuameh, M. S., Basciotta, M. D., Brasefield, J. A., Zhu, C., Asriyan, Y., Lapointe, D. S., Sinha, S., Wolfe, S. A., & Brodsky, M. H. (2011). FlyFactorSurvey: A database of Drosophila transcription factor binding specificities determined using the bacterial one-hybrid system. *Nucleic Acids Research*, *39*(Database issue), D111–D117. https://doi.org/10.1093/nar/gkq858

Zielke, N., Querings, S., Rottig, C., Lehner, C., & Sprenger, F. (2008). The anaphase-promoting complex/cyclosome (APC/C) is required for rereplication control in endoreplication cycles. *Genes & Development*, *22*(12), 1690–1703. https://doi.org/10.1101/gad.469108

Zielke, N., Kim, K. J., Tran, V., Shibutani, S. T., Bravo, M.-J., Nagarajan, S., van Straaten, M., Woods, B., von Dassow, G., Rottig, C., Lehner, C. F., Grewal, S. S., Duronio, R. J., & Edgar, B. A. (2011). Control of Drosophila endocycles by E2F and CRL4CDT2. *Nature*, *480*(7375), 123–127. https://doi.org/10.1038/nature10579

Zielke, N., Korzelius, J., van Straaten, M., Bender, K., Schuhknecht, G. F. P., Dutta, D., Xiang, J., & Edgar, B. A. (2014). Fly-FUCCI: A Versatile Tool for Studying Cell Proliferation in Complex Tissues. *Cell Reports*, *7*(2), 588–598. https://doi.org/10.1016/j.celrep.2014.03.020

Zoog, S. J., Schiller, J. J., Wetter, J. A., Chejanovsky, N., & Friesen, P. D. (2002). Baculovirus apoptotic suppressor P49 is a substrate inhibitor of initiator caspases resistant to P35 in vivo. The EMBO Journal, 21(19), 5130–5140. https://doi.org/10.1093/emboj/cdf520

# Appendix A: Methods Related

## A.1 Genetic Stocks

| STOCK | SOURCE (BDSC = Bloomington Drosophila Stock Center) | Reed Lab Stock Collection Number |
|---|---|---|
| **Hindsight Overexpression Lines** | | |
| ***w; Sp/CyO; 1xUAS-peb$^{attP2}$/TM3, Sb**** | **Freeman Lab** | **1293** |
| ***w; Sp/CyO; 5xUAS-peb::myc/TM3, Sb**** | **Freeman Lab** | **1301** |
| ***w; Sp/CyO; 10xUAS-peb/TM3, Sb**** | **Freeman Lab** | **1299** |
| **Notch Overexpression Lines** | | |
| ***UAS-N$^{\Delta 34a}$* (also known as UAS-Dl::N.ΔECN)** | **Giniger Lab** | **959** |
| ***UAS-NICD/CyO-GFP ; Sb/TM6,TbHu*** | **Arama Lab** | |
| **Other UAS Lines** | | |
| ***UAS-p35$^{TTRO33}$*** | **Made in Reed Lab by Δ23 transposase mobilization of BDSC (#6298) to II chromosome** | **491** |
| ***UAS-stg*** *(w[1118]; P{w[+mC]=UAS-stg.N}16/CyO, P{ry[+t7.2]=sevRas1.V12}FK1)* | **BDSC (#4777)** | **1358** |
| ***UAS-cdc2-RNAi*** *(y[1] sc[*] v[1] sev[21]; P{y[+t7.7] v[+t1.8]=TRiP.GL00262}attP2)* | **BDSC (#35350)** | **1063** |
| **Reporter Lines** | | |
| ***w[1118]; P{w[+mC]=UAS-GFP.NLS}8*** | **BDSC (#4776)** | **127** |
| ***w[*]; P{w[+mC]=UAS-mCherry.NLS}3*** | **BDSC (#38424)** | **757** |
| ***w[1118]; P{w[+m*]=NRE-EGFP.S}5A*** | **BDSC (#30727)** | **1006** |
| ***His2AvGFP,hsFLP; His2AvRFP*** *(y[1] w[*] P{w[+mC]=His2Av[T:Avic\GFP-S65T]}1 P{ry[+t7.2]=hsFLP}122 P{ry[+t7.2]=neoFRT}19A; P{w[+mC]=His2Av-mRFP1}III.1/TM6B, Tb[1])* (may be segregating *Fm7)* | **BDSC (#30563)** | **610** |

*(Continued on next page…)*

| GAL4 Lines | | |
|---|---|---|
| ***retn-GAL4*** *(w[1118]; P{y[+t7.7] w[+mC]=GMR9F06-GAL4}attP2)* | **BDSC (#47433)** | **1317** |
| ***Mmp1-GAL4*** *(y[1] w[*]; Mi{Trojan-GAL4.1}Mmp1[MI03010-TG4.1])* | **BDSC (#76161)** | **1356** |
| **Other** | | |
| ***y[1] w[1118] P{ry[+t7.2]=neoFRT}19A*** **(standard lab control)** | **BDSC (#1744)** | **597** |
| ***w hnt$^{345x}$ hsFLP FRT19A/Fm7Kr ; + ; +*** | **Freeman Lab** | **1300** |
| ***w hsFLP FRT19A ; + ; +*** | **Freeman Lab** | **1295** |

**Table A.1.1 List of Genetic Stocks.** ***** *UAS-peb* constructs will be known as *UAS-hnt* constructs throughout this document.

## A.2 Crossing Schemes

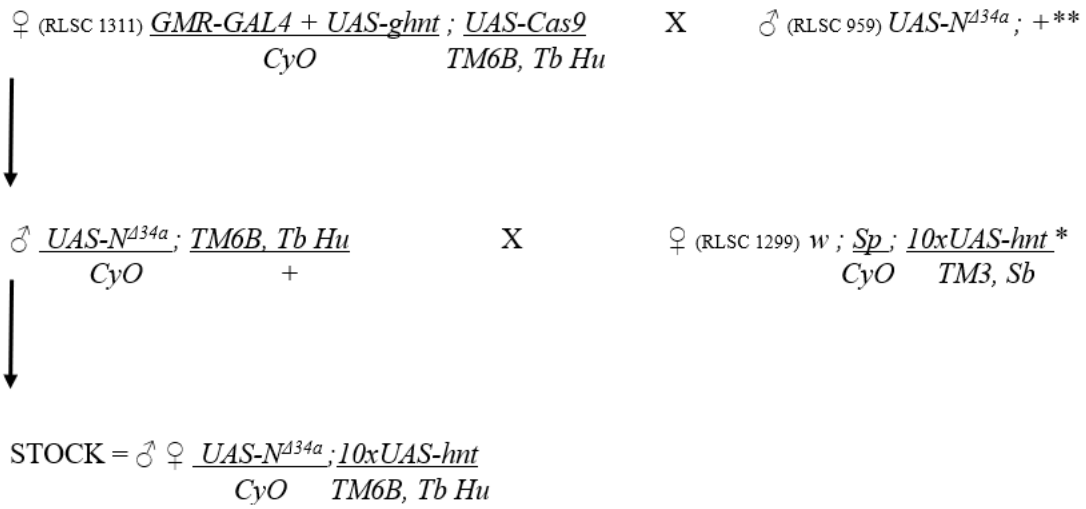



**Figure A.2.1 Representative crossing scheme to generate *Drosophila* stocks.** Standard *Drosophila* phenotypic markers are used to select progeny that have inherited the desired chromosome. + indicates wildtype chromosome; * can be replaced with a stock that has desired construct on second chromosome. ** can be replaced with a stock that has desired construct on third chromosome.

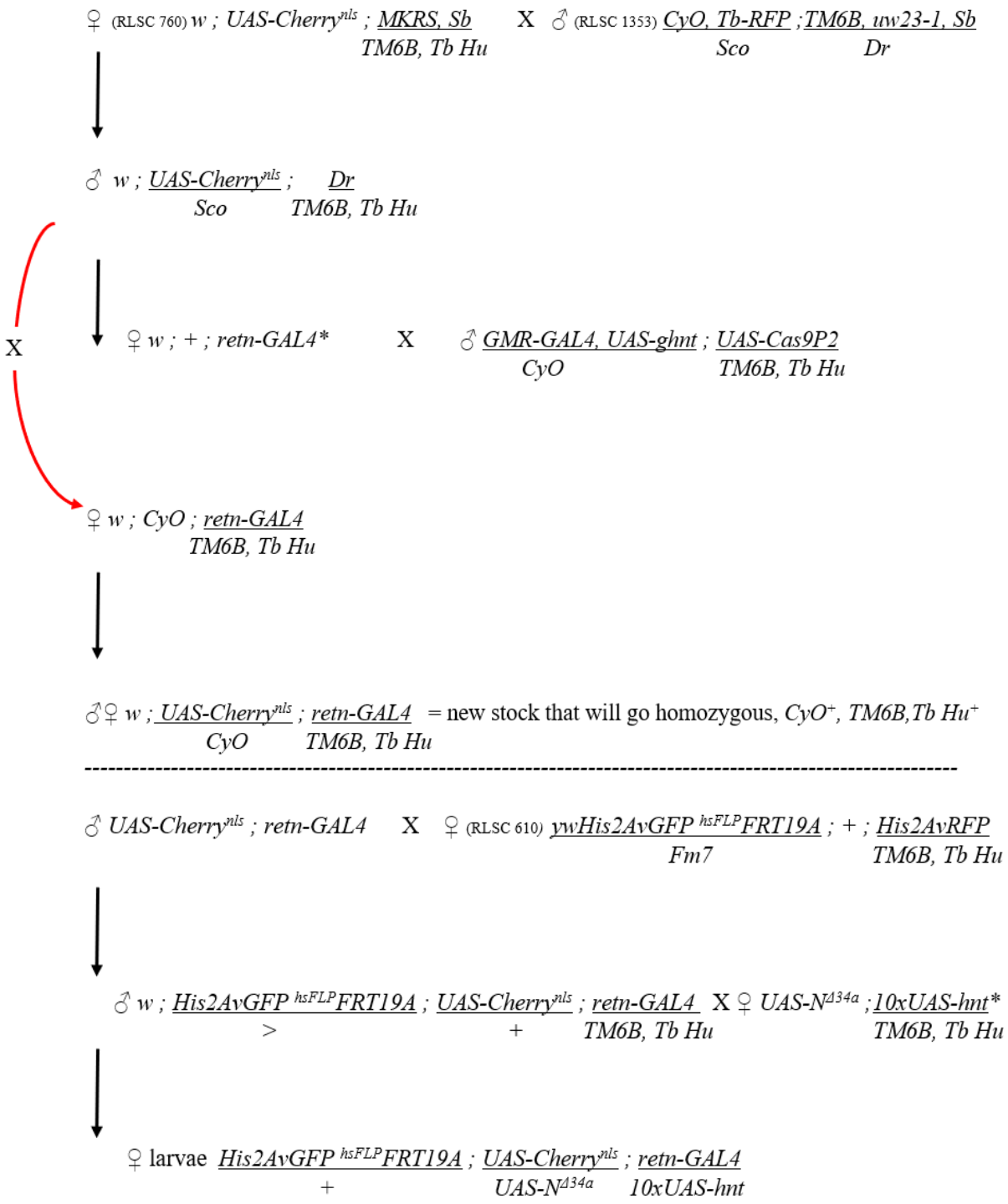



**Figure A.2.2 Crossing scheme to generate fluorescent reporter system.** *Drosophila* phenotypic markers are used to select progeny that have inherited the desired chromosome. + indicates wildtype chromosome; > represents Y chromosome; * stock can be replaced by any stock with *UAS* constructs to observe phenotype

## A.3 Extended larval state (ELS) with Notch-induced overproliferation

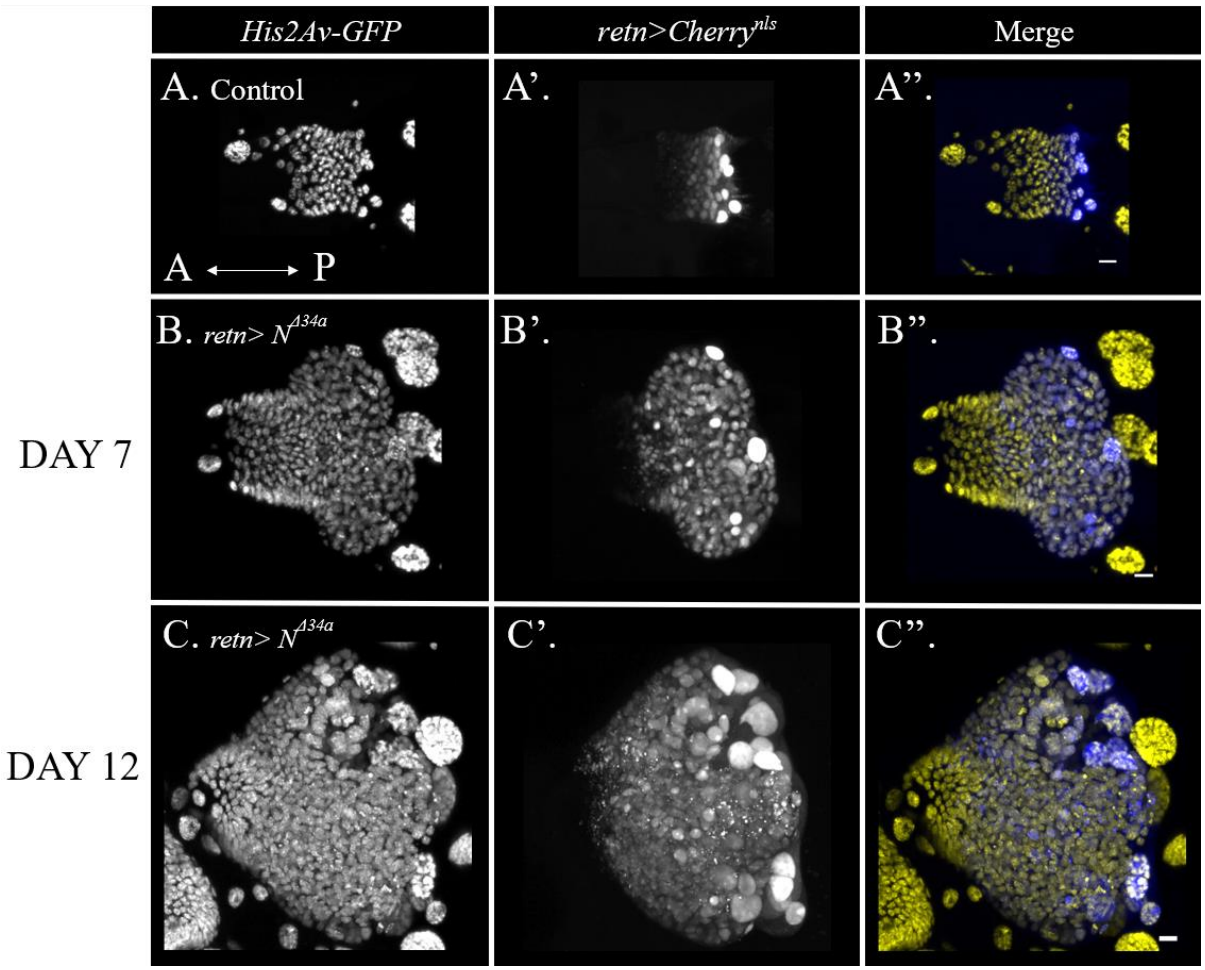



**Figure A.3.1 Notch-induced overproliferation in SGIR increases with extended larval state (ELS).** (A-A") Control SGIR with *retn>GFP*$^{nls}$. Third instar *retn>N*$^{\Delta 34a}$ larvae that have entered an ELS (C-C") possess greater proliferation and larger nuclei than larvae that have not (B-B"). *His2Av-GFP* was utilized as background to identify all nuclei. SGIRs are oriented in the same manner with anterior to the left. Scale bar: 10μm.

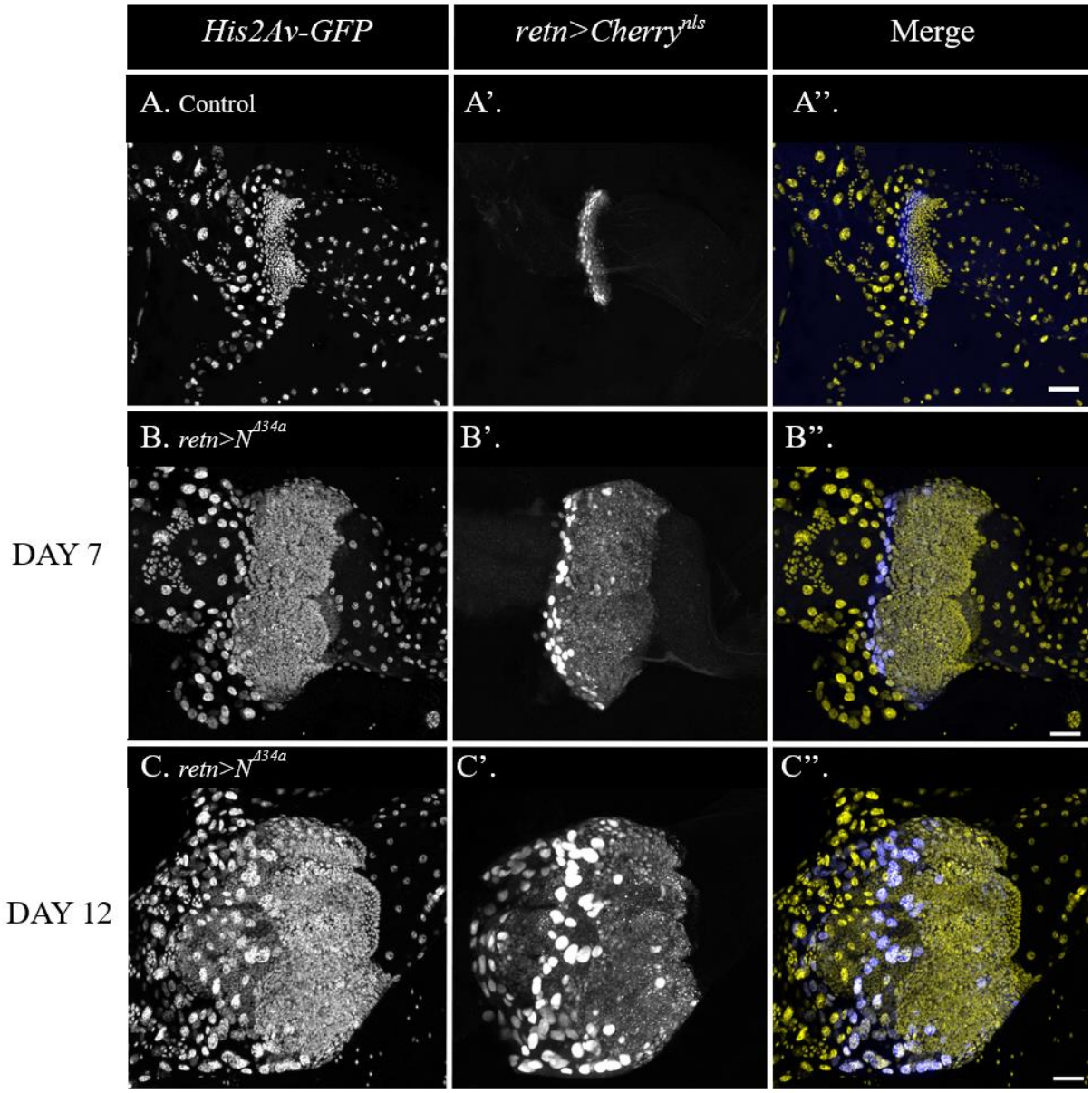



**Figure A.3.2 Notch-induced overproliferation in HIR increases with extended larval state (ELS).** (A-A") Control SGIR with *retn>GFP*$^{nls}$. Third instar *retn>N*$^{\Delta 34a}$ larvae that have entered an ELS (C-C") possess greater proliferation and larger nuclei than larvae that have not (B-B"). *His2Av-GFP* was utilized as background to identify all nuclei. SGIRs are oriented in the same manner with anterior to the left. Scale bar: 40µm.

# Appendix B: Raw Data and Calculations Associated with Results

## B.1 Cell counts and Student T-Tests

| Control | | *Mmp1>cdc2-RNAi* | | *retn>cdc2-RNAi* | |
|---|---|---|---|---|---|
| **SGIR** | **Total number of cells** | **SGIR** | **Total number of cells** | **SGIR** | **Total number of cells** |
| 1 | 87 | 1 | 89 | 1 | 42 |
| 2 | 63 | 2 | 69 | 2 | 40 |
| 3 | 94 | 3 | 98 | 3 | 35 |
| 4 | 90 | 4 | 82 | 4 | 50 |
| 5 | 85 | 5 | 91 | 5 | 45 |
| 6 | 55 | 6 | 79 | 6 | 27 |
| 7 | 79 | 7 | 76 | 7 | 51 |
| 8 | 81 | 8 | 86 | 8 | 21 |
| 9 | 69 | 9 | 123 | 9 | 46 |
| 10 | 73 | 10 | 107 | 10 | 50 |
| 11 | 97 | 11 | 100 | 11 | 63 |
| 12 | 86 | 12 | 84 | 12 | 62 |
| 13 | 88 | 13 | 88 | 13 | 55 |
| 14 | 82 | 14 | 93 | 14 | 48 |
| 15 | 81 | 15 | 83 | 15 | 49 |
| 16 | 110 | 16 | 72 | 16 | 64 |
| 17 | 107 | 17 | 76 | 17 | 57 |
| 18 | 88 | 18 | 47 | 18 | 81 |
| 19 | 72 | 19 | 60 | | |
| 20 | 75 | | | **AVERAGE** | 49.22 |
| 21 | 71 | **AVERAGE** | 84.37 | **STANDARD DEVIATION** | 14.01 |
| 22 | 67 | **STANDARD DEVIATION** | 16.91 | | |
| 23 | 82 | | | | |
| 24 | 92 | | | | |
| 25 | 87 | | | | |
| 26 | 81 | | | | |
| 27 | 75 | | | | |
| | | | | | |
| **AVERAGE** | 82.11 | | | | |
| **STANDARD DEVIATION** | 12.38 | | | | |

| **Student T Test** | |
|---|---|
| | **Control & *Mmp1>cdc2-RNAi*** |
| **p =** | 0.623486906 |
| | NS |
| **p =** | **Control & *retn>cdc2-RNAi*** |
| | 2.34812E-09 |
| | *** |

**Table B.1.1 *cdc2-RNAi* knockdown SGIR experiment cell counts and statistical analysis.** Data in table was used to create Table 3.1. The average and standard deviation of each class was calculated. Student T-Tests were conducted to identify if the difference between means of classes is significant. All calculations performed in Microsoft Excel. *** $p < 0.001$; NS = not significant.

## CONTROL

| SGIR | GFP+/RFP+ | GFP-/RFP+ | Total | GFP-/RFP+ % of SGIR |
|---|---|---|---|---|
| 1 | 94 | 11 | 105 | 10.5 |
| 2 | 57 | 17 | 74 | 23.0 |
| 3 | 74 | 15 | 89 | 16.9 |
| 4 | 89 | 13 | 102 | 12.7 |
| 5 | 82 | 46 | 128 | 35.9 |
| 6 | 82 | 18 | 100 | 18.0 |
| 7 | 104 | 35 | 139 | 25.2 |
| 8 | 60 | 45 | 105 | 42.9 |
| 9 | 91 | 14 | 105 | 13.3 |
| 10 | 79 | 8 | 87 | 9.2 |
| 11 | 123 | 16 | 139 | 11.5 |
| 12 | 80 | 13 | 93 | 14.0 |
| 13 | 114 | 20 | 134 | 14.9 |
| 14 | 75 | 36 | 111 | 32.4 |
| 15 | 113 | 29 | 142 | 20.4 |
| 16 | 73 | 12 | 85 | 14.1 |
| 17 | 89 | 25 | 114 | 21.9 |
| 18 | 90 | 23 | 113 | 20.4 |
| 19 | 88 | 24 | 112 | 21.4 |
| 20 | 92 | 10 | 102 | 9.8 |
| 21 | 89 | 11 | 100 | 11.0 |
| 22 | 101 | 12 | 113 | 10.6 |
| 23 | 92 | 8 | 100 | 8.0 |
| 24 | 91 | 22 | 113 | 19.5 |
| **AVERAGE** | **88.42** | **20.13** | **108.54** | **18.2** |
| **STANDARD DEVIATION** | **15.59** | **11.00** | **17.80** | **8.85** |

(*Continued on following page…)*

| *hnt^345x* | | | | |
|---|---|---|---|---|
| **SGIR** | **GFP+/RFP+** | **GFP-/RFP+** | **Total** | **GFP-/RFP+ % of SGIR** |
| 1 | 86 | 16 | 102 | 15.7 |
| 2 | 77 | 55 | 132 | 41.7 |
| 3 | 109 | 26 | 135 | 19.3 |
| 4 | 105 | 38 | 143 | 26.6 |
| 5 | 100 | 22 | 122 | 18.0 |
| 6 | 87 | 48 | 135 | 35.6 |
| 7 | 72 | 74 | 146 | 50.7 |
| 8 | 120 | 14 | 134 | 10.4 |
| 9 | 89 | 34 | 123 | 27.6 |
| 10 | 93 | 10 | 103 | 9.7 |
| 11 | 100 | 16 | 116 | 13.8 |
| 12 | 95 | 33 | 128 | 25.8 |
| 13 | 94 | 31 | 125 | 24.8 |
| 14 | 119 | 11 | 130 | 8.5 |
| 15 | 58 | 45 | 103 | 43.7 |
| 16 | 100 | 28 | 128 | 21.9 |
| 17 | 92 | 20 | 112 | 17.9 |
| 18 | 76 | 27 | 103 | 26.2 |
| 19 | 66 | 33 | 99 | 33.3 |
| 20 | 141 | 23 | 164 | 14.0 |
| 21 | 93 | 26 | 119 | 21.8 |
| 22 | 115 | 28 | 143 | 19.6 |
| 23 | 85 | 26 | 111 | 23.4 |
| 24 | 90 | 23 | 113 | 20.4 |
| 25 | 82 | 35 | 117 | 29.9 |
| 26 | 76 | 49 | 125 | 39.2 |
| 27 | 107 | 24 | 131 | 18.3 |
| 28 | 124 | 9 | 133 | 6.8 |
| 29 | 102 | 24 | 126 | 19.0 |
| | | | | |
| **AVERAGE** | **94.93** | **29.24** | **124.17** | **23.6** |
| | | | | |
| **STANDARD DEVIATION** | **18.32** | **14.43** | **15.15** | **10.88** |
| | | | | |
| **STUDENT T TEST** | | | | |
| **p =** | **0.1681** | **0.0119** | **0.0014** | **0.0543** |
| | **NS** | * | ** | **NS** |

**Table B.1.2 Control and *hnt*$^{345x}$ mosaic cell count data and statistical analysis.** This data was used to create Table 3.2. Cell counts of both control and *hnt*$^{345x}$ SGIRs. The average and standard deviation of each class was calculated. Student T-Tests were conducted to identify if the difference in means between classes is significant. All calculations performed in Microsoft Excel. * $p < 0.05$; ** $p < 0.01$; NS = not significant.

| Control | | *retn>stg+5xUAS-hnt* | |
|---|---|---|---|
| **SGIR** | **Total number of cells** | **SGIR** | **Total number of cells** |
| 1 | 87 | 1 | 176 |
| 2 | 63 | 2 | 41 |
| 3 | 94 | 3 | 41 |
| 4 | 90 | 4 | 46 |
| 5 | 85 | 5 | 108 |
| 6 | 55 | 6 | 112 |
| 7 | 79 | 7 | 91 |
| 8 | 81 | 8 | 40 |
| 9 | 69 | 9 | 59 |
| 10 | 73 | 10 | 77 |
| 11 | 97 | 11 | 40 |
| 12 | 86 | 12 | 113 |
| 13 | 88 | 13 | 53 |
| 14 | 82 | 14 | 88 |
| 15 | 81 | 15 | 14 |
| 16 | 110 | 16 | 13 |
| 17 | 107 | 17 | 31 |
| 18 | 88 | 18 | 40 |
| 19 | 72 | 19 | 136 |
| 20 | 75 | 20 | 144 |
| 21 | 71 | 21 | 78 |
| 22 | 67 | 22 | 94 |
| 23 | 82 | 23 | 96 |
| 24 | 92 | 24 | 75 |
| 25 | 87 | 25 | 19 |
| 26 | 81 | 26 | 9 |
| 27 | 75 | 27 | 21 |
| | | 28 | 22 |
| **AVERAGE** | 82.11 | | |
| **STANDARD DEVIATION** | 12.38 | **AVERAGE** | 67.04 |
| | | **STANDARD DEVIATION** | 44.03 |

| *retn>5xUAS-hnt* | | *retn>stg* | |
|---|---|---|---|
| **SGIR** | **Total number of cells** | **SGIR** | **Total number of cells** |
| 1 | 3 | 1 | 123 |
| 2 | 19 | 2 | 107 |
| 3 | 13 | 3 | 79 |
| 4 | 15 | 4 | 113 |
| 5 | 3 | 5 | 97 |
| 6 | 3 | 6 | 98 |
| 7 | 12 | 7 | 123 |
| 8 | 11 | 8 | 112 |
| 9 | 50 | 9 | 110 |
| 10 | 43 | 10 | 104 |
| 11 | 11 | 11 | 95 |
| 12 | 44 | 12 | 73 |
| 13 | 19 | 13 | 109 |
| 14 | 44 | 14 | 127 |
| 15 | 16 | 15 | 95 |
| 16 | 11 | 16 | 111 |
| 17 | 3 | 17 | 134 |
| | | | |
| **AVERAGE** | 18.82 | **AVERAGE** | 106.47 |
| **STANDARD DEVIATION** | 16.03 | **STANDARD DEVIATION** | 16.09 |

*(Continued on following page…)*

| | Student T Test |
|---|---|
| | **Control & *retn>stg*** |
| **p =** | 1.16407E-05 |
| | *** |
| | |
| | **Control & *retn>5xUAS-hnt*** |
| **p =** | 6.61723E-12 |
| | *** |
| | |
| | **Control & *retn>stg+5xUAS-hnt*** |
| **p =** | 0.091319965 |
| | NS |
| | |
| | ***retn>stg* & *retn>5xUAS-hnt*** |
| **p =** | 9.41009E-17 |
| | *** |
| | |
| | ***retn>5xUAS-hnt* & *retnstg+5xUAS-hnt*** |
| **p =** | 6.46486E-06 |
| | *** |
| | ***retn>stg* & *retn>stg+5xUAS-hnt*** |
| **p =** | 0.000122009 |
| | *** |

**Table B.1.3 *5xUAS-hnt* and *stg* SGIR rescue experiment cell counts and statistical analysis.** Data in table was used to create Table 3.3. The average and standard deviation of each class was calculated. Student T-Tests were conducted to identify if the difference between means of classes is significant. All calculations performed in Microsoft Excel. *** $p < 0.001$; NS = not significant.